9-25-2014 12:00 AM

# Dynamic Image Processing for Guidance of Off-pump Beating Heart Mitral Valve Repair

Feng Li
*The University of Western Ontario*

Supervisor
Terry M. Peters
*The University of Western Ontario*

Graduate Program in Biomedical Engineering
A thesis submitted in partial fulfillment of the requirements for the degree in Doctor of Philosophy

# DYNAMIC IMAGE PROCESSING FOR GUIDANCE OF OFF-PUMP BEATING HEART MITRAL VALVE REPAIR

(Thesis format: Integrated Article)

by

Feng Li

Graduate Program in Biomedical Engineering

A thesis submitted in partial fulfillment
of the requirements for the degree of
Doctor of Philosophy

The School of Graduate and Postdoctoral Studies
Western University
London, Ontario, Canada

# Abstract

Compared to conventional open heart procedures, minimally invasive off-pump beating heart mitral valve repair aims to deliver equivalent treatment for mitral regurgitation with reduced trauma and side effects. However, minimally invasive approaches are often limited by the lack of a direct view to surgical targets and/or tools, a challenge that is compounded by potential movement of the target during the cardiac cycle. For this reason, sophisticated image guidance systems are required in achieving procedural efficiency and therapeutic success. The development of such guidance systems is associated with many challenges. For example, the system should be able to provide high quality visualization of both cardiac anatomy and motion, as well as augmenting it with virtual models of tracked tools and targets. It should have the capability of integrating pre-operative images to the intra-operative scenario through registration techniques.The computation speed must be sufficiently fast to capture the rapid cardiac motion. Meanwhile, the system should be cost effective and easily integrated into standard clinical workflow.

This thesis develops image processing techniques to address these challenges, aiming to achieve a safe and efficient guidance system for off-pump beating heart mitral valve repair. These techniques can be divided into two categories, using 3D and 2D image data respectively. When 3D images are accessible, a rapid multi-modal registration approach is proposed to link the pre-operative CT images to the intra-operative ultrasound images. The ultrasound images are used to display the real time cardiac motion, enhanced by CT data serving as high quality 3D context with annotated features. I also developed a method to generate synthetic dynamic CT images, aiming to replace real dynamic CT data in such a guidance system to reduce the radiation dose applied to the patients. When only 2D images are available, an approach is developed to track the feature of interest, i.e. the mitral annulus, based on bi-plane ultrasound images and a magnetic tracking system. The concept of modern GPU-based parallel computing is employed in most of these approaches to accelerate the computation in order to capture the rapid cardiac motion with desired accuracy.

Validation experiments were performed on phantom, animal and human data. The overall accuracy of registration and feature tracking with respect to the mitral annulus was about 2-3mm with computation time of 60-400ms per frame, sufficient for one update per cardiac cycle. It was also demonstrated in the results that the synthetic CT images can provide very similar anatomical representations and registration accuracy compared to that of the real dynamic CT images. These results suggest that the approaches developed in the thesis have good potential for a safer and more effective guidance system for off-pump beating heart mitral valve repair.

**Keywords:** Mitral valve repair, Minimally invasive, Off-pump, Beating heart, Image guidance, Real time, Dynamic image processing, Ultrasound, CT, Synthetic CT, Registration, Feature Tracking

# Acknowlegements

First and formost I would like to express my deepest gratitude to my supervisor, Dr. Terry M. Peters, who offered me this great opportunity to study in his lab in Robarts Research Institute. Over the years, he has been a continuous source of guidance and support with his enthusiasm in research, immense knowledge, and sparkling insights. The amazing environment Terry has created in his lab allows us to perform cutting edge research with a very collabrative manner, with access to tremendous equipments and resources. He has also provided me many opportunities of communicating and collabrating with people from different disciplines, including scientists, engineers, clinicians, and even businessmen from start-up company. Those marvellous experience has motivated me to think beyond my previous comfort zone and helped me to acquire new skills. In addition, Terry is very patient in helping me reviewing and editing my manuscripts, to which I am extremely grateful.

As all should know, this thesis would not have been possible without the contribution of many people who have helped me all the way along the journey. I want to express my sincere appreciation to my advisory committee members, Dr. Maria Drangova, Dr. James A. White, and Dr. Gerard Guiraudon, for their invaluable mentorship and advises. Special recoginitions shall be send to Dr. Chu, Dr. Kiaii, Dr. Bainbridge, and Dr. Guiraudon for their expertise, clinical insights, and collabrations, especially in the NeoNav project. I would also like to thank Dr. McCarty and Dr. Goela for providing the data for experiments and educating me about cardiology. The cardiac group in the lab, including Martin Rajchl, Pencilla Lang, and Maria Currie, has been a great source of creative and insightful discussions and I am very happy to be part of the group. Special thanks go to John Moore and Dr. Elvis Chen, for they have provided great help in designing experiments, analyzing data, and discussing the structure of my manuscripts and thesis. Thanks Chris Wedlake for the fundimental development of the Echelon platform, which is an essential for the mitral valve trakcing project.

Further I would like to give my gratitude to all my colleagures in Dr. Peters' VASST lab

and all the friends I have made at Robarts. Thank you all for making the study experience here such a great one. It has been a great pleasure to spend time around people who are creative and enthusiastic in science.

Finally, I want to thank my parents, Xiahong Zhu and Juming Li, and my wife, Zhuoxin Wu, who have always been very supportive over the years. Without you, I would never have the chance to get here and I am extremely grateful for all the things you have done for me.

# Contents

# List of Figures

# List of Tables

# List of Appendices

# List of Abbreviations, Symbols, and Nomenclature

| | |
|---|---|
| 2D | Two Dimensional |
| 3D | Three Dimensional |
| 4D | Four Dimensional (3D + time) |
| ARF | Acute Renal Failure |
| BH | Beating Heart |
| Cine MR | Cine Magnetic Resonance imaging |
| CPB | CardioPulmonary Bypass |
| CPU | Central Processing Unit |
| CT | Computed Tomography |
| CUDA | Compute Unified Device Architecture |
| DoF | Degree of Freedom |
| DSC | Dice Similarity Coefficient |
| DynCT | Dynamic CT |
| ECG | ElectroCardioGraphy |
| F3D | Fast Free Form Deformation |
| FOV | Field of View |
| FFD | Free Form Deformation |
| GPU | Graphics Processing Unit |
| GPGPU | General Purpose computation on Graphics Processing Unit |
| ICE | Intra-Cardiac Echocardiography |
| ICP | Iterative Closest Point |
| Intra-op | Intra-operative |
| LA | Left Atrium |
| LV | Left Ventricle |
| ME | Mid-Esophageal |
| MI | Minimally Invasive |
| MR | Mitral Regurgitation |
| MRI | Magnetic Resonance Imaging |
| MVA | Mitral Valve Annulus |
| MVR | Mitral Valve Repair |
| NCC | Normalized Cross Correlation |
| NMI | Normalized Mutual Information |
| Peri-op | Peri-operative |
| Pre-op | Pre-operative |
| RF | Regurgitant Fraction |
| ROI | Region of Interest |
| RMS | Root Mean Square |
| RMSE | Root Mean Sqaure Error |
| SAD | Sum of Absolute Differences |
| SIFT | Scale Invariant Feature Transform |
| SSD | Sum of Squared Differences |
| SynCT | Synthetic CT |
| TAVI | Transcatheter Aortic Valve Implantation |

| | |
|---|---|
| TAVR | Transcatheter Aortic Valve Replacement |
| TEE | TransEsophageal Echocardiogram |
| TRE | Target Registration Error |
| US | UltraSound |

# Chapter 1

# An Introduction to Guidance of Minimally Invasive Off-pump Beating Heart Mitral Valve Repair

Minimally invasive off-pump closed beating heart mitral valve repair is being developed to deliver the same quality of repair as conventional open-heart surgery. However, this approach precludes the direct vision of the surgical targets and tools, which must be substituted by an image-guidance system that displays all the critical features of the target for optimal visualization of lesions and tools for optimal repair. This chapter first introduces the clinical background of minimally invasive off-pump closed beating heart mitral valve repair, the requirements and challenges of the image guidance system for it, the limitations of the current imaging modalities. It then outlines the contributions made in this thesis to address these challenges by using ultrasound guidance augmented by mixed reality visualization techniques.

## 1.1 Mitral Valve Anatomy

The mitral valve (MV), also known as the bicuspid valve, is a complex structure, located between the left atrium (LA) and left ventricle (LV) of the heart, comprising several components working in synchrony. It is designed to ensure the oxygenized blood flows unidirectionally from the LA to the LV. Its components include the leaflets, annulus, chordae tendineae, and papillary muscles [1], and some literature considers the posterior left atrium wall and the left ventricle wall as part of the mitral valve as well [2].

***Leaflets:*** The mitral valve has two leaflets, anterior and posterior (see Figure 1.1). Each leaflet can be further divided into three regions, A1-A3 for the anterior and P1-P3 for the posterior leaflets respectively. The posterior leaflet is narrow and usually extends two-thirds of the annular circumference around the left atrioventricular junction, whereas the anterior leaflet occupies the remaining third. The basal-to-edge distance of the anterior leaflet can be two or more times than that of the posterior leaflet, which makes it more mobile, whereas the smaller posterior leaflet fulfills a secondary or supporting role in the valve closure [3]. Historically, the mitral leaflets had been viewed as passive connective structures, but some investigations have found an active function which is assigned to the striated muscle bundles that form part of the valve tissue [4]. However, it is still uncertain as to whether or not these muscle fibres play important roles in the valve closure.

***Annulus:*** Strictly speaking, the mitral annulus (MVA) is a non-existent structure, being the virtual space at the transition (or junction) of the endocardial layer of the LA, the valve tissue, and the endocardium and myocardium of the LV [5]. Generally, the MVA is described as having a saddle shape, although the detailed shape of the MVA is unique for each individual. The orifice area of the mitral valve at the annulus level is approximately 6.5 $cm^2$ and 8 $cm^2$, and the circumference of the annulus is about 9 cm and 10 cm for women and men respectively [6]. Because the annulus moves outwards with the posterior wall of the left ventricle and dilates to a certain extent during diastole, the shape of the annulus becomes more circular and the area of the orifice larger, the actual size of the annulus can vary between systole and diastole by as

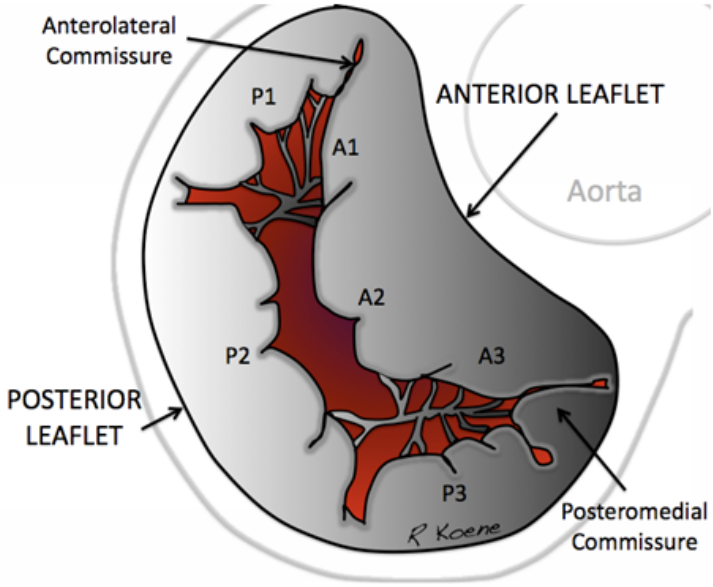


http://upload.wikimedia.org/wikipedia/en/4/44/Mitral_Valve_RK.png
Picture available under Creative Commons CC0 1.0 Universal Public Domain Dedication. No permission required for re-distribution.

Figure 1.1: Anatomy of the mitral valve leaflets

much as 30% [7].

***Chordae tendineae:*** Chordae tendineae are string-like structures that connect the mitral valve leaflets and the papillary muscles (see Figure 1.2). There are three types of chordae tendineae depending on where they attach. The marginal (primary) chords attach to the free edge of the rough zone of the leaflets preventing the eversion of the free edge into the LA during systole. The intermediate (secondary) chords attach to the body surface of the leaflets preventing the doming. The basal (tertiary) chords attach near to or in the annulus supporting the centre of the leaflets [1, 5].

***Papillary muscles:*** There are two papillary muscles located at the inner wall of the LV supporting the chordae tendineae. One of them is usually seen at the border of the anterolateral and inferolateral walls, whereas the other is usually positioned over the inferior wall of the LV. In most adults, each papillary muscle can have up to three heads [8]. The major function of these structures is to maintain proper tension to the mitral valve leaflets through the chordae tendineae, preventing the leaflets from prolapsing into the LA.

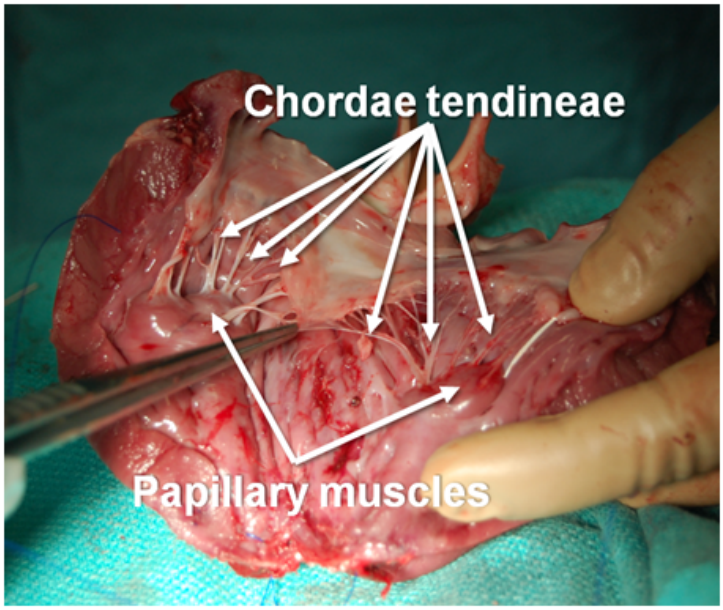


Figure 1.2: Anatomy of the chordae tendineae and the papillary muscles

## 1.2 Mitral Regurgitation

Mitral Regurgitation (MR) is a very common heart disorder in which the mitral valve cannot close properly during systole resulting in blood flowing back from the LV to the LA, referred as the regurgitation (see Figure 1.3). The prevalence of MR is approximately 2-3% of the population in North America in 2001 with no gender predominance [9]. This disorder decreases the efficiency of the LV pumping oxygenized blood through the aorta to the entire body, which can lead to symptoms as shortness of breath, pulmonary edema, orthopnea, and decreased exercise tolerance [10].

The severity of the mitral regurgitation is measured by the regurgitant fraction, which is defined as

$$RegurgitantFraction = \frac{(V_{mitral} - V_{aortic})}{V_{mitral}} \tag{1.1}$$

where $V_{mitral}$ is the volume of blood flowed through the mitral valve during diastole and $V_{aortic}$ is the volume of blood flowed through the aortic valve during systole. The degree of severity is determined to be mild with RF less than 20% and severe with RF more than 60%.

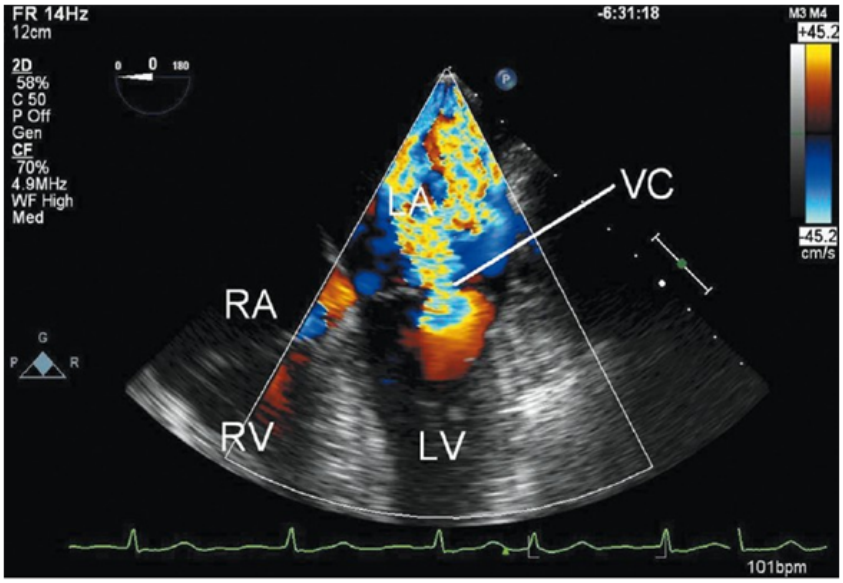


http://www.annals.in/viewimage.asp?img=AnnCardAnaesth_2012_15_2_144_95080_f16.jpg



Figure 1.3: A transesophageal echocardiogram image with mid-esophageal 4-chamber view showing mitral regurgitation with Doppler color flow

There are many different causes and mechanisms for MR. Generally, the causes of MR can be divided into non-ischemic and ischemic, i.e. related to coronary artery diseases, and the mechanisms can be divided into functional and degenerative (organic) [11]. In functional MR cases, the valve itself remains structurally normal and the MR results from failure of coaptation of the mitral valve leaflets, caused by abnormalities in segmental LV wall motion, annular and/or LV dilation, or papillary muscle displacement and/or dysfunction. On the other hand, degenerative MR is associated with structural abnormalities of the leaflets or the subvalvular apparatus, such as the chordae tendineae.

***Degenerative MR*** is most commonly associated with mitral valve prolapse (prolapse of one or both of the mitral leaflets into the LA). The diagnosis of mitral valve prolapse was once highly prevalent, as much as 35% among teenage girls [12], due to incorrect assumption that the shape of the mitral valve is planar. This over-diagnosis was then corrected after the important work in echocardiography that refined the normal mitral anatomy [13–15]. Currently, the more precise definition of mitral valve prolapse is that one or both of the leaflets prolapse at least

2mm beyond the long-axis annular plane, with or without leaflet thickening. According to this definition, the prevalence of prolapse in 2005 is about 2-3% equality distributed among men and women [16].

***Functional MR*** can occur without any abnormalities in the valve itself. It usually results from a primary ventricular pathology that leads to ventricular remodeling and/or dysfunction [17]. There are two major ways whereby ventricular dilation can cause functional MR. First a dilated ventricle leads to papillary muscle displacement, which means the distances between the papillary muscles and the proper valve closure position, i.e. tethering distances, are enlarged. Since the chordae tendineae are not extensible, which constrains the movement of the leaflets, the displaced papillary muscles tend to prevent the leaflets from closing properly. Second, a dilated ventricle may lead to the dilation of the mitral annulus as well. As the size of the leaflets is not changed, a dilated annulus can naturally lead to insufficient coaptation. However, some recent studies have shown that ventricular dilation does not necessarily lead to functional MR, because in some patients who have LV dilation, the mitral valve leaflets can be enlarged spontaneously by as much as 31%, as compensation to the LV dilation, to provide sufficient coaptation [18, 19]. The question why the mitral leaflets enlarge in some patient with LV dilation but does not enlarge in others so far remains unanswered.

## 1.3 Surgical Treatments for Mitral Regurgitation

Although pharmacological treatments are available to alleviate the symptoms and, in some cases, to reduce the severity of regurgitation, they do not actually prevent or correct the physical damage to the heart caused by MR. Mitral valve surgery is the only treatment for MR that provides sustained relief of symptoms and prevents the development of heart failure [20]. Studies have shown that early surgical treatment should be recommended for patients with severe MR, even when they have no or minimal symptoms because of the low operative risk and low postoperative mortality, especially when mitral valve repair is feasible [21]. The two main

surgical options for MR are mitral valve repair and mitral valve replacement.

### 1.3.1 Mitral Valve Repair

Mitral valve repair (MVR) includes a set of valvular, subvalvular, and annular procedures that aim to restore normal leaflet coaptation, i.e. normal valvular function. The choice between repair and replacement is based on many factors including patients general health, the condition of the valve, and expected benefits of the surgery. However, in the recent years a trend has been formed among surgeons to favor repair to replacement in most cases when the former is feasible, due to lower mortality and morbidity rate and the development of related techniques [22–24].

#### Surgical repair for degenerative MR

Most causes for degenerative MR are chordae-related, such as ruptured and elongated chordae, among which the posterior chordal rupture is probably the most common with a prevalence twice that of elongated chordae, and more times than that of anterior chordal rupture [25]. One typical and traditional technique to repair prolapsed posterior leaflet is achieved by resection of the prolapsed segment, sometimes along with the damaged chordae, in conjunction with posterior annulus placation sutures. However, removing part of the leaflet can decrease the overall valve leaflets area when the size of the annulus remains the same, which may lead to leakage. Consequently, mitral annuloplasty may also need to be performed after the resection to reduce the size of the annulus. One approach that is gaining in popularity is to repair the stretched or ruptured chordae by implanting artificial chordae without resecting the prolapsed leaflets. The repair of the prolapsed anterior leaflets is more challenging than that for posterior leaflets. The reconstructive techniques include chordal replacement, shortening, or transposition, folding plasty, and triangular resection [26]. Another technique that does not directly deal with the chordae is to create a double orifice valve by suturing or clipping part of the edges of both leaflets together, which can also enforce the correct coaptation of the leaflets [27].

**Surgical repair for functional MR**

In functional MR, the repair is mainly achieved by remodeling the distorted mitral annulus aiming to reduce its size (diameter), i.e. annuloplasty. The conventional means of performing mitral valve annuloplasty is to attach a ring to the annulus, which reshapes the annulus to the shape of the ring. In the past, the ring was designed with a flat or curved outline. However, new insight into the 3D dynamic behavior of the mitral valve has promoted a redesign of the ring to be saddle-shaped, which is closer to the natural shape of the annulus [28, 29]. Some modern techniques have also been developed to perform percutaneous mitral annuloplasty, which can be delivered through a minimally invasive procedure [30, 31].

### 1.3.2 Mitral Valve Replacement

Mitral valve replacement, as its name implies, involves the implantation of a biological or mechanical prosthesis as a replacement of the original valve. Biological valves are usually made from animal tissue or, in some cases, from tissue from the patients themselves. Such valves are associated with lower risk of thromboembolic disorders, but they may only last for 10-15 years [32]. Mechanical valves are usually made from metal or pyrolytic carbon and last longer than biological valves, but patients with mechanical valves may have to take blood-thinning medications regularly to prevent clotting. The choice of valve types to implant depends on the patient's age, general health conditions, preferences with medication, and life expectations.

## 1.4 Approaches to Deliver the Surgical Therapy

With a history of about 60 years, cardiac surgery is considered to be a very young discipline in medicine. Although it has been a long time since human beings tried to pursue knowledge about the heart, it was not until early 20th century that cardiac surgery was attempted. For example, Dr. Werner Forssmann first documented right heart catheterization in humans with

radiographic techniques in 1929 [33] and Dr. Robert E. Gross performed closure of patent ductus arteriosus in 1939, which is considered to be the first surgical correction of a congenital heart defect [34]. There are many difficulties that have to be resolved before it is possible to perform operations on the heart, among which one of the most important is to maintain sufficient blood circulation for the patient to survive during the surgery. Dr John H. Gibbon, Jr. attempted to resolve this difficulty by introducing a heart lung machine (see Figure 1.4), also referred as cardiopulmonary bypass (CPB), which was designed to maintain extracorporeal circulation during the surgery. Dr. Gibbon performed the first successful open-heart operation with the use this device in Philadelphia on May 6th, 1953, which brought modern open heart surgery to its infancy [35].

However, it is noteworthy that much of the surgical trauma in open heart surgery is not a result of action on the surgical target itself, but rather occurs during the process of gaining access to it. Dr. Gerard Guiraudon has divided a surgical procedure into three components [36]: ***the target***, - the pathological tissue/organ to be treated; ***the bullet***, - the therapeutic agent that defines the actual therapy to be performed on the target; and ***the gun***, - the surgical procedure that delivers the therapy to the target, but does not affect the target directly. This description characterizes most surgical procedures as the means of delivering therapy, and this leads to the idea that it is the delivery procedures that causes most of the morbidity or even mortality in surgery. This concept promoted the development of minimally invasive surgery, which aims to deliver equivalent or similar therapy to that of open heart surgery through minimized incisions; and off-pump beating heart surgery, which aims to operate on the beating heart without the use of the heart lung machine. The next subsections discuss these different approaches to deliver the surgical therapy.

### 1.4.1 Open Heart Surgery

Conventional open heart surgery usually starts with a procedure called a “sternotomy”, in which a 15-to-25 cm vertical incision is made along the sternum (or breastbone) after which



Figure 1.4: 1955 heart-lung machine

the sternum itself is split. The purpose of this procedure is to provide visual and surgical access to the heart. The heart lung machine is attached to the patients cardiovascular system, and the heart is arrested. Via the Heart-Lung machine, blood is drained from the heart, oxygenized by the machine, and pumped back to the patients body temporarily taking over the function of the heart during surgery.

Open heart surgery with heart lung machine is a great innovation, because it has made many complicated operations on the heart possible to be performed. Nowadays, open heart surgery is routinely performed in many clinical centres worldwide and studies have suggested that elderly patients with comorbidities and advanced cardiovascular disease benefit more from cardiac surgery than from medical therapy alone [37]. However, this technique is associated with a large amount of many side-effects, such as chest pain, risk of stroke, renal dysfunction, and cognitive complications. Some of the side effects are discussed below.

***Chest Pain:*** One of the most salient side effects is the pain associated with the long incision along the chest caused by the media sternotomy [38]. Since the breastbone is broken during the surgery, the patient has to suffer from great pain in the chest for about six weeks after the surgery. Even normal breathing becomes difficult and painful during that period.

***Infection & Inflammation:*** Postoperative infection is one of the major factors that increases the risk of postoperative mortality. This may come from the surgical incisions as with any other surgical procedure, as well as from the use of cardiopulmonary bypass [39]. The overall incidence of infections after open heart surgery is around 3% [40], while this number can be higher (9%) in developing countries [41]. It has been reported that the frequency of infection for patients with postoperative acute renal failure ranged from 23.7% to 58.5% depending on whether or not they required dialysis [42].

***Arrhythmia & Atrial fibrillation:*** Arrhythmia is very common after open heart surgery, especially associated with the use of heart lung machines, with the reported incidence of postoperative arrhythmia after open heart surgery being over 70%, while the incidence of severe arrhythmia can still be over 40% [43, 44]. Atrial fibrillation, the most common arrhythmia occurring postoperatively with incidence rate around 30% [45], increases the risk of stroke and mortality [46] and also leads to longer hospital stay and increased health-care costs.

***Renal Dysfunction:*** Acute renal insufficiency or renal failure (ARF) is another major complication associated with open heart procedures. The incidence of patients having ARF that requires dialysis, ranges from 1% to 4% in different studies [47–49]. The more important fact is that the mortality rate of patients with ARF is significantly greater (in excess 60%) [50] than those with no ARF, while the general mortality after open heart surgery is 2-8% [51–53].

***Central Nervous System Complications:*** Neurological complications can be categorized into two groups. Type I complications include fatal or non-fatal stroke, stupor, or coma at discharge, whereas type II complications include chronic syndromes of cognitive decline, such as inattention, amnesia, aphasia, and apraxia [54]. Stroke is one of the most fatal complications after open heart surgery. The general frequency of this complication varies from 1.6% to 5.6%

in different studies [55–57], and rate is much higher in patients over 75 years of age (almost 9%) and patients undergoing valve surgery (~16%) [58]. The incidence of peri-operative overt stroke has declined progressively since the invention of open heart surgery thanks to improvements in technology. However, the cognitive complication has remained with high incidence and in some respects has become the most important side-effect [54, 59]. Newman et al. [60] reported a cognitive decline in 53% of patients at discharge, 36% at 6 weeks, 24% at 6 months, and 42% at 5 years with a significant decline defined as 20% reduction from baseline. Cognitive complication can greatly affect the patients' post-operative quality of life, although it may not lead to mortality.

### 1.4.2 Minimally Invasive Heart Surgery

Minimally invasive (MI) cardiac surgery, as its name implies, aims to minimize the incisions applied on patients for the access to the surgical targets. In other words, it attempts to replace the median sternotomy with small incision(s). Many incision techniques have been developed to replace conventional median sternotomy, including right mini-sternotomy, which is probably the most common incision type for now [61–63], J-sternotomy [64, 65], left thoracotomy [66, 67], right infra-axillary thoracotomy [68], trans-sternal approach [69], inverted T-sternotomy [70], and V-incision [71].

Mitral valve surgery has been one of the areas of cardiac surgery that is most widely influenced by MI approaches. The first MI valve surgery was performed by Cosgrove in 1996 [72], while in the same year Carpentier performed the first video assisted mitral valve repair with minithoracotomy [73]. In 1998, Carpentier advanced his work by performing the first completely robotic mitral valve repair using the surgical robotic, Da Vinci (Intuitive Surgical Inc., CA, USA) [74]. Since then, the development of alternative methodologies and technologies in terms of new incision approaches, new surgical tools, new CPB techniques, especially cannulation techniques, and new image guidance approaches, have been promoted and developed with a rapid pace.

Although some studies have shown that there is no difference in mortality between MI surgery and open heart surgery [75–78], MI approaches have many advantages including decreased length of stay in hospital, decreased surgical trauma, reduced pain, improved patient satisfaction, and potentially reduced hospital resource utilization.

### 1.4.3 Off-pump Beating Heart Surgery

When MI heart surgery was first introduced, it did not eliminate the use of the heart lung machine. On the contrary, some studies showed that MI approaches may lead to increased operating time, and consequently increased CPB time [79], which can raise the incidence of some CPB-related side effects [80]. This problem can be resolved by performing MI off-pump procedures, in which the patients heart keeps on beating and the blood flows through the heart as normal.

Although it is interesting to note that there are actually on-pump beating heart surgeries, in which the heart is perfused normally through the aortic root [81–83] and off-pump beating heart (BH) surgery with full sternotomy [84], minimally invasive off-pump beating heart (BH) surgery has gained more interest and popularity. Many studies have shown evidence that compared to on-pump procedures, off-pump procedures lead to lower risks and morbidity [85–87] and lower cost [88]. The next section describes some commercially available MI off-pump BH mitral valve repair techniques.

### 1.4.4 Existing Techniques for MI Off-pump BH Mitral Valve Repair

#### Transapical Artificial Chordae Implantation

NeoChord©DS1000 (NeoChord Inc., MN, USA) is a device designed to perform off-pump beating heart mitral valve repair for degenerative MR, especially mitral valve prolapse [23, 89]. The therapy it delivers is to implant artificial chordae tendineae to a ruptured leaflet. The device is introduced into the left ventricle through a 2 to 3 inch incision between the ribs and a hole at

the apex of the heart (see Figure 1.5). A jaw close to the tip of the device can be opened and used to grasp the leaflets. A needle can go through a channel built inside the device and apply a suture on the leaflet. After the suture is applied, the device comes out of the heart and the other end of the suture is tied at the apex. This procedure may need to be repeated several times to apply multiple sutures to the leaflets. The sutures then limit the movement of the leaflets and prevent them from prolapsing into the left atrium at systole.


Figure 1.5: An illustration of NeoChord DS1000 device and the related transapical procedure for artificial chordae implantation

One of the difficulties in conventional chordae implantation procedures is the determination of the length of the implanted chordae. This difficulty is resolved in the NeoChord procedure, because it allows the surgeons to adjust the length of the implanted chordae and assess the result by intra-operative Doppler echocardiogram, before they tighten the chordae and secure it at the apex.

**Percutaneous Edge-to-Edge Leaflets Clipping**

MitraClip©(Abbott Laboratories, IL, USA) is a percutaneous mitral valve repair system designed to perform edge-to-edge leaflets clipping that creates a double orifice valve. This device and its related procedure is currently under a randomized controlled clinical trial coded as

EVEREST (endovascular valve edge-to-edge repair study trial) [90, 91]. The system consists of implant catheters and the MitraClip clip device with the clip device attached to the tip of a catheter. The procedure starts with inserting the catheter through the femoral vein to the left atrium. The clip is then carefully positioned to grasp both mitral valve leaflets and to clip the two leaflets together. By doing this, a double orifice valve is created to allow greater valve closure and less regurgitation. This procedure has the potential of treating both degenerative and functional MR.

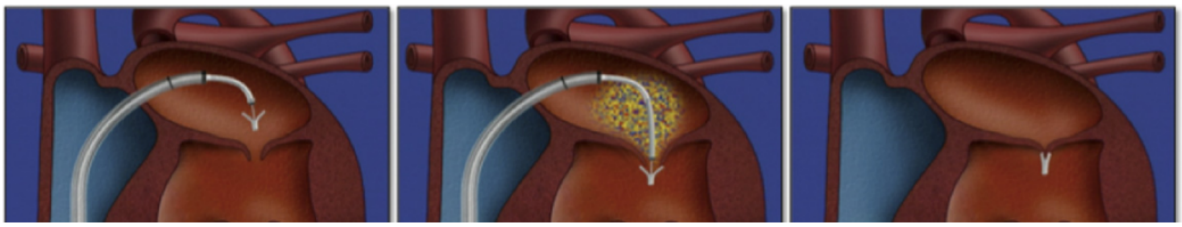


Figure 1.6: An illustration of MitraClip device and its related procedure

The advantage of this technique is that the interventionist can release the clip and re-grasp the leaflets multiple times before the clip is detached from the catheter, so that they can assess the result through Doppler echocardiography and adjust the grasping position accordingly. When the expected result is achieved, the clip is detached from the catheter and left in the heart attached to the valve leaflets, and the catheter removed. This approach can treat mitral valve prolapse without directly dealing with the chordae tendinae. However, some criticism has suggested this is using mitral stenosis to treat MR.

**Percutaneous Direct Mitral Annuloplasty**

Mitralign©(Mitralign Inc. MA, USA) is a percutaneous annuloplasty device that is designed to perform mitral annuloplasty with a minimally invasive manner on a beating heart [92]. It begins by introducing a guide catheter through the aortic valve and positioning it on the posterior side of the left ventricle. Wires are then introduced through the catheter and placed in the mitral annulus with a predefined distance in between. Pledgets are delivered over the wires

(one plegdget over each wire) and attached to the annulus. After the deployment, the pledgets are pulled together and locked in place, which folds part of the annulus and reduces its circumference.

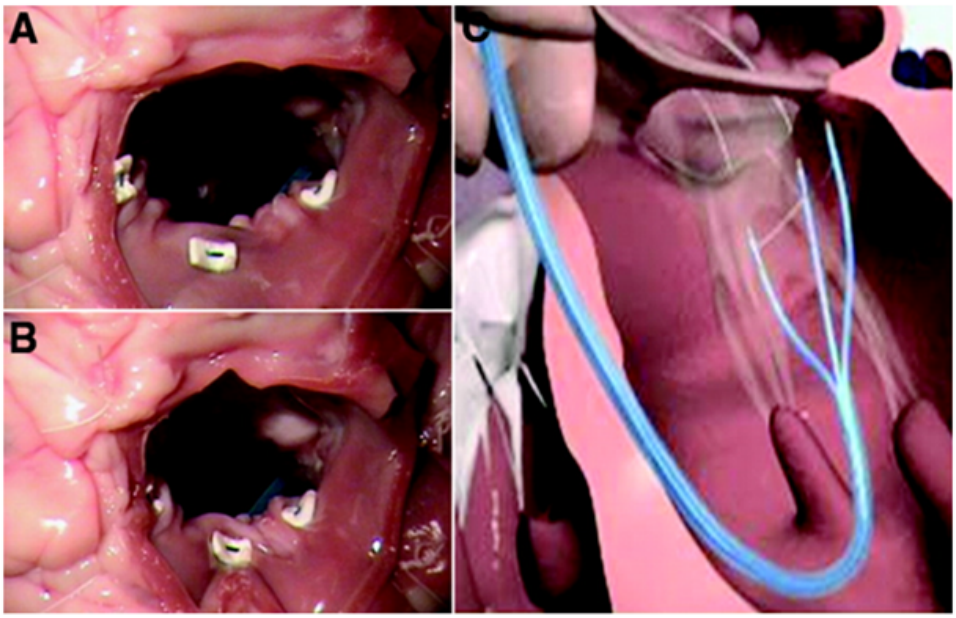


http://circinterventions.ahajournals.org/content/2/2/140/F6.expansion.html
Adapted from J. Masson, MD and J.G. Webb, MD, "Percutaneous Treatment of Mitral Regurgitation"

Figure 1.7: An illustration of Mitralign and its related procedure

This approach does not involve the attachment of an artificial ring that remodels the shape of the annulus. The feasibility of this approach is suggested by some literature [93, 94] that shows suture plication of the posterior portion of the annulus can offer benefit even without a ring.

**Percutaneous Indirect Mitral Annuloplasty**

The MONARC©device (Edwards Lifesciences, Irvine, CA, USA) is designed to perform mitral annuloplasty by implanting a curved device within the coronary sinus to reduce the size of mitral annulus [95, 96]. The MONARC system consists of a nickel-titanium alloy implant and the delivering catheters. The implant itself comprises a spring-like "bridge" and two self-expanding anchors at both ends of the bridge. The compressed implant can be introduced

from the jugular vein through the guide catheter and positioned within the coronary sinus. The sheath is then removed to allow the anchor to expand, providing fixation.

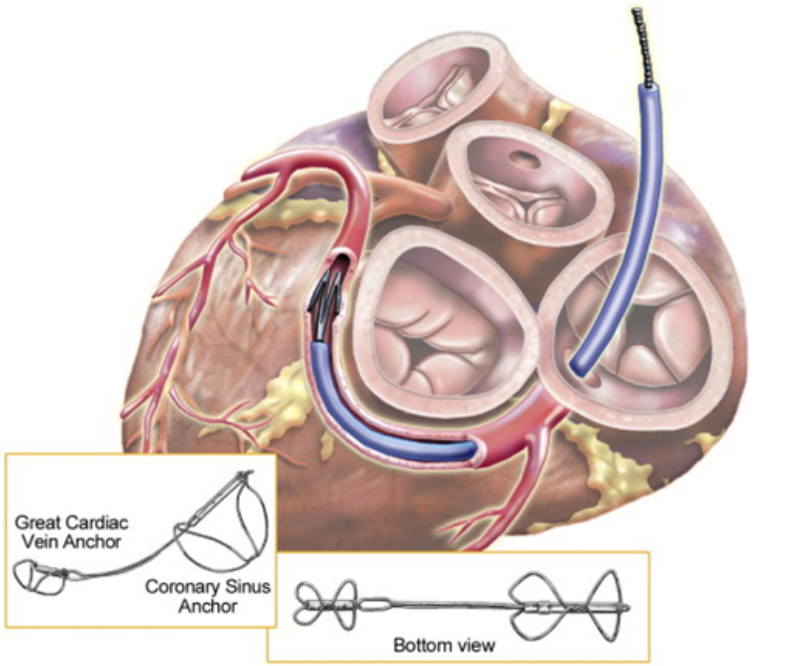


Figure 1.8: An illustration of MONARC device and its related procedure

This approach has raised many concerns. For example, it has been noted that the coronary sinus and great cardiac vein typically lie on the atrial side of the mitral annulus rather than immediately in the mitral annulus plane. The anatomic relationship between the sinus and the mitral annulus is highly variable. These concerns were confirmed in many studies [97–99]. In addition, clinical experience has shown that coronary artery compression, ischemia and infarction may occur after this type of procedure [100].

## 1.5 Image Guidance: An Essential Assistance for MI Off-pump BH Surgery

Lack of direct visual access to either the surgical targets or tools is an intrinsic limitation of MI procedures and off-pump beating heart intracardiac procedures have one more limitation due to the flowing blood in the heart chambers that makes normal endoscopic camera impractical for such procedures. To enable such procedures, some sort of assistance must be provided, so that the surgeons can know what they are operating on. Image guidance provides such assistance by providing a model of the surgical environment complemented by intra-operative real-time information from a variety of imaging sources and tool tracking systems [101].

The most important event that led to the start of the "image-guided procedure" is probably the discovery of X-ray by Roentgen on November 8th 1895 [102, 103]. A few months after that, Cox [104] successfully removed a bullet from the leg of a victim based on the radiograph of the limb at McGill University in Montreal, which was a very rapid translation from a scientific discovery to clinical practice. In the past few decades, image guidance has gained more and more interest thanks to the tremendous advancement in imaging techniques and modern computers. Today image guidance has been wildly adopted and become a state-of-art component in most of the MI cardiac procedures.

## 1.6 Challenges for Image Guidance

### 1.6.1 Requirements of Image Guidance for MI BH Surgery

General requirements of image guidance for MI surgery include the capabilities of visualizing the surgical targets, the surrounding anatomical context, and the status of the tools in real time. For the BH surgery, the visualization of the cardiac motion is also necessary. Specific requirements in terms of image quality vary among different procedures and/or even different stages in one procedure. Those requirements are discussed below.

***Temporal resolution:*** Temporal resolution defines the precision of the measurements with respect to time, which is a key concern for imaging a beating heart. Using the NeoChord and MitraClip procedures as examples, those two approaches require very high temporal resolution for the surgeon to grasp the leaflet(s) with the tools due to the fast motion of the leaflets [105, 106]. This explains why the surgeons prefer to use 2D echocardiography, which can provide very high temporal resolution (>30 Hz), as the imaging modality for leaflets grasping. On the other hand, guiding a catheter through the femoral vein has a much lower requirement for temporal resolution.

***Spatial resolution:*** Spatial resolution, often confused with pixel size, is measured by how close two lines can be placed to each other and still be resolved in an imaging system. Small pixel size does not necessarily lead to good spatial resolution. Better spatial resolution usually leads to more detailed images. For example, in the indirect annuloplasty procedures, identifying the ostium of the coronary sinus requires the spatial resolution to be better than 5mm [107], which is not difficult to achieve for modern imaging techniques.

***Field of view (FOV):*** FOV is the region of the observable space that an imaging system can provide at a given moment. Figure 1.9 shows an example of two transesophageal echocardiogram (TEE) images both with mid-esophageal (ME) 4-chamber view. The left image has a larger FOV in which the complete left ventricle is contained, whereas the right image has a smaller FOV which focuses on the mitral valve. The requirement for FOV may also change during a procedure. For example, in the NeoChord procedure, a relatively large FOV showing the entire left ventricle is required for guiding the tool moving from the apex to the mitral valve area. When the tool tip is close to the leaflets, a smaller but more detailed view may be required to show the position and motion of the leaflets. The image guidance system should be able to adjust the view according to the procedure's requirements to provide most informative and intuitive visualization to the surgeons. However, trade-offs must often be made among FOV, spatial resolution, and temporal resolution.

***Soft tissue contrast:*** Most medical images use grayscale to represent image intensity, so

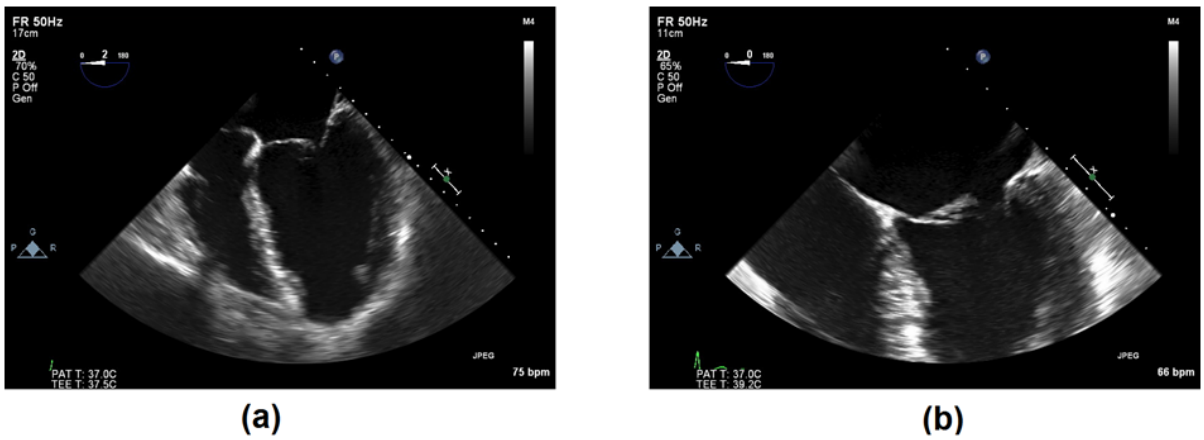


(a) (b)

Figure 1.9: An example of two TEE images with the same view but different FOV

the soft tissue contrast is basically the difference in intensity that makes a one soft tissue distinguishable from another. Figure 1.10 shows the comparison between a cardiac TEE image and an X-ray fluoroscopy image. The TEE image shows excellent contrast between the intracardiac structures, whereas the fluoroscopy image can barely show any of them. A basic requirement for image contrast is that the target and the tools must be recognizable in the image. In the mitral valve repair procedure, echocardiography is a good choice, because it provides excellent contrast between the mitral valve leaflets and the blood. In some situations a contrast agent can be applied to improve the contrast of a certain tissues, typically the blood (angiography) in BH surgery.

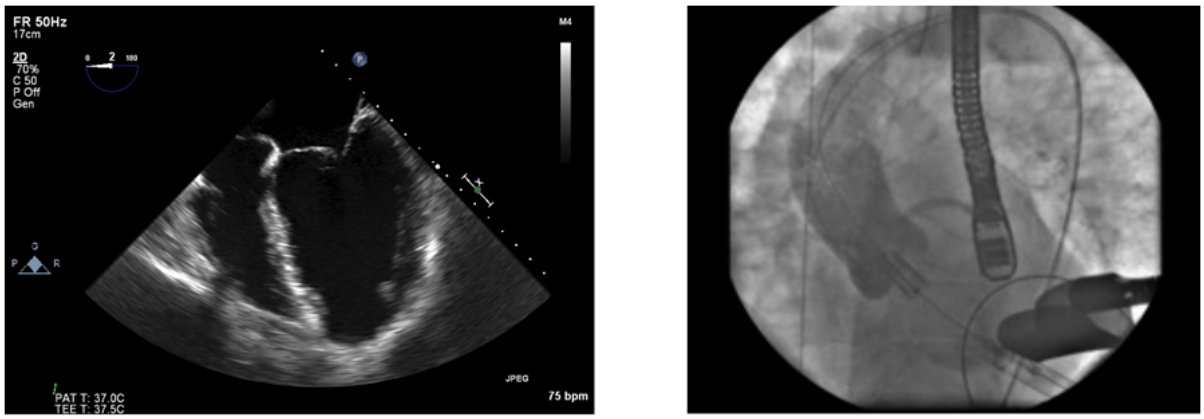


(a) (b)

Figure 1.10: A TEE image and a fluoroscopy image showing different soft tissue contrast

Some other requirements that are not related to image quality include incorporating pre-operative images and surgical plans to intra-operative environment, radiation dose management and economic cost.

***Incorporating pre-operative images and surgical plans:*** Pre-operative images usually have better image quality, in terms of larger FOV, higher resolution, better signal-to-noise ratio, and better soft tissue contrast, than intra-operative images and surgical plans are usually made based on pre-operative images. These attributes motivate the idea of incorporating pre-operative images, together with the surgical plan, into the intra-operative environment. This is usually achieved through image registration techniques (detailed discussion in section 1.9).

***Radiation dose:*** Any X-ray based imaging modalities, such as CT and fluoroscopy, are associated with ionizing radiation dose, which can be harmful to those exposed to it, both patients and the clinicians. Since good image contrast, high resolution, and long scanning times can all lead to high radiation dose, a compromise must be made regarding factors to ensure sufficiently high image quality while minimizing radiation dose.

***Economic cost:*** The economic cost of the guidance system is not directly related to its effectiveness. However, it affects the affordability and consequently the availability of the guidance system. In countries where the patient is responsible for a large portion of or even the entire cost of the medical procedure, economic cost can also have the impact on who can or cannot receive a certain type of medical treatment. For example, although interventional MRI is capable of providing real time cardiac images with excellent image quality, its popularity has been greatly limited by its extremely high cost and general lack of availability in interventional cardiac suites.

### 1.6.2 Limitations of the Current Imaging Modalities

Common imaging modalities used for guidance of cardiac surgery include X-ray fluoroscopy, 2D/Bi-plane/3D ultrasound, CT, interventional MRI, and endoscopy. Although these modalities have been used as standard practice for the guidance of cardiac interventional procedures

for many years, there are limitations of each, which renders them unable to fully resolve the challenges in guiding minimally invasive and off-pump beating heart procedures.

***X-ray fluoroscopy:*** X-ray fluoroscopy has been the standard imaging modality for many percutaneous intracardiac procedures for some time [108], and is still widely used in many clinical centres. It provides real time intra-operatively projection images that can provide good visualization of the surgical tools and catheters. However, the soft tissue contrast in those images is relatively low and intracardiac structures can barely be recognized (see Figure 1.10b). In addition, radiation dose is also a serious concern, especially for long exposure. Many studies have been performed for radiation dose management to reduce or control its negative effects [109], but it still remains a serious concern, particularly for long procedures. The use of x-ray contrast agents can also lead to renal damage.

***Ultrasound:*** Transesophageal echocardiography (TEE), both 2D and 3D, has become popular for both diagnostic and interventional cardiac procedures. The high temporal resolution of TEE, especially for 2D imaging, makes it perfect for analyzing the cardiac motion, especially the motion of the valve leaflets, which is too rapid for most of the other imaging modalities to capture. Also, ultrasound has no ionizing radiation dose, which makes it safe for extended imaging. The limitation of 2D TEE, either single plane or bi-plane, is that it is difficult to maintain both the surgical target and tools in the imaging plane, which is important for navigating the tool to reach the target [110, 111]. 3D TEE can overcome this limitation to some extent, but at the cost of decreased temporal and spatial resolution in a restricted field of view (FOV). Another limitation of 3D TEE is that it can only be performed for a few minutes before it has to be switched back to 2D due to the heat generated by the transducer. Further, the signal-to-noise ratio of 3D TEE is rather low.

***Interventional MRI:*** Other than the high economic cost, interventional MRI has some other technical limitations as well. First, as an MRI, it requires specifically designed non-ferromagnetic tools to be used within the operation area. It also needs to deal with radiofrequency heating at the tips of guide wires, catheters, and other wire-shaped devices [112]. In

addition, the space for the surgeons to perform operations is highly restricted.

### 1.6.3 Multi-stage or Single-stage? No One-size-fits-all

The idea of using one imaging modality or one constant setting for the guidance of the entire procedure is not appropriate for the increased demand of guidance accuracy and effectiveness. Image guidance should be considered as a multi-stage task. Some studies have suggested that for better guidance quality, a surgical procedure needs to be broken down into smaller steps, that for each such step the most suitable guidance solution should be determined [113] and that each solution could consist of multiple modalities or the use of mixed reality [114].

A general way of breaking down a guidance procedure is to divide it into two major components: navigation and positioning. Navigation refers to the operation of guiding the tool from an entry point to an area very close to the target, whereas positioning deals with delivery of the therapy to the target with required accuracy and precision. For example, in the NeoChord procedure, navigation involves guiding the tool tip from the apex of the heart to the centre of mitral annulus, while positioning implies deploying the artificial chordae on the leaflet at the correct positions.

The guidance requirements for navigation and positioning can be very different. In a perfect scenario, the only change within the surgical environment after the navigation stage should be the position of the tool. This concept suggests that navigation is about getting the tool to the destination with minimized negative impacts to the other aspects of the operation, such as causing danger to the surrounding tissues, extending operation time, or increasing surgeons' mental/physical workflow. On the other hand, the details of the target are not the most important concern in the navigation stage. For example, when a surgeon introduces a catheter through the aorta in a transcatheter aortic valve implantation (TAVI) procedure, the position of the catheter tip is more important than the appearance or movement of the aortic valve leaflets.

However, in the positioning stage visualization of the details of the target becomes one of the most important factors for deploying the therapy at the planned position. The final

deployment position of the therapy can very often be the key reason for operation success or failure. For example, when placing a MitraClip device, the cardiologist must find the position that leads to minimal, if not zero, mitral regurgitation, while making sure the clipped tissues are sufficiently strong to hold the device. Applying multiple sutures in the NeoChord procedure requires them to be placed with uniform intervals on the leaflets. Placing a stent in a TAVI procedure has to make sure the stent does not block the ostia feeding the coronary arteries. The major task of image guidance in the positioning stage is to help the surgeon to deliver the therapy accurately at the planned position with confidence. Two facts make a positioning task very different from a navigation task. First, after successful navigation, the tool is already very close to the final target and the movement of the tool must be constrained to be within a smaller region. Second, the requirement of guidance accuracy and image resolution (both spatial and temporal) may become higher than that during the navigation task. Because of these two differences, the image guidance for the positioning stage does not need to provide a very large FOV, but it requires more details of the target.

If we use driving a car to a shopping mall as an example, a navigation task is similar to driving the car from the start point to the parking lot of the mall using a GPS, while the positioning task is similar parking the car into a certain lot with the help of a back-up camera. A navigation task focuses on where the destination is and what the route leading the car from the start point to the destination is. On the other hand, a positioning task focuses on the details of the surroundings to ensure the final deployment is at the correct position. Using a navigation tool, e.g. GPS, for a positioning task, e.g. parking, can lead to very inaccurate results, while using a positioning tool, e.g. a back camera, for a navigation task, e.g. long distance drive, could easily get lost, because it focus primarily on the surrounding details without providing any useful information about the location of the destination. Different tools are required for guiding the two tasks, and using the wrong tool for the task may end in failure.

This same concept also applies to image guided procedures. A surgical operation is a very complicated task that requires many specific tools for each specific step in the procedure

and so should the guidance. The idea of viewing image guidance as a multi-stage task is not completely new, and some procedures have already adapted this idea in their workflow. The MitraClip procedure for example, uses fluoroscopy, 2D TEE, and 3D TEE for guidance at different stages. Actually, Altiok et al. [113] divided the MitraClip procedure into eleven tasks (not including guiding the catheter with fluoroscopy) in their study and compared the guidance with 2D and 3D TEE to decide the optimal modality for each task. NeoChord applies the same idea in their current guidance solution. 3D TEE is used to verify the position of the tool tip before it is moved through the mitral valve area, while 2D TEE is used for grasping the leaflets. In summary, image guidance system should not be considered as a single tool that can hopefully solve all the problems, but a toolbox that can provide the optimal tools for every specific task according to its requirements.

## 1.7 Solution to the Challenges: Mixed-reality

As discussed above, no single intra-operative imaging modality can fulfill all the requirements and resolve all the challenges for the guidance of minimally invasive off-pump beating heart interventions. A solution to this problem that has been widely adopted by researchers and clinicians is to introduce mixed-reality to the guidance systems [114]. According to Milgram et al. [115] who first defined this concept, mixed-reality covers a whole spectrum from pure real environment to pure virtual environment, e.g. computer simulations. A mixed-reality based guidance system attempts to consolidate all the useful information from pre-operative (pre-op) images, intra-operative (intra-op) images, anatomical models or atlases, surgical plans, tool tracking systems, and video cameras into a unified platform and visualize them in a way that can be easily interpreted and understood by the surgeon. It aims to provide more important information than any single imaging modality can achieve, ease the navigation task, and eventually improve the procedural safety, efficiency, and even outcomes. Many studies have demonstrated the feasibility and benefits of using mixed-reality platform for the guidance of

MI off-pump BH interventions [101, 110, 111, 116–123].

## 1.8 Principal Components in a Mixed-reality Guidance System

A mixed-reality based guidance system usually consists of the following major components: pre-operative images or models, intra-operative images, tool tracking system, image processing programs, and visualization programs (see Figure 1.11).

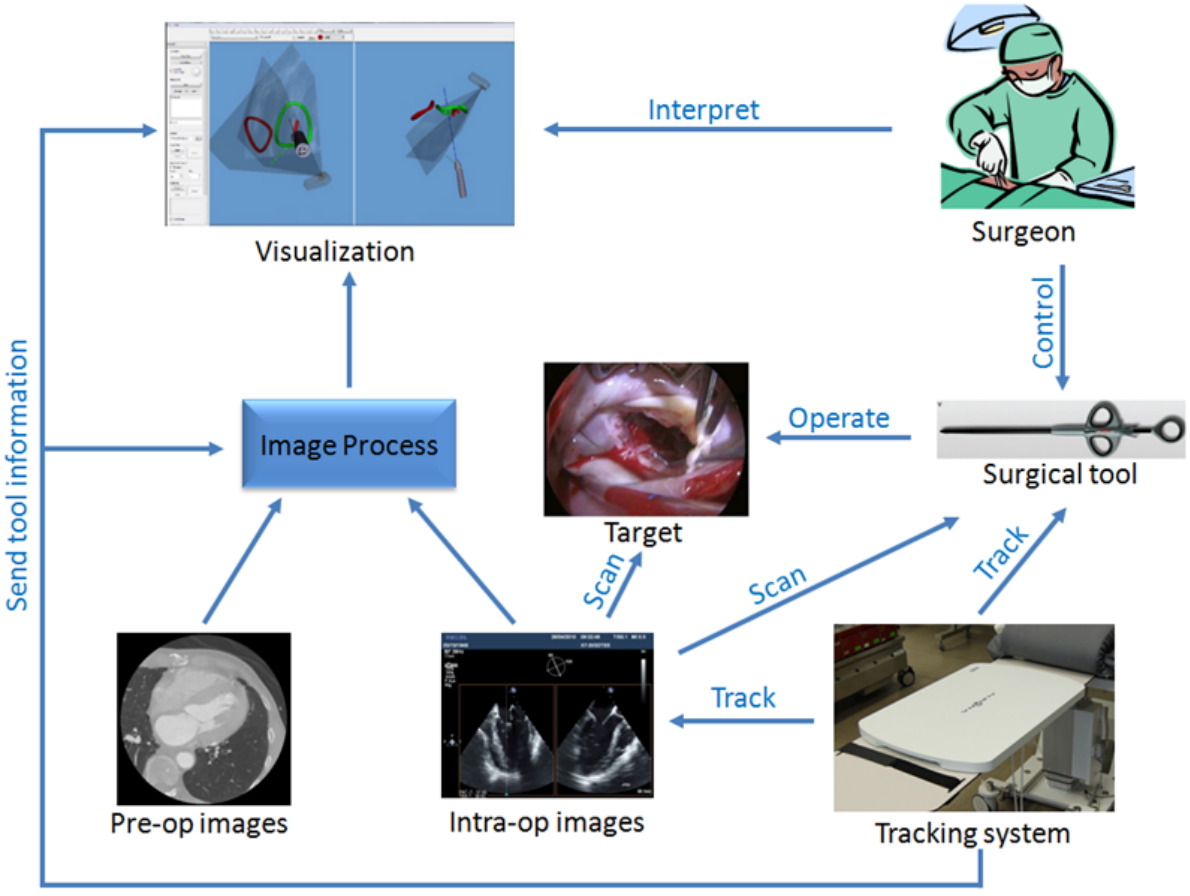


Figure 1.11: Overview of an Image Guidance System

### 1.8.1 Pre-operative Images

Pre-operative images and models are mostly used for diagnosis and surgery planning. They can also be integrated into the intra-operative guidance system to provide high quality images as enhancement to the intra-operative images. Pre-operatively defined models can also provide useful information that may be difficult to obtain or to produce during the operation, such as planned surgical path, clearly defined target position, annotations of surrounding tissues, and customized fusion and visualization of multiple images. However, the limitation of pre-operative images is that they may not present the true intra-operative patient state. Many factors differentiate pre-operative images from their intra-operative counterparts, such as different imaging modalities, different scanning positions or poses, deformed tissues, surgical tool presence, and changes in lesions or surrounding tissues. Image registration techniques are commonly required for using pre-operative images during the surgery.

### 1.8.2 Intra-operative Images

Intra-operative images show the true state of a patient during the surgery. They can be the same or different imaging modalities as the pre-operative images. The importance of having intra-operative images is that they can show not only the anatomy and motion of the patient, but also the surgical tools and the interaction between the tools and the tissues. The latter cannot be found in the pre-operative images. However, it is a general requirement that the procedure of obtaining an intra-operative image should not significantly interfere with the OR workflow. Waiting half an hour or maybe even ten minutes to get an image is usually not acceptable in the OR. Furthermore, in beating heart interventions, it is also important to show the real time heart motion. Inside a beating heart, some tissues, such as valve leaflets, can move rapidly, requiring high temporal resolution of the imaging modality, which means the scanning process for one image, must be accomplished within a very short period of time.

### 1.8.3 Tool Tracking Systems

Tool tracking systems continuously track the position and orientation of the surgical tools and send the updated information to the guidance system. Common choices of tracking systems are optical tracking, visual tracking, magnetic tracking, and image based tracking. Optical tracking systems usually use two cameras to locate the positions of infrared-emitting or retro-reflective markers, usually spheres, and compute the positions and orientations of the tracked tool based on the markers positions. The accuracy is generally excellent, in many cases better than one millimeter. However, the line-of-sight is a common limitation for optical tracking, implying that the markers should not be blocked from the camera by any objects at any time for the tracker to be able to work. Visual tracking is similar to optical tracking, but it uses geometric patterns attached to the tools for tracking. It is cheaper and can be more scalable than optical tracking, but it also has the occlusion issue and the general accuracy is not determined yet. Magnetic tracking systems employ a field generator to generate a magnetic field and sensor coils placed in the tracking area induce different voltages according to the varying magnetic fields, which can be used to calculate the position and orientation of the sensors. A major advantage of magnetic tracking is that it does not have the "line-of-sight" constraint. Sensor coils can be placed anywhere inside a human body and will operate as long as they are within the sensitive volume of the field generator. However, metal tools may greatly affect the tracking accuracy, although medical grade stainless steel and titanium are claimed to be non-problematic. Also, the general accuracy of magnetic tracking is worse than optical tracking. Image based tracking doesn't rely on any external devices other than the imaging devices themselves, and the position and orientation of the tool is calculated based on the tools appearance in the images. It is a good option when the other three techniques are not applicable, but accuracy of this technique relies largely on the image quality and the image processing techniques.

### 1.8.4 Image Processing Techniques

Image processing programs act as the linkage between pre-operative images/models, the intra-operative image, and visualization programs. They are used to bring all the useful information together from available images, either pre-operative or intra-operative, and make them more salient and easier to interpret for the surgeons. For example, locating and dynamically updating the position of the surgical target, if possible, often receive the most attention in any image guidance systems; marking the regions that may cause potential danger if the tool accidently gets into is helpful for improving the overall safety of the procedure; and incorporating high quality pre-operative image to the system can help the surgeon to better interpret the anatomy, when intra-operative images have relatively low quality.

In terms of processing techniques, segmentation, registration, and image filtering including regularization, enhancing, feature extraction, and thresholding are the most commonly used.

***Segmentation*** usually forms the basis for generating anatomical and/or functional models, locating surgical targets, and quantitative measurements within the area of interest. For medical purposes, the segmentation results are usually expected to be highly accurate ($\leq$1mm). However, this level of accuracy is often very hard to achieve. Many segmentation approaches that give satisfactory results are then very computationally intensive, which limits the opportunity of using them intra-operatively. Thus, most of the segmentation work is still performed pre-operatively, which also allows review and correction by the clinician.

***Registration*** is the key component for linking multiple images together, especially for aligning pre-operative images to intra-operative images. Many factors can lead to variations between pre-operative and intra-operative images, such as tissue deformation, changes in lesions, inter-modality intensity distribution differences, and different coordinate system used by the imaging systems. In most cases, these factors are combined in various ways, so the choice of using either rigid or non-rigid registration and the selection of a similarity metric depend on applications. The factors to be considered are the differences in image presentation, computational efficiency of the approach versus requirement of the efficiency of the application,

general accuracy of the approach versus tolerance of registration error of the application, extra time and efforts required for implementing a certain approach versus estimated benefits of using this approach.

***Image filters*** are commonly used in the pre-processing step before segmentation or registration. They can smooth or sharpen images, enhance contrast, and detect geometrical features, etc. In some cases, a well chosen filter can be the difference between success and failure. Histogram matching, for example, may greatly improve the performance of mono-modality registration. Such steps are often referred to as engineering tricks as they are not always reported in publications.

### 1.8.5 Visualization

Visualization platforms obtain data from the image processing programs and the tool tracking systems and display them on the screen. There are many different ways of visualizing an image or a virtual model, such as maximum intensity projection, volume rendering of the whole image, showing orthogonal slices, rendering a model as polygon or surfaces with shading, and overlaying/fusing images together. It is not always necessary to show everything that the image processing programs can provide on the screen. Actually, in many situation, showing too much is as bad as showing too little. The optimal choice of what to visualize at each certain stage during the procedure needs careful studies. A general criterion is that the visualization should ease the mental workload of the surgeons but not add to workload.

## 1.9 Image Registration Techniques for Guidance of MI Off-pump BH Procedures

Image registration has two important roles in image guidance system for beating heart intervention. First, it is the core technique that connects the pre-operative images/models and intra-operative images together. Second, it is essential for analyzing the cardiac motion. Trade-

off between registration accuracy and efficiency is one of the most important decisions when choosing registration approaches for the guidance of BH procedures. Many non-rigid registration approaches aim to achieve excellent registration accuracy, but place little emphasis on efficiency. Some of them may take hours to finish the computation on one dataset [124, 125]. These approaches are not plausible for intra-operative BH applications. On the other hand, most of the guidance applications require the root mean square error (RMSe) of the registration to be within a reasonable range, typically less than 5mm. This means that the registration approach guidance of BH procedures should be both fast and accurate.

There are hundreds of image registration techniques designed for different applications and requirements, but basically all of them can be classified into a few categories according to some simple rules.

### 1.9.1 Transformation Models

Transformation models define the degrees of freedom (DoF) involved in mapping the moving image to the reference (fixed) image. To list some of the transformation models from low DoF to high DoF, there are rigid, procrustes, affine, and non-rigid transformation. Rigid transformation allows only rotation and translation of the moving image. For a 3D registration problem, a rigid transformation allows three degrees of freedom in rotation and three degrees of freedom in translation, i.e. 6 DoF in total. Procrustes transformation adds uniform scaling to the rigid transformation. Affine transformation preserves only points, straight lines, and planes. Parallel lines remain parallel after an affine transformation, but the angles between lines and distances between points are not necessarily preserved. Non-rigid transformation allows local non-linear deformation to the extent of individual pixel/voxels, and provides the highest freedom, but the validation of non-rigid registration remains a complicated question. Figure 1.12 shows how a square shape changes when different transformation models are applied to it.

Rigid transformation can be computed very efficiently, but it does not deal with tissue deformation. On the other hand, non-rigid transformation can deal with all kinds of deformation

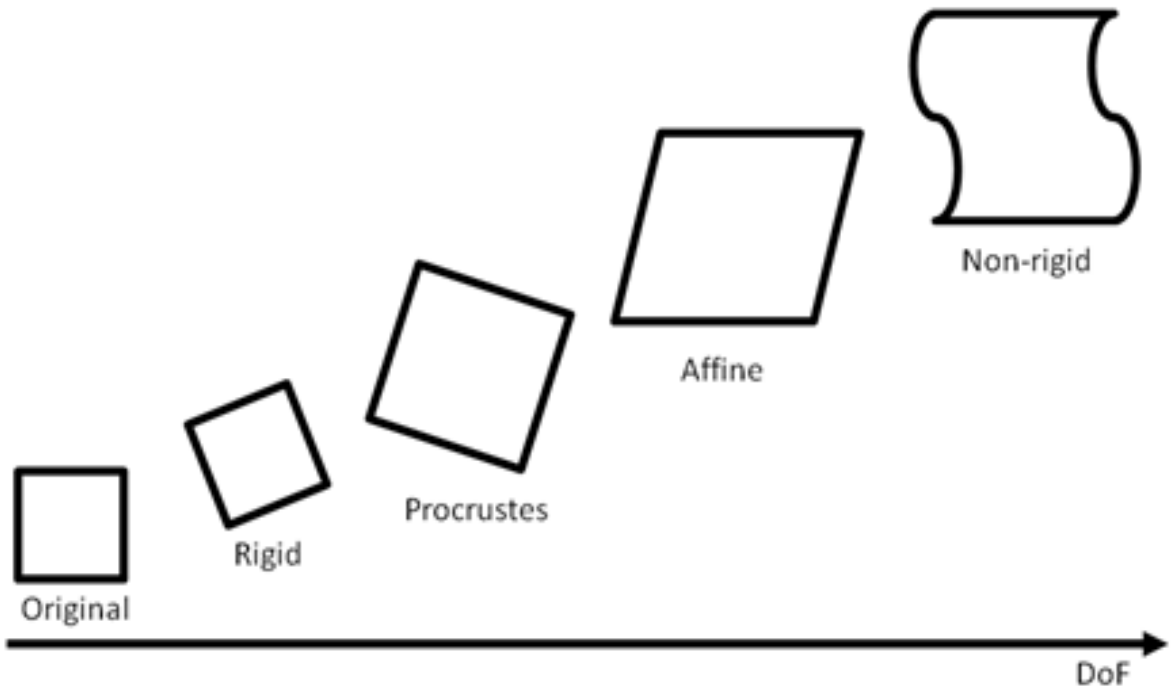


Figure 1.12: An illustration of transformation models

in images, even the changes in intensities (e.g. Level-sets based method [126]), but it is usually computationally intensive and the regularization can be tricky.

***Non-rigid transformation*** has been very widely used to estimate the cardiac motion. The results are often used to generate dynamic heart motion models or atlases both for diagnosis and guidance purposes.

For example, Wierzbicki et al. [127, 128] introduced and validated an approach of generating dynamic heart models using non-rigid registration. This approach was tested on CT animal images and MRI human images. With properly selected similarity metrics, the accuracy of the models was reported to be approximately 1mm. Phatak et al. [129] and Veress et al. [130] used an hyperelastic warping approach to measure the strain of the left ventricle during systole with untagged cine-MR images. The circumferential and radial strains computed based on the warping were compared to the results obtained from tagged MR images and showed good correlation. Shi et al. [131] described a approach that registered tagged and untagged MR images from the same patient simultaneously to a common spatio-temporal reference to estimate the

cardiac motion. The results were reported to be better than using either tagged or untagged images alone. Sundar et al. [132] introduced a 4D registration approach that registered all the 3D images in one cardiac cycle simultaneously. This approach provided better smoothness in deformation fields between adjacent frames than approaches that register the images frame by frame. The accuracy of this approach was reported to be 1-2mm compared to tagged MR images.

The use of ultrasound images for cardiac motion estimation was once limited to 2D images [133]. However, with the introduction of the matrix transducers 3D ultrasound images are gaining more and more interest for cardiac motion estimation as well. For example, Elen et al. [134] used non-rigid registration to estimate the left ventricle strain based on the 3D ultrasound data of three different left ventricle phantoms and achieved sub-millimeter RMSe in phantom studies. The development of 3D speckle tracking techniques has also been shown to be a clinically reliable method for estimating the left ventricle wall function [135, 136].

Most of the non-rigid registration approaches are computationally intensive, which prevent them from being used for real-time applications. Some studies have accelerated the registration speed to be faster than 30 seconds per frame with graphic processing unit (GPU) based implementations [137–139], but so far there have been no reports of sub-second computation times for non-rigid registrations.

***Rigid transformation*** previously had very few applications in cardiac imaging, because it cannot deal with the image deformation caused by cardiac motion. Recently, the development of modern GPU hardware and the programming platform for general-purpose computing on graphics processing units (GPGPU) have made it possible to perform 3D rigid registration in real time. This has prompt many studies using rigid registration to develop real time intra-operative guidance for MI BH procedures.

Although the limitations related to deformation still remain, researchers have attempted to reduce its negative impact by minimizing the temporal spacing (within the cardiac cycle) between the images to be registered. For the registration between adjacent images from the same

sequence, this is achieved by using images with high temporal resolution, typically ultrasound. For example, Schneider et al. [140] introduced a feature based approach to register a sequence of 3D ultrasound volumes in real time as the basis for stitching the volumes to expand the field of view. The accuracy of this approach is approximately 1 mm and they claimed the registration speed can be as fast as the image acquisition. Kutter et al. [141] used the similar idea to perform ultrasound mosaicing using an intensity based registration approach. For the registration of images from different sequences, a temporal alignment, usually based on gating information, is first performed to identify images with corresponding cardiac phases. Many studies have adopted this idea including the works of Huang et al. [142, 143], Li et al. [144, 145], Lang et al. [121], Okumura et al. [146], and Zhang et al. [147]. The gating information can be obtained from either electrocardiography (ECG) signals [142, 147] or image based phasing techniques [148].

***Procrustes transformation*** adds one more DoF to rigid transformation in terms of uniform scaling. Although there are some studies suggesting that in the transcatheter aortic valve replacement/implantation (TAVR or TAVI) procedure the diameter of the aortic valve measured in TEE can be underestimated by 1-2mm compared to that in CT [149], the importance of using procrustes transformation for cardiac procedures has not been supported by other studies.

***Affine transformation*** is often used to provide a good initialization for non-rigid registration to reduce the computation time as it can partially deal with the deformation [127], but very few applications in cardiac interventions use affine transformation as the main transformation model. However, it is reasonable to predict that real time affine registration can become possible soon in the future with further development in GPU based parallel computing, which may replace rigid registration in intra-operative applications due to better registration accuracy.

### 1.9.2 Feature Based and Intensity Based

***Feature based approaches*** require the definition of corresponding feature points to align the moving and target (fixed) images. The type of feature can vary from a few selected points to

a large surface containing thousands of points. For example, if the task is to align the images of a rigid phantom with some salient geometric features, a few non-symmetric feature points can be sufficient to obtain an accurate registration result. However, this approach requires the corresponding feature points represent exactly the same point in the real world, otherwise the result can be heavily biased by the inaccuracy of feature point selection. This requirement can be very difficult to achieve for some anatomy based features, e.g. the tip of the apex of the heart. Thus, in many applications, an entire surface of a certain anatomical structure is selected as the feature, e.g. the inner wall of the left ventricle or the aortic root. Since there are more geometric features included in a surface, small selection errors in one place can be compensated by the other part of the surface, which makes this approach more robust.

Schneider et al. [140] and Ni et al. [150] chose to use the first type of feature, i.e. several feature points, in their 3D ultrasound registration approaches and 3D scale invariant feature transform SIFT algorithm was used for feature extraction. The registration speed of these approaches is very fast (over 20Hz in Schneiders study), since only a small number of points are required for registration. However, the accuracy of this type of approach highly relies on the repeatability and consistency of the feature extraction, which is the reason that high temporal resolution imaging and a close-to-stationary probe are required in those studies to ensure that the features extracted from the two adjacent volumes represent the same physical feature. Furthermore, this approach may not work with multi-modality registration, because the feature extraction cannot guarantee finding the corresponding feature points.

The second type of feature, i.e. surfaces, is usually obtained by segmentation and registration with an iterative closest point (ICP) algorithm [116]. The segmentation of the features can be achieved manually, semi-automatically, or completely automatically. However, most of the segmentation approaches are too slow for the beating heart interventions. Although some automatic approaches have been introduced, which can segment a 3D volume in 5- 90 seconds [151–153], it is still much slower than the heart rate and the imaging rate of ultrasound.

***Intensity based approaches*** do not require predefined features, and instead compare the

intensity patterns between the images using similarity metrics, such as sum of squared differences (SSD), sum of absolute differences (SAD), normalized correlation coefficient (NCC), and (normalized) mutual information (NMI). There is no fixed rule for which similarity metric to choose for a certain application. The common factors to be considered are the image modalities, the required efficiency, and workload of implementation. The most commonly used metrics for multi-modal registrations are mutual information and/or normalized mutual information [154–160], because they don't assume linear relationships between intensities of corresponding features in different images, which is an essential requirement for some other metrics, such as SAD and SSD. The computation of the similarity metrics can be achieved using all or a subset of the image, e.g. a thresholded image. Using a sub-set of the images usually leads to better computational efficiency but not necessarily worse accuracy, if the sub-set is well selected [142, 144].

### 1.9.3 Single Modality and Multi-Modality

As the name implies, single modality registration means that the images to be registered are produced with the same imaging modality, while images in multi-modality registrations are produced with different modalities. Both of the two techniques are very commonly used in guidance of beating heart interventions.

Single modality registration is often used for analyzing cardiac motion from a sequence of images covering one or several cardiac cycles [131, 161–164] or providing real time mosaicing of the streaming images [140, 141, 150]. Ultrasound images, retrospectively gated CT images, and cine MRI images are the most popular modalities for this approach.

Multi-modality registration is used to combine images, which contain unique information, to provide a fused visualization that gives more information than any single imaging modality can achieve. This method is used in two ways. One is to fuse the pre-operative (pre-op) images, together with the pre-defined anatomical models, tags, and surgical plans to the intra-operative (intra-op) images or patients. Typical applications include registering pre-op CT to

intra-op ultrasound images [143, 145, 165, 166], pre-op MRI to intra-op ultrasound images [147, 166], and pre-op CT/MRI to intra-op X-ray fluoroscopy [167]. The other is to fuse two intra-op modalities together in real time. TEE and X-ray fluoroscopy are the two most frequently used modalities for this approach [168–170]. The fluoroscopy images are used to visualize the tools, while the TEE images are used for accurate positioning. There is also a commercially available guidance platform using this approach called EchoNavigator ©[171] (Philips, Amsterdam, Netherlands).

## 1.10 Thesis Outline

The objective of this thesis is to develop rapid image processing techniques and integrate them in the image guidance system for minimally invasive off-pump beating heart mitral valve repair procedure. The proposed approaches are designed to provide augmented reality/virtuality for the guidance system through real time image registration that provides the linkage between pre- and intra-operative images and anatomical feature tracking that tracks and enhances the feature of interest during the procedure. Chapter 2 describes an approach to generate synthetic dynamic CT images to be used as high quality pre-operative images in the guidance system. Chapter 3 introduces an approach to perform real time CT-TEE registration that can be used to enhance the ultrasound guidance with real or synthetic CT images, while Chapter 4 describes the development of a real time mitral annulus tracking approach using 2D bi-plane TEE images.

### 1.10.1 Synthetic CT Generation

Chapter 2 proposes an approach to generate synthetic dynamic CT images based on a static CT image and a sequence of 3D US images. The role of synthetic CT images is to replace actual dynamic CT images obtained from retrospectively gated CT scans in the guidance system to reduce radiation dose and cost. This approach obtains the cardiac motion information in terms of image deformation field through non-rigid registration and applies that information to a

static CT image to produce animation. Validation experiments are described comparing the anatomical region of interest, left ventricle in this chapter, in the synthetic CT images, to that in actual CT images. Results demonstrated that the synthetic CT images can provide very similar anatomical representations as the real CT images.

### 1.10.2 CT Enhanced Ultrasound Guidance

Chapter 3 introduces an approach to enhance ultrasound guidance with dynamic CT images. A rapid registration method is developed to register the pre-operative CT images to intra-operative 3D TEE images both temporally and spatially in real time. Validation experiments were performed with the mitral annulus as the target, demonstrating the ability to achieve acceptable target registration error (TRE) (~3mm). We also compared the registration results between using synthetic and real dynamic CT images and found no significant difference between them, supporting the concept of using synthetic CT images in our guidance system.

### 1.10.3 Ultrasound Based Mitral Anuulus Tracking

Chapter 4 describes a mitral annulus tracking approach using 2D bi-plane images. This approach uses no pre-operative images. All the feature tracking is based on intra-operative images and magnetic tracking systems. We validated the approach with a dynamic heart phantom as well as data collected from animal studies. The results showed excellent tracking accuracy ($\leq$2mm) on both phantom and animal data when the shift of the annulus is within 2cm.

## 1.11 Co-authorship Statement

In Chapters 2-4, I was responsible for study design, conducting experiments, data analysis and the principal contribution to the manuscripts. None of these chapters would have been completed without the contribution and expertise of many people involved, so within the thesis I refer to the authors as 'we'.

Chapter 2 is adapted from the papers:

- **Feng P. Li**, James A. White, Martin Rajchl, Aashish Goela, and Terry M. Peters, Generation of Synthetic 4D Cardiac CT Images by Deformation from Cardiac Ultrasound. In: Workshop on Augmented Environments for Computer-Assisted Interventions (AE-CAI). Lecture Notes in Computer Science. Springer Berlin / Heidelberg, 2012

- **Feng P. Li**, Martin Rajchl, James A. White, Aashish Goela, and Terry M. Peters, Generation of Synthetic 4D Cardiac CT Images for Guidance of Minimally Invasive Beating Heart Interventions. Information Processing in Computer- Assisted Interventions (IPCAI), 2013

Chapter 3 is adapted from the papers:

- **Feng Li**, Pencilla Lang, Martin Rajchl, Elvis C.S. Chen, Gerard Guiraudon, Terry M. Peters, Towards Real-time 3D US-CT Registration on the Beating Heart for Guidance of Minimally Invasive Cardiac Interventions, SPIE Medical Imaging Conference, San Diego, Feb. 4-9, 2012

- **Feng P. Li**, Martin Rajchl, James A. White, Aashish Goela, and Terry M. Peters, Towards CT Enhanced Ultrasound Guid- ance for Off-pump Beating Heart Mitral Valve Repair. In: MIAR/AE-CAI 2013.

- **Feng P. Li**, Martin Rajchl, James A. White, Aashish Goela, and Terry M. Peters, Ultrasound Guidance for Beating Heart Mitral Valve Repair Augmented by Synthetic Dynamic CT, IEEE Transaction on Medical Imaging (submitted)

Chapter 4 is adapted from the papers:

- **Feng P. Li**, Martin Rajchl, John Moore, Terry M. Peters, Ultrasound based mitral valve annulus tracking for off-pump beating heart mitral valve repair, SPIE Medical Imaging, 2014

- **Feng P. Li**, Martin Rajchl, John Moore, and Terry M. Peters, A Mitral Annulus Tracking Approach for Navigation of Off-pump Beating Heart Mitral Valve Repair, Medical Physics (submitted)

# Bibliography

[1] K. P. McCarthy, L. Ring, and B. S. Rana, "Anatomy of the mitral valve: understanding the mitral valve complex in mitral regurgitation.," *European journal of echocardiography : the journal of the Working Group on Echocardiography of the European Society of Cardiology*, vol. 11, pp. i3–9, Dec. 2010.

[2] J. K. Perloff and W. C. Roberts, "The Mitral Apparatus: Functional Anatomy of Mitral Regurgitation," *Circulation*, vol. 46, pp. 227–239, Aug. 1972.

[3] R. C. Brock, "The surgical and pathological anatomy of the mitral valve," *British Heart Journal*, vol. 14, no. 4, pp. 489–513, 1952.

[4] M. M. Montiel, "Muscular apparatus of the mitral valve in man and its involvement in left-sided cardiac hypertrophy," *The American Journal of Cardiology*, vol. 26, no. 4, pp. 341–344, 1970.

[5] G. L. van Rijk-Zwikker, B. J. Delemarre, and H. a. Huysmans, "Mitral valve anatomy and morphology: relevance to mitral valve replacement and valve reconstruction.," *Journal of cardiac surgery*, vol. 9, pp. 255–61, Mar. 1994.

[6] M. Chiechi, W. Lees, and R. Thompson, "Functional anatomy of the normal mitral valve," *Journal of thoracic cardiovascular surgery*, pp. 378–398, 1956.

[7] J. A. Ormiston, P. M. Shah, C. Tei, and M. Wong, "Size and motion of the mitral valve annulus in man. I. A two- dimensional echocardiographic method and findings in normal subjects," *Circulation*, vol. 64, pp. 113–120, July 1981.

[8] I. E. Rusted, C. H. Scheifley, and J. E. Edwards, "Studies of the Mitral Valve. I. Anatomic Features of the Normal Mitral Valve and Associated Structures," *Circulation*, vol. 6, pp. 825–831, Dec. 1952.

[9] E. C. Jones, R. B. Devereux, M. J. Roman, J. E. Liu, D. Fishman, E. T. Lee, T. K. Welty, R. R. Fabsitz, and B. V. Howard, "Prevalence and correlates of mitral regurgitation in a population-based sample (the Strong Heart Study).," *The American journal of cardiology*, vol. 87, pp. 298–304, Feb. 2001.

[10] E. D. Agabegi and S. S. Agabegi, "Step-Up to Medicine (Step-Up Series) Chapter 1:Diseases of the Cardiovascular system ¿ Section: Valvular Heart Disease," ch. Chapter 1:, Wolters Kluwer — Lippincott Williams & Wilkins, 3rd editio ed., 2008.

[11] G. B. Pedrazzini, F. Faletra, G. Vassalli, S. Demertzis, and T. Moccetti, "Mitral regurgitation," *Swiss medical weekly*, vol. 140, pp. 36–43, Jan. 2010.

[12] D. Warth, M. King, J. Cohen, V. Tesoriero, E. Marcus, and A. Weyman, "Prevalence of mitral valve prolapse in normal children," *Journal of American College of Cardiology*, vol. 5, no. 5, pp. 1173–1177, 1985.

[13] R. A. Levine, M. O. Triulzi, P. Harrigan, and A. E. Weyman, "The relationship of mitral annular shape to the diagnosis of mitral valve prolapse," *Circulation*, vol. 75, pp. 756–767, Apr. 1987.

[14] R. A. Levine, E. Stathogiannis, J. B. Newell, P. Harrigan, and a. E. Weyman, "Reconsideration of echocardiographic standards for mitral valve prolapse: lack of association between leaflet displacement isolated to the apical four chamber view and independent echocardiographic evidence of abnormality.," *Journal of the American College of Cardiology*, vol. 11, pp. 1010–9, May 1988.

[15] R. A. Levine, M. D. Handschumacher, A. J. Sanfilippo, A. A. Hagege, P. Harrigan, J. E. Marshall, and A. E. Weyman, "Three-dimensional echocardiographic reconstruction of the mitral valve, with implications for the diagnosis of mitral valve prolapse," *Circulation*, vol. 80, pp. 589–598, Sept. 1989.

[16] E. Hayek, C. N. Gring, and B. P. Griffin, "Mitral valve prolapse," *Lancet*, vol. 365, no. 9458, pp. 507–18, 2005.

[17] J. D. Schmitto, L. S. Lee, S. a. Mokashi, R. M. Bolman, L. H. Cohn, and F. Y. Chen, "Functional mitral regurgitation," *Cardiology in review*, vol. 18, no. 6, pp. 285–91, 2010.

[18] J. Beaudoin, M. D. Handschumacher, X. Zeng, J. Hung, E. L. Morris, R. a. Levine, and E. Schwammenthal, "Mitral valve enlargement in chronic aortic regurgitation as a compensatory mechanism to prevent functional mitral regurgitation in the dilated left ventricle.," *Journal of the American College of Cardiology*, vol. 61, pp. 1809–16, Apr. 2013.

[19] M. Chaput, M. D. Handschumacher, F. Tournoux, L. Hua, J. L. Guerrero, G. J. Vlahakes, and R. a. Levine, "Mitral leaflet adaptation to ventricular remodeling: occurrence and adequacy in patients with functional mitral regurgitation.," *Circulation*, vol. 118, pp. 845–52, Aug. 2008.

[20] J. Shuhaiber and R. J. Anderson, "Meta-analysis of clinical outcomes following surgical mitral valve repair or replacement.," *European journal of cardio-thoracic surgery*, vol. 31, pp. 267–75, Feb. 2007.

[21] C. M. Tribouilloy, M. Enriquez-Sarano, H. V. Schaff, T. a. Orszulak, K. R. Bailey, a. J. Tajik, and R. L. Frye, "Impact of Preoperative Symptoms on Survival After Surgical Correction of Organic Mitral Regurgitation : Rationale for Optimizing Surgical Indications," *Circulation*, vol. 99, pp. 400–405, Jan. 1999.

[22] R. R. Moss, K. H. Humphries, M. Gao, C. R. Thompson, J. G. Abel, G. Fradet, and B. I. Munt, "Outcome of mitral valve repair or replacement: a comparison by propensity score analysis.," *Circulation*, vol. 108 Suppl, pp. II90–7, Sept. 2003.

[23] P. Bajona, W. E. Katz, R. C. Daly, K. J. Zehr, and G. Speziali, "Beating-heart, off-pump mitral valve repair by implantation of artificial chordae tendineae: an acute in vivo

animal study.," *The Journal of thoracic and cardiovascular surgery*, vol. 137, pp. 188–93, Jan. 2009.

[24] H. H. H. Feringa, L. J. Shaw, D. Poldermans, S. Hoeks, E. E. van der Wall, R. a. E. Dion, and J. J. Bax, "Mitral valve repair and replacement in endocarditis: a systematic review of literature.," *The Annals of thoracic surgery*, vol. 83, pp. 564–70, Feb. 2007.

[25] A. M. Gillinov, D. M. Cosgrove, E. H. Blackstone, R. Diaz, J. H. Arnold, B. W. Lytle, N. G. Smedira, J. F. Sabik, P. M. McCarthy, and F. D. Loop, "Durability of mitral valve repair for degenerative disease," *The Journal of thoracic and cardiovascular surgery*, vol. 116, pp. 734–43, Nov. 1998.

[26] H. Morimoto, K. Tsuchiya, M. Nakajima, and O. Akashi, "Mitral valve repair for anterior leaflet prolapse: surgical techniques review and 16-year follow-up results.," *Journal of cardiac surgery*, vol. 23, no. 5, pp. 426–30, 2008.

[27] O. Alfieri, M. De Bonis, E. Lapenna, T. Regesta, F. Maisano, L. Torracca, and G. La Canna, "Edge-to-edge repair for anterior mitral leaflet prolapse," *Seminars in Thoracic and Cardiovascular Surgery*, vol. 16, pp. 182–187, June 2004.

[28] M. O. Jensen, H. Jensen, M. Smerup, R. a. Levine, A. P. Yoganathan, H. Nygaard, J. M. Hasenkam, and S. L. Nielsen, "Saddle-shaped mitral valve annuloplasty rings experience lower forces compared with flat rings.," *Circulation*, vol. 118, pp. S250–5, Sept. 2008.

[29] A. F. Carpentier, A. Lessana, J. Y. Relland, E. Belli, S. Mihaileanu, a. J. Berrebi, E. Palsky, and D. F. Loulmet, "The "physio-ring": an advanced concept in mitral valve annuloplasty.," *The Annals of thoracic surgery*, vol. 60, pp. 1177–85; discussion 1185–6, Nov. 1995.

[30] S. Sack, P. Kahlert, L. Bilodeau, L. a. Pièrard, P. Lancellotti, V. Legrand, J. Bartunek, M. Vanderheyden, R. Hoffmann, P. Schauerte, T. Shiota, D. S. Marks, R. Erbel, and S. G.

Ellis, "Percutaneous transvenous mitral annuloplasty: initial human experience with a novel coronary sinus implant device.," *Circulation. Cardiovascular interventions*, vol. 2, pp. 277–84, Aug. 2009.

[31] J. G. Webb, J. Harnek, B. I. Munt, P. O. Kimblad, M. Chandavimol, C. R. Thompson, J. R. Mayo, and J. O. Solem, "Percutaneous transvenous mitral annuloplasty: initial human experience with device implantation in the coronary sinus.," *Circulation*, vol. 113, pp. 851–5, Feb. 2006.

[32] T. Burdon, D. Miller, P. Oyer, R. Mitchell, E. Stinson, V. Starnes, and N. Shunmway, "Durability of porcine valves at fifteen years in a representative North American patient population," *The Journal of thoracic and cardiovascular surgery*, vol. 103, no. 2, pp. 238–251, 1992.

[33] Nobelprize.org. Nobel Media, "Werner Forssmann - Biographical," 2013.

[34] R. E. Gross and J. P. Hubbard, "Surgical ligation of patent ductus arteriosus; report of first successful case," *JAMA*, vol. 112, no. 8, pp. 729–731, 1939.

[35] L. H. Cohn, "Fifty years of open-heart surgery," *Circulation*, vol. 107, pp. 2168–70, May 2003.

[36] G. M. Guiraudon, "Musing while cutting," *Journal of cardiac surgery*, vol. 13, pp. 156–62, Mar. 1998.

[37] T. Ferguson, B. G. Hammill, E. D. Peterson, E. R. DeLong, and F. L. Grover, "A decade of changerisk profiles and outcomes for isolated coronary artery bypass grafting procedures, 19901999: a report from the STS National Database Committee and the Duke Clinical Research Institute," *The Annals of Thoracic Surgery*, vol. 73, pp. 480–489, Feb. 2002.

[38] M. Ono, N. Fukushima, S. Ohtake, H. Ichikawa, K. Kagisaki, T. Matsushita, and H. Matsuda, "The clinical pathway for fast track recovery of school activities in children after minimally invasive cardiac surgery, pp. 4448, 2003.in children after minimally invasive cardiac surgery," *Cardiol Young*, pp. 44–48, 2003.

[39] R. Freeman, B. King, and M. H. Hambling, "Infective complications of open-heart surgery and the monitoring of infections by the NBT test," *Thorax*, vol. 28, pp. 617–621, Sept. 1973.

[40] G. M. Barker, S. M. O'Brien, K. F. Welke, M. L. Jacobs, J. P. Jacobs, D. K. Benjamin, E. D. Peterson, J. Jaggers, and J. S. Li, "Major infection after pediatric cardiac surgery: a risk estimation model.," *The Annals of thoracic surgery*, vol. 89, pp. 843–50, Mar. 2010.

[41] S. Kakar, B. Mishra, S. Khanna, and A. Mandel, "Wound Infections After Open Heart Surgery," *Indian Journal of Thoracic and Cardiovascular Surgery*, vol. 12, no. 1-2, pp. 21–25, 1996.

[42] C. V. Thakar, J.-P. Yared, S. Worley, K. Cotman, and E. P. Paganini, "Renal dysfunction and serious infections after open-heart surgery," *Kidney international*, vol. 64, pp. 239–46, July 2003.

[43] G. Gursel, a. Karamehmetoglu, a. Y. Bozer, and a. Saylam, "Postoperative Arrhythmias in Open-Heart Surgery: A Study On Fifty Cases," *Vascular and Endovascular Surgery*, vol. 10, pp. 30–37, Jan. 1976.

[44] R. Smith, W. Grossman, L. Johnson, H. Segal, J. Collins, and J. Dalen, "Arrhythmias following Cardiac Valve Replacement," *Circulation*, vol. 45, pp. 1018–1023, May 1972.

[45] G. H. Almassi, T. Schowalter, a. C. Nicolosi, a. Aggarwal, T. E. Moritz, W. G. Henderson, R. Tarazi, a. L. Shroyer, G. K. Sethi, F. L. Grover, and K. E. Hammermeister,

"Atrial fibrillation after cardiac surgery: a major morbid event?," *Annals of surgery*, vol. 226, pp. 501–11; discussion 511–3, Oct. 1997.

[46] L. L. Creswell, R. B. Schuessler, M. Rosenbloom, and J. L. Cox, "Hazards of postoperative atrial arrhythmias," *The Annals of thoracic surgery*, vol. 56, no. 3, pp. 539–549, 1993.

[47] G. Mangos, M. Brown, W. Chan, D. Horton, P. Trew, and J. Whitworth, "Acute renal failure following cardiac surgery: incidence, outcomes and risk factors," *Aust N Z J Med*, vol. 25, no. 4, pp. 284–289, 1995.

[48] S. Slogoff, G. Reul, A. Keats, G. Curry, M. Crum, B. Elmquist, N. Giesecke, J. Jistel, L. Rogers, and J. Soderberg, "Role of perfusion pressure and flow in major organ dysfunction after cardiopulmonary bypass," *Annual Thoracic Surgery*, vol. 50, no. 6, pp. 911–918, 1990.

[49] E. W. Young, A. Diab, and M. M. Kirsh, "Intravenous diltiazem and acute renal failure after cardiac operations.," *The Annals of thoracic surgery*, vol. 65, pp. 1316–9, May 1998.

[50] C. V. Thakar, S. Arrigain, S. Worley, J.-P. Yared, and E. P. Paganini, "A clinical score to predict acute renal failure after cardiac surgery.," *Journal of the American Society of Nephrology : JASN*, vol. 16, pp. 162–8, Jan. 2005.

[51] C. R. Bridges, F. H. Edwards, E. D. Peterson, and L. P. Coombs, "The effect of race on coronary bypass operative mortality.," *Journal of the American College of Cardiology*, vol. 36, pp. 1870–6, Nov. 2000.

[52] J. W. Kennedy, G. C. Kaiser, L. D. Fisher, J. K. Fritz, W. Myers, J. G. Mudd, and T. J. Ryan, "Clinical and angiographic predictors of operative mortality from the collaborative study in coronary artery surgery (CASS)," *Circulation*, vol. 63, pp. 793–802, Apr. 1981.

[53] T. L. Higgins, F. G. Estafanous, F. D. Loop, G. J. Beck, J. C. Lee, N. J. Starr, W. a. Knaus, and D. M. Cosgrove, "ICU admission score for predicting morbidity and mortality risk after coronary artery bypass grafting.," *The Annals of thoracic surgery*, vol. 64, pp. 1050–8, Oct. 1997.

[54] M. F. Newman, J. P. Mathew, H. P. Grocott, G. B. Mackensen, T. Monk, K. a. Welsh-Bohmer, J. a. Blumenthal, D. T. Laskowitz, and D. B. Mark, "Central nervous system injury associated with cardiac surgery.," *Lancet*, vol. 368, pp. 694–703, Aug. 2006.

[55] J. Ricotta, G. Faqqioli, A. Castilone, and J. Hassett, "Risk factors for stroke after cardiac surgery: Buffalo Cardiac-Cerebral Study Group," *Journal of Vascular Surgery*, vol. 21, no. 2, pp. 359–363, 1995.

[56] J. Craver, W. Weintraub, E. Jones, R. Guyton, and C. Hatcher Jr., "Predictors of mortality, complications, and length of stay in aortic valve replacement for aortic stenosis," *Circulation*, vol. 78, no. 3, pp. 185–190, 1988.

[57] T. Gardner, P. Horneffer, T. Manolio, T. Pearson, V. Gott, W. Baumgartner, A. Borkon, L. Watkins Jr., and B. Reitz, "Stroke following coronary artery bypass grafting: a ten-year study," *Annual Thoracic Surgery*, vol. 40, no. 6, pp. 574–581, 1985.

[58] C. W. Hogue, S. F. Murphy, K. B. Schechtman, and V. G. Davila-Roman, "Risk Factors for Early or Delayed Stroke After Cardiac Surgery," *Circulation*, vol. 100, pp. 642–647, Aug. 1999.

[59] K. A. Sotaniemi, "Brain damage and neurological outcome after open-heart surgery.," *Journal of Neurology, Neurosurgery & Psychiatry*, vol. 43, pp. 127–135, Feb. 1980.

[60] M. K. Newman, J. L. Kirchner, B. Phillips-Bute, V. Gaver, H. Grocott, R. H. Johnes, D. B. Mark, J. G. Reves, and J. A. Blumenthal, "Longitudinal assessment of neurocognitive function after coronary-artery bypass surgery," *The New England Journal of Medicine*, vol. 344, pp. 395–402, June 2001.

[61] A. Iribarne, M. J. Russo, R. Easterwood, K. N. Hong, J. Yang, F. H. Cheema, C. R. Smith, and M. Argenziano, "Minimally invasive versus sternotomy approach for mitral valve surgery: a propensity analysis.," *The Annals of thoracic surgery*, vol. 90, pp. 1471–7; discussion 1477–8, Nov. 2010.

[62] A. Gillinov and D. Cosgrove, "Minimally invasive mitral valve surgery: mini-sternotomy with extended transseptal approach," *Semin Thorac Cardiovasc Surg*, vol. 11, no. 3, pp. 206–211, 1999.

[63] D. Loulmet, A. Carpentier, P. Cho, A. Berrebi, N. D'Attellis, C. Austin, J. Couetil, and P. Lajos, "Less invasive techniques for mitral valve surgery," *Journal of thoracic cardiovascular surgery*, vol. 115, no. 4, pp. 772–779, 1998.

[64] L. G. Svensson and R. S. D'Agostino, ""J" incision minimal-access valve operations," *The Annals of thoracic surgery*, vol. 66, pp. 1110–2, Sept. 1998.

[65] H. E. Maechler, P. Bergmann, M. Anelli-monti, D. Dacar, P. Rehak, I. Knez, L. Salaymeh, E. Mahla, B. Rigler, C. Surgery, and C. Anesthesia, "Minimally Invasive Versus Conventional Aortic Valve Operations: A Prospective Study in 120 Patients," *The Annals of thoracic surgery*, vol. 4975, no. 99, 1999.

[66] T. Walther, S. Lehmann, V. Falk, C. Walther, N. Doll, A. Rastan, S. Metz, J. Schneider, J. Gummert, and F. W. Mohr, "Midterm results after stentless mitral valve replacement," *Circulation*, vol. 108 Suppl, pp. II85–9, Sept. 2003.

[67] E. Grossi, A. Galloway, A. LaPietra, G. Ribakove, P. Ursomanno, J. Delianides, A. Culliford, C. Bizekis, R. Esposito, F. Raumann, M. Kanchuger, and S. Colvin, "Minimally invasive mitral valve surgery: a 6-year experience with 714 patients," *The Annals of thoracic surgery*, vol. 74, no. 3, pp. 660–663, 2002.

[68] D. Wang, Q. Wang, X. Yang, Q. Wu, and Q. Li, "Mitral valve replacement through a

minimal right vertical infra-axillary thoracotomy versus standard median sternotomy.," *The Annals of thoracic surgery*, vol. 87, pp. 704–8, Mar. 2009.

[69] L. H. Cohn, D. H. Adams, G. S. Couper, D. P. Bichell, D. M. Rosborough, S. P. Sears, and S. F. Aranki, "Minimally invasive cardiac valve surgery improves patient satisfaction while reducing costs of cardiac valve replacement and repair.," *Annals of surgery*, vol. 226, pp. 421–6; discussion 427–8, Oct. 1997.

[70] F. Farhat, Z. Lu, M. Lefevre, P. Montagna, P. Mikaeloff, and O. Jegaden, "Total Sternotomy and Ministernotomy for Aortic Valve Replacement," *Journal of cardiac surgery*, vol. 18, no. 5, pp. 396–401, 2003.

[71] P. Corbi, M. Rahmati, E. Donal, H. Lanquetot, C. Jayle, P. Menu, and J. Allal, "Prospective comparison of minimally invasive and standard techniques for aortic valve replacement: initial experience in the first hundred patients.," *Journal of cardiac surgery*, vol. 18, no. 2, pp. 133–9.

[72] D. M. Cosgrove III, J. F. Sabik, and J. L. Navia, "Minimally Invasive Valve Operations," *Annual Thoracic Surgery*, vol. 4975, no. 98, pp. 1535–1539, 1998.

[73] A. Carpentier, D. Loulmet, E. Le Bret, B. Haugades, P. Dassier, and P. Guibourt, "Open heart operation under videosurgery and minithoracotomy. First case (mitral valvuloplasty) operated with success," *C R Acad Sci III*, vol. 319, no. 3, pp. 219–223, 1996.

[74] A. Carpentier, P. Guibourt, A. Fiemeyer, B. Auppcle, D. Mgard, and P. Richomme, "Computer assisted open heart surgery. First case operated on with success," *Medical Sciences*, vol. 321, no. 5, pp. 437–442, 1998.

[75] E. A. Grossi, A. LaPietra, G. H. Ribakove, J. Delianides, R. Esposito, a. T. Culliford, C. C. Derivaux, R. M. Applebaum, I. Kronzon, B. M. Steinberg, F. G. Baumann, a. C. Galloway, and S. B. Colvin, "Minimally invasive versus sternotomy approaches for mi-

tral reconstruction: comparison of intermediate-term results.," *The Journal of thoracic and cardiovascular surgery*, vol. 121, pp. 708–13, Apr. 2001.

[76] V. A. Gaudiani, G. L. Grunkemeier, L. J. Castro, A. L. Fisher, and Y. Wu, "Mitral valve operations through standard and smaller incisions.," *The heart surgery forum*, vol. 7, pp. E337–42, Jan. 2004.

[77] J. Gammie, S. Bartlett, and B. Griffith, "Small-incision mitral valve repair: safe, durable, and approaching perfection," *Ann Surg*, vol. 250, no. 3, pp. 409–415, 2009.

[78] C. de Vaumas, I. Philip, G. Daccache, J.-P. Depoix, J.-B. Lecharny, D. Enguerand, and J.-M. Desmonts, "Comparison of minithoracotomy and conventional sternotomy approaches for valve surgery," *Journal of Cardiothoracic and Vascular Anesthesia*, vol. 17, pp. 325–328, June 2003.

[79] L. G. Svensson, F. a. Atik, D. M. Cosgrove, E. H. Blackstone, J. Rajeswaran, G. Krishnaswamy, U. Jin, a. M. Gillinov, B. Griffin, J. L. Navia, T. Mihaljevic, and B. W. Lytle, "Minimally invasive versus conventional mitral valve surgery: a propensity-matched comparison.," *The Journal of thoracic and cardiovascular surgery*, vol. 139, pp. 926–32.e1–2, Apr. 2010.

[80] J. S. Gammie, Y. Zhao, E. D. Peterson, S. M. O'Brien, J. S. Rankin, and B. P. Griffith, "Less-invasive mitral valve operations: trends and outcomes from the Society of Thoracic Surgeons Adult Cardiac Surgery Database," *The Annals of thoracic surgery*, vol. 90, pp. 1401–8, 1410.e1; discussion 1408–10, Nov. 2010.

[81] A. J. Rastan, H. B. Bittner, J. F. Gummert, T. Walther, C. V. Schewick, E. Girdauskas, and F. W. Mohr, "On-pump beating heart versus off-pump coronary artery bypass surgery-evidence of pump-induced myocardial injury.," *European journal of cardio-thoracic surgery : official journal of the European Association for Cardio-thoracic Surgery*, vol. 27, pp. 1057–64, June 2005.

[82] E. Ferrari, N. Stalder, and L. K. von Segesser, "On-pump beating heart coronary surgery for high risk patients requiring emergency multiple coronary artery bypass grafting.," *Journal of cardiothoracic surgery*, vol. 3, p. 38, Jan. 2008.

[83] S. F. Katircioglu, F. Cicekcioglu, U. Tutun, A. I. Parlar, S. Babaroglu, U. Mungan, and A. Aksoyek, "On-pump beating heart mitral valve surgery without cross-clamping the aorta.," *Journal of cardiac surgery*, vol. 23, no. 4, pp. 307–11, 2006.

[84] T. Bottio, G. Rizzoli, L. Caprili, G. Nesseris, G. Thiene, and G. Gerosa, "Full-Sternotomy Off-Pump versus On-Pump Coronary Artery Bypass Procedures," *Texas Heart Institute Journal*, vol. 30, no. 4, pp. 261–267, 2001.

[85] G. D. Angelini, F. C. Taylor, B. C. Reeves, and R. Ascione, "Early and midterm outcome after off-pump and on-pump surgery in Beating Heart Against Cardioplegic Arrest Studies (BHACAS 1 and 2): a pooled analysis of two randomised controlled trials.," *Lancet*, vol. 359, pp. 1194–9, Apr. 2002.

[86] D. van Dijk, a. P. Nierich, E. W. Jansen, H. M. Nathoe, W. J. Suyker, J. C. Diephuis, W.-J. van Boven, C. Borst, E. Buskens, D. E. Grobbee, E. O. Robles de Medina, and P. P. de Jaegere, "Early Outcome After Off-Pump Versus On-Pump Coronary Bypass Surgery: Results From a Randomized Study," *Circulation*, vol. 104, pp. 1761–1766, Oct. 2001.

[87] D. Van Dijk, E. W. L. Jansen, R. Hijman, A. P. Neirich, J. C. Diephuis, K. G. M. Moons, J. R. Lahpor, C. Borst, A. M. A. Keizer, H. M. Nathoe, D. E. Grobbee, P. P. T. De Jaegere, and C. J. Kalkman, "Cognitive Outcome After Off-Pump and On-Pump Coronary Artery Bypass Graft Surgery," *Journal of American Medical Association*, vol. 287, no. 11, pp. 1405–1412, 2002.

[88] R. Ascione, C. T. Lloyd, M. J. Underwood, a. a. Lotto, a. a. Pitsis, and G. D. Angelini,

"Economic outcome of off-pump coronary artery bypass surgery: a prospective randomized study.," *The Annals of thoracic surgery*, vol. 68, pp. 2237–42, Dec. 1999.

[89] "http://www.neochord.com/."

[90] T. Feldman, E. Foster, M. Qureshi, B. Whisenant, J. Williams, D. Glower, and L. Mauri, "TCT-788 The EVEREST II Randomized Controlled Trial (RCT): Three Year Outcomes," *Journal of the American College of Cardiology*, vol. 60, pp. B229–B230, Oct. 2012.

[91] "http://www.abbottvascular.com/int/mitraclip.html#overview."

[92] "http://www.mitralign.com/,"

[93] C. W. Barlow, Z. a. Ali, E. Lim, J. B. Barlow, and F. C. Wells, "Modified technique for mitral repair without ring annuloplasty.," *The Annals of thoracic surgery*, vol. 75, pp. 298–300, Jan. 2003.

[94] P. Fundaro, P. M. Tartara, E. Villa, P. Fratto, S. Campisi, and E. O. Vitali, "Mitral Valve Repair: Is There Still a Place for Suture Annuloplasty?," *Asian Cardiovascular and Thoracic Annals*, vol. 15, pp. 351–358, Aug. 2007.

[95] J. Harnek, J. G. Webb, K.-H. Kuck, C. Tschope, A. Vahanian, C. E. Buller, S. K. James, C. P. Tiefenbacher, and G. W. Stone, "Transcatheter implantation of the MONARC coronary sinus device for mitral regurgitation: 1-year results from the EVOLUTION phase I study (Clinical Evaluation of the Edwards Lifesciences Percutaneous Mitral Annuloplasty System for the Treatment of Mitral R," *JACC. Cardiovascular interventions*, vol. 4, pp. 115–22, Jan. 2011.

[96] "http://www.edwards.com/."

[97] D. Maselli, F. Guarracino, F. Chiaramonti, F. Mangia, G. Borelli, and G. Minzioni, "Percutaneous mitral annuloplasty: an anatomic study of human coronary sinus and its

relation with mitral valve annulus and coronary arteries.," *Circulation*, vol. 114, pp. 377–80, Aug. 2006.

[98] E. Lansac, I. Di Centa, N. Al Attar, D. Messika-Zeitoun, R. Raffoul, A. Vahanian, and P. Nataf, "Percutaneous mitral annuloplasty through the coronary sinus: an anatomic point of view.," *The Journal of thoracic and cardiovascular surgery*, vol. 135, pp. 376–81, Feb. 2008.

[99] A. J. Choure, M. J. Garcia, B. Hesse, M. Sevensma, G. Maly, N. L. Greenberg, L. Borzi, S. Ellis, E. M. Tuzcu, and S. R. Kapadia, "In vivo analysis of the anatomical relationship of coronary sinus to mitral annulus and left circumflex coronary artery using cardiac multidetector computed tomography: implications for percutaneous coronary sinus mitral annuloplasty.," *Journal of the American College of Cardiology*, vol. 48, pp. 1938–45, Nov. 2006.

[100] S. Goldberg, R. van Bibber, J. Schofer, A. Ebner, T. Siminiak, U. Hoppe, M. Haude, J.-P. Herrman, S. Duffy, D. Reuter, and D. Kaye, "The frequency of coronary artery compression and management using a removable mitral annuloplasty device in the coronary sinus," *Journal of American College of Cardiology*, vol. 51, no. 10 Suppl B, p. 28, 2008.

[101] T. M. Peters, "Image-guidance for surgical procedures," *Physics in medicine and biology*, vol. 51, pp. R505–40, July 2006.

[102] Roentgen, "Uber eine neue Art von Strahlen (About a new type of radiation)," *Phys Med Gesellsch*, vol. 9, pp. 132–141, 1895.

[103] H. J. W. Dam, "The new marvel in photography," *McLure's Mag*, vol. 6, p. 403, 1896.

[104] J. Cox and R. Kirkpatrick, "The new photography with report of a case in which a bullet was photographed in the leg," *Montreal Med J.*, vol. 24, pp. 661–665, 1896.

[105] G. Anastasios, D. A. Gordon, Y. Mathieu, and I. Lipton, "Motion of both mitral valve leaflets: a cineroentgenographic study in intact dogs," *Journal of Applied Physiology*, vol. 39, no. 3, pp. 359–366, 1975.

[106] S. Saito, Y. Araki, A. Usui, T. Akita, H. Oshima, J. Yokote, and Y. Ueda, "Mitral valve motion assessed by high-speed video camera in isolated swine heart.," *European journal of cardio-thoracic surgery : official journal of the European Association for Cardio-thoracic Surgery*, vol. 30, pp. 584–91, Oct. 2006.

[107] G. S. Mak, A. J. Hill, F. Moisiuc, and S. C. Krishnan, "Variations in Thebesian valve anatomy and coronary sinus ostium: implications for invasive electrophysiology procedures.," *Europace : European pacing, arrhythmias, and cardiac electrophysiology : journal of the working groups on cardiac pacing, arrhythmias, and cardiac cellular electrophysiology of the European Society of Cardiology*, vol. 11, pp. 1188–92, Sept. 2009.

[108] D. R. Holmes, M. A. Wondrow, J. E. Gray, R. J. Vetter, J. L. Fellows, and P. R. Julsrud, "Effect of Pulsed Progressive Fluoroscopy on Reduction of Radiation Dose in the Cardiac Catheterization laboratory," *Journal of American College of Cardiology*, vol. 15, no. 1, pp. 159–162, 1990.

[109] K. Chida, H. Saito, H. Otani, M. Kohzuki, S. Takahashi, S. Yamada, K. Shirato, and M. Zuguchi, "Relationship between fluoroscopic time, dose-area product, body weight, and maximum radiation skin dose in cardiac interventional procedures.," *AJR. American journal of roentgenology*, vol. 186, pp. 774–8, Mar. 2006.

[110] J. T. Moore, M. W. A. Chu, B. Kiaii, D. Bainbridge, G. Guiraudon, C. Wedlake, M. Currie, M. Rajchl, R. V. Patel, and T. M. Peters, "A navigation platform for guidance of beating heart transapical mitral valve repair.," *IEEE transactions on bio-medical engineering*, vol. 60, pp. 1034–40, Apr. 2013.

[111] M. W. Chu, J. Moore, T. M. Peters, D. Bainbridge, D. McCarty, G. M. Guiraudon, C. Wedlake, P. Lang, M. Rajchl, M. E. Currie, R. C. Daly, and B. Kiaii, "Augmented reality image guidance improves navigation for beating heart mitral valve repair," *Innovations*, vol. 7, no. 4, pp. 274–281, 2012.

[112] C. J. Yeung, R. C. Susil, and E. Atalar, "RF Safety of Wires in Interventional MRI : Using a Safety Index," *Magnetic resonance in medicine*, vol. 193, no. September 2001, pp. 187–193, 2002.

[113] E. Altiok, M. Becker, S. Hamada, S. Reith, N. Marx, and R. Hoffmann, "Optimized guidance of percutaneous edge-to edge repair of the mitral valve using real-time 3-D transesophageal echocardiography," *Clinical research in cardiology : official journal of the German Cardiac Society*, vol. 100, pp. 675–81, Aug. 2011.

[114] C. A. Linte, J. White, R. Eagleson, G. M. Guiraudon, and T. M. Peters, "Virtual and augmented medical imaging environments: enabling technology for minimally invasive cardiac interventional guidance.," *IEEE reviews in biomedical engineering*, vol. 3, pp. 25–47, Jan. 2010.

[115] P. Milgram, H. Takemura, A. Utsumi, and F. Kishino, "Augmented Reality: A class of displays on the reality-virtuality continuum," in *SPIE 2351, Telemanipulator and Telepresence Technologies*, vol. 2351, pp. 282–292, 1994.

[116] C. A. Linte, J. Moore, C. Wedlake, D. Bainbridge, G. M. Guiraudon, D. L. Jones, and T. M. Peters, "Inside the beating heart: an in vivo feasibility study on fusing pre- and intra-operative imaging for minimally invasive therapy.," *International journal of computer assisted radiology and surgery*, vol. 4, pp. 113–23, Mar. 2009.

[117] C. Linte, M. Wierzbicki, J. Moore, G. Guiraudon, D. L. Jones, and T. M. Peters, "On enhancing planning and navigation of beating-heart mitral valve surgery using preoperative cardiac models.," *Conference proceedings : ... Annual International Confer-*

*ence of the IEEE Engineering in Medicine and Biology Society. IEEE Engineering in Medicine and Biology Society. Conference*, vol. 2007, pp. 475–8, Jan. 2007.

[118] D. Bainbridge, D. L. Jones, G. M. Guiraudon, and T. M. Peters, "Ultrasound image and augmented reality guidance for off-pump, closed, beating, intracardiac surgery.," *Artificial organs*, vol. 32, pp. 840–5, Nov. 2008.

[119] H. Liao, N. Hata, and T. Dohi, "Image-guidance for Cardiac Surgery Using Dynamic Autostereoscpic Display System," in *IEEE International Symposium on Biomedical Imaging*, pp. 265–268, 2004.

[120] S. De Buck, F. Maes, J. Ector, J. Bogaert, S. Dymarkowski, H. Heidbüchel, and P. Suetens, "An augmented reality system for patient-specific guidance of cardiac catheter ablation procedures.," *IEEE transactions on medical imaging*, vol. 24, pp. 1512–24, Nov. 2005.

[121] P. Lang, M. Rajchl, F. Li, and T. M. Peters, "Towards Model-Enhanced Real-Time Ultrasound Guided Cardiac Interventions," in *Proc. 2011 International Conference on Intelligent Computation and Bio-Medical Instrumentation*, pp. 89–92, Ieee, Dec. 2011.

[122] P. Rajiah and P. Schoenhagen, "The role of computed tomography in pre-procedural planning of cardiovascular surgery and intervention.," *Insights into imaging*, vol. 4, pp. 671–89, Oct. 2013.

[123] M. Carminati, M. Agnifili, C. Arcidiacono, N. Brambilla, C. Bussadori, G. Butera, M. Chessa, M. Heles, A. Micheletti, D. G. Negura, L. Piazza, A. Saracino, L. Testa, M. Tusa, and F. Bedogni, "Role of imaging in interventions on structural heart disease.," *Expert review of cardiovascular therapy*, vol. 11, pp. 1659–76, Dec. 2013.

[124] G. Wu, Q. Wang, J. Lian, and D. Shen, "Reconstruction of 4D-CT from a single free-breathing 3D-CT by spatial-temporal image registration," in *Information processing in medical imaging : proceedings of the conference*, vol. 22, pp. 686–98, Jan. 2011.

[125] M. P. Heinrich, M. Jenkinson, M. Bhushan, T. Matin, F. V. Gleeson, S. M. Brady, and J. a. Schnabel, "MIND: modality independent neighbourhood descriptor for multi-modal deformable registration," *Medical image analysis*, vol. 16, pp. 1423–35, Oct. 2012.

[126] B. C. Vemuri, J. Ye, Y. Chen, and C. M. Leonard, "Image registration via level-set motion : Applications to atlas-based segmentation," *Medical image analysis*, vol. 7, pp. 1–20, 2003.

[127] M. Wierzbicki, M. Drangova, G. Guiraudon, and T. Peters, "Validation of dynamic heart models obtained using non-linear registration for virtual reality training, planning, and guidance of minimally invasive cardiac surgeries.," *Medical image analysis*, vol. 8, pp. 387–401, Sept. 2004.

[128] M. Wierzbicki, M. Drangova, and G. Guiraudon, "Mapping Template Heart Models to Patient Data Using Image Registration," in *Medical Image Computing and Computer-Assisted Intervention*, pp. 671–678, 2004.

[129] N. S. Phatak, S. a. Maas, A. I. Veress, N. a. Pack, E. V. R. Di Bella, and J. a. Weiss, "Strain measurement in the left ventricle during systole with deformable image registration.," *Medical image analysis*, vol. 13, pp. 354–61, Apr. 2009.

[130] A. I. Veress, G. T. Gullberg, and J. A. Weiss, "Measurement of Strain in the Left Ventricle during Diastole with cine-MRI and Deformable Image Registration," *Journal of Biomechanical Engineering*, vol. 127, p. 1195, July 2005.

[131] W. Shi, X. Zhuang, H. Wang, S. Duckett, D. V. N. Luong, C. Tobon-gomez, K. Tung, P. J. Edwards, K. S. Rhode, R. S. Razavi, S. Ourselin, and D. Rueckert, "A Comprehensive Cardiac Motion Estimation Framework Using Both Untagged and 3-D Tagged MR Images Based on Nonrigid Registration," *IEEE transactions on medical imaging*, vol. 31, no. 6, pp. 1263–1275, 2012.

[132] H. Sundar, H. Litt, and D. Shen, "Estimating Myocardial Motion by 4D Image Warping," *Pattern Recognitioin*, vol. 42, no. 11, pp. 2514–2526, 2010.

[133] M. J. Ledesma-Carbayo, J. Kybic, M. Desco, A. Santos, M. Sühling, P. Hunziker, and M. Unser, "Spatio-temporal nonrigid registration for ultrasound cardiac motion estimation," *IEEE transactions on medical imaging*, vol. 24, pp. 1113–26, Sept. 2005.

[134] A. Elen, H. F. Choi, D. Loeckx, H. Gao, P. Claus, P. Suetens, F. Maes, and J. D'hooge, "Three-dimensional cardiac strain estimation using spatio-temporal elastic registration of ultrasound images: a feasibility study," *IEEE transactions on medical imaging*, vol. 27, pp. 1580–91, Nov. 2008.

[135] Y. Seo, T. Ishizu, Y. Enomoto, H. Sugimori, M. Yamamoto, T. Machino, R. Kawamura, and K. Aonuma, "Validation of 3-dimensional speckle tracking imaging to quantify regional myocardial deformation.," *Circulation. Cardiovascular imaging*, vol. 2, pp. 451–9, Nov. 2009.

[136] H. Geyer, G. Caracciolo, H. Abe, S. Wilansky, S. Carerj, F. Gentile, H.-J. Nesser, B. Khandheria, J. Narula, and P. P. Sengupta, "Assessment of myocardial mechanics using speckle tracking echocardiography: fundamentals and clinical applications," *Journal of the American Society of Echocardiography : official publication of the American Society of Echocardiography*, vol. 23, pp. 351–369, Apr. 2010.

[137] R. Shams, P. Sadeghi, R. Kennedy, and R. Hartley, "Parallel computation of mutual information on the GPU with application to real-time registration of 3D medical images," *Computer Methods and Programs in Biomedicine*, vol. 99, no. 2, pp. 133–146, 2009.

[138] R. Shams, P. Sadeghi, R. A. Kennedy, and R. I. Hartley, "A Survey of Medical Image Registration on Multicore and the GPU," *IEEE Signal Processing Magzine*, no. March, pp. 50–60, 2010.

[139] A. Eklund, P. Dufort, D. Forsberg, and S. M. Laconte, "Medical image processing on the GPU - Past, present and future," *Medical image analysis*, vol. 17, pp. 1073–1094, June 2013.

[140] R. J. Schneider, D. P. Perrin, N. V. Vasilyev, G. R. Marx, P. J. Del Nido, and R. D. Howe, "Real-time image-based rigid registration of three-dimensional ultrasound," *Medical image analysis*, vol. 16, pp. 402–14, Feb. 2012.

[141] O. Kutter, W. Wein, and N. Navab, "Multi-modal registration based ultrasound mosaicing," *Medical image computing and computer-assisted intervention : MICCAI ... International Conference on Medical Image Computing and Computer-Assisted Intervention*, vol. 12, pp. 763–70, Jan. 2009.

[142] X. Huang, J. Ren, G. Guiraudon, D. Boughner, and T. M. Peters, "Rapid dynamic image registration of the beating heart for diagnosis and surgical navigation," *IEEE transactions on medical imaging*, vol. 28, pp. 1802–14, Nov. 2009.

[143] X. Huang, J. Moore, G. Guiraudon, D. L. Jones, D. Bainbridge, J. Ren, and T. M. Peters, "Dynamic 2D ultrasound and 3D CT image registration of the beating heart," *IEEE transactions on medical imaging*, vol. 28, pp. 1179–89, Aug. 2009.

[144] F. Li, P. Lang, M. Rajchl, E. C. S. Chen, G. Guiraudon, and T. M. Peters, "Towards real-time 3D US-CT registration on the beating heart for guidance of minimally invasive cardiac interventions," in *Proc. SPIE 8316, Medical Imaging 2012* (D. R. Holmes III and K. H. Wong, eds.), vol. 8316, p. 831615, Feb. 2012.

[145] F. P. Li, M. Rajchl, J. A. White, A. Goela, and T. M. Peters, "Towards CT Enhanced Ultrasound Guidance for Off-pump Beating Heart Mitral Valve Repair," in *Augmented Reality Environments for Medical Imaging and Computer-Assisted Interventions Lecture Notes in Computer Science, Volume 8090*, pp. 136–143, 2013.

[146] Y. Okumura, B. D. Henz, S. B. Johnson, T. J. Bunch, C. J. O'Brien, D. O. Hodge, A. Altman, A. Govari, and D. L. Packer, "Three-dimensional ultrasound for image-guided mapping and intervention: methods, quantitative validation, and clinical feasibility of a novel multimodality image mapping system," *Circulation. Arrhythmia and electrophysiology*, vol. 1, pp. 110–9, June 2008.

[147] W. Zhang, J. Noble, and J. Brady, "Real Time 3-D Ultrasound to MR Cardiovascular Image Registration Using a Phase-Based Approach," *3rd IEEE International Symposium on Biomedical Imaging: Macro to Nano, 2006.*, pp. 666–669, 2006.

[148] H. Sundar, A. Khamene, L. Yatziv, and C. Xu, "Automatic Image-Based Cardiac and Respiratory Cycle Synchronization and Gating of Image Sequences," in *Medical image computing and computer-assisted intervention*, pp. 381–388, 2009.

[149] V. Kurra, S. R. Kapadia, E. M. Tuzcu, S. S. Halliburton, L. Svensson, E. E. Roselli, and P. Schoenhagen, "Pre-procedural imaging of aortic root orientation and dimensions: comparison between X-ray angiographic planar imaging and 3-dimensional multidetector row computed tomography.," *JACC. Cardiovascular interventions*, vol. 3, pp. 105–13, Jan. 2010.

[150] D. Ni, Y. Qul, X. Yang, Y. P. Chui, T.-T. Wong, S. S. M. Ho, and P. A. Heng, "Volumetric ultrasound panorama based on 3D SIFT," *Medical image computing and computer-assisted intervention : MICCAI ... International Conference on Medical Image Computing and Computer-Assisted Intervention*, vol. 11, pp. 52–60, Jan. 2008.

[151] G. Carneiro and J. C. Nascimento, "Multiple dynamic models for tracking the left ventricle of the heart from ultrasound data using particle filters and deep learning architectures," *2010 IEEE Computer Society Conference on Computer Vision and Pattern Recognition*, pp. 2815–2822, June 2010.

[152] R. J. Schneider, D. P. Perrin, N. V. Vasilyev, G. R. Marx, P. J. del Nido, and R. D.

Howe, "Mitral annulus segmentation from four-dimensional ultrasound using a valve state predictor and constrained optical flow," *Medical image analysis*, vol. 16, pp. 497–504, Feb. 2012.

[153] R. J. Schneider, D. P. Perrin, N. V. Vasilyev, G. R. Marx, P. J. del Nido, and R. D. Howe, "Mitral annulus segmentation from 3D ultrasound using graph cuts," *IEEE transactions on medical imaging*, vol. 29, pp. 1676–87, Sept. 2010.

[154] J. P. W. Pluim, J. B. A. Maintz, and M. a. Viergever, "Mutual-information-based registration of medical images: a survey," *IEEE transactions on medical imaging*, vol. 22, pp. 986–1004, Aug. 2003.

[155] M. P. Heinrich, M. Jenkinson, S. J. M. Brady, and J. A. Schnabel, "Textural Mutual Information Based on Cluster Trees for Multimodal Deformable Registration," in *2012 9th IEEE International Symposium on Biomedical Imaging (ISBI)*, no. i, pp. 2–5, 2012.

[156] P. Thévenaz and M. Unser, "Optimization of mutual information for multiresolution image registration," *IEEE transactions on image processing : a publication of the IEEE Signal Processing Society*, vol. 9, pp. 2083–99, Jan. 2000.

[157] F. Maes, A. Collignon, D. Vandermeulen, G. Marchal, and P. Suetens, "Multimodality image registration by maximization of mutual information," *IEEE transactions on medical imaging*, vol. 16, pp. 187–98, Apr. 1997.

[158] D. Rueckert, M. J. Clarkson, D. L. G. Hill, and D. J. Hawkes, "Non-rigid Registration Using Higher-Order Mutual Information," in *Proceedings of SPIE Vol. 3979* (K. M. Hanson, ed.), vol. V, pp. 438–447, Mar. 2000.

[159] Z. Yi and S. Soatto, "Multimodal registration via spatial-context mutual information," *Information processing in medical imaging : proceedings of the ... conference*, vol. 22, pp. 424–35, Jan. 2011.

[160] D. Loeckx, P. Slagmolen, F. Maes, D. Vandermeulen, and P. Suetens, "Nonrigid Image Registration Using Conditional Mutual Information," *IEEE transactions on medical imaging*, vol. 29, no. 1, pp. 19–29, 2010.

[161] M. Wierzbicki and T. M. Peters, "Determining Epicardial Surface Motion Using Elastic Registration : Towards Virtual Reality Guidance of Minimally Invasive Cardiac Interventions," in *Medical Image Computing and Computer-Assisted Intervention*, pp. 722–729, 2003.

[162] R. I. Ionasec, I. Voigt, B. Georgescu, Y. Wang, H. Houle, F. Vega-Higuera, N. Navab, and D. Comaniciu, "Patient-specific modeling and quantification of the aortic and mitral valves from 4-D cardiac CT and TEE," *IEEE transactions on medical imaging*, vol. 29, pp. 1636–51, Sept. 2010.

[163] D. Shen, H. Sundar, Z. Xue, Y. Fan, and H. Litt, "Consistent estimation of cardiac motions by 4D image registration," *Medical image computing and computer-assisted intervention : MICCAI ... International Conference on Medical Image Computing and Computer-Assisted Intervention*, vol. 8, pp. 902–10, Jan. 2005.

[164] T. Mansi, X. Pennec, M. Sermesant, H. Delingette, and N. Ayache, "iLogDemons: A Demons-Based Registration Algorithm for Tracking Incompressible Elastic Biological Tissues," *International Journal of Computer Vision*, vol. 92, pp. 92–111, Nov. 2010.

[165] W. Wein, S. Brunke, A. Khamene, M. R. Callstrom, and N. Navab, "Automatic CT-ultrasound registration for diagnostic imaging and image-guided intervention.," *Medical image analysis*, vol. 12, pp. 577–85, Oct. 2008.

[166] Y. Sun, S. Kadoury, Y. Li, M. John, J. Resnick, G. Plambeck, R. Liao, F. Sauer, and C. Xu, "Image guidance of intracardiac ultrasound with fusion of pre-operative images," *Medical image computing and computer-assisted intervention : MICCAI ... Interna-*

*tional Conference on Medical Image Computing and Computer-Assisted Intervention*, vol. 10, pp. 60–7, Jan. 2007.

[167] J. Ector, S. De Buck, J. Adams, S. Dymarkowski, J. Bogaert, F. Maes, and H. Heidbüchel, "Cardiac three-dimensional magnetic resonance imaging and fluoroscopy merging: a new approach for electroanatomic mapping to assist catheter ablation.," *Circulation*, vol. 112, pp. 3769–76, Dec. 2005.

[168] P. Lang, P. Seslija, M. W. a. Chu, D. Bainbridge, G. M. Guiraudon, D. L. Jones, and T. M. Peters, "US-fluoroscopy registration for transcatheter aortic valve implantation," *IEEE transactions on bio-medical engineering*, vol. 59, pp. 1444–53, May 2012.

[169] A. Jain, L. Gutierrez, and D. Stanton, "3D TEE Registration with X-Ray Fluoroscopy for Interventional Cardiac Applications," in *FIMH '09 Proceedings of the 5th International Conference on Functional Imaging and Modeling of the Heart*, pp. 321–329, 2009.

[170] C. R. Hatt, M. A. Speidel, and A. N. Raval, "Efficient feature-based 2D/3D registration of transesophageal echocardiography to x-ray fluoroscopy for cardiac interventions," in *SPIE Medical Imaging* (Z. R. Yaniv and D. R. Holmes, eds.), vol. 9036, p. 90361J, Mar. 2014.

[171] "http://www.healthcare.philips.com/main/products/interventional_xray/product/ interventional_cardiology/echonavigator/."

# Chapter 2

# Generation of Synthetic 4D Cardiac CT Images for Guidance of Minimally Invasive Beating Heart Interventions

This chapter is adapted from the papers:

- Feng P. Li, James A. White, Martin Rajchl, Aashish Goela, and Terry M. Peters, Generation of Synthetic 4D Cardiac CT Images by Deformation from Cardiac Ultrasound. In: Workshop on Augmented Environments for Computer-Assisted Interventions (AE-CAI). Lecture Notes in Computer Science. Springer Berlin / Heidelberg, 2012

- Feng P. Li, Martin Rajchl, James A. White, Aashish Goela, and Terry M. Peters, Generation of Synthetic 4D Cardiac CT Images for Guidance of Minimally Invasive Beating Heart Interventions. Information Processing in Computer- Assisted Interventions (IPCAI), 2013

## 2.1 Introduction

Compared to conventional cardiac surgery procedures, minimally invasive beating heart interventions limit the need for thoracic trauma and remove the need to arrest the heart [1, 2]. While these approaches have grown in popularity recently, they are often limited by the lack of a direct view of surgical targets and/or tools, a challenge that is compounded by potential movements of the target during the cardiac cycle. For this reason, sophisticated image-guided navigation systems are required to assist in procedural efficiency and therapeutic success [3].

For minimally invasive beating heart surgical procedures, the optimal navigation system would show both the pertinent cardiac anatomy and the dynamic motion of the surgical targets throughout the cardiac cycle. It should also be cost efficient and be easily integrated into standard workflow within the operating room. Such a goal is however difficult to accomplish successfully using a single imaging modality. For example, fluoroscopy can only provide 2D projection images and barely shows the anatomical structures. Intra-operative MRI has the capability of displaying cardiac anatomy and motion dynamically during interventions [4], but is very expensive, requires developments of novel, non-ferromagnetic tools and devices, and is unavailable in most institutions. On the other hand, intra-operative trans-esophageal ultrasound is more accessible and clinically feasible, but its field of view remains relatively restricted. Furthermore, artifacts, such as acoustic shadowing [5], can limit the capacity to accurately develop volumetric models. Another cardiac imaging technique, retrospectively gated CT, can provide dynamic volumetric imaging, but the temporal resolution is limited by the gantry rotation speed and radiation dose exposure can be many times that of a static scan [6, 7]. Accordingly, no single imaging modality appears to be ideal for the provision of 4D cardiac modeling to plan and guide cardiovascular procedures.

Some previous work has suggested the use of pre-operative high spatial resolution CT and intra-operative 4D ultrasound images within a navigation system [8, 9], both of which are commonly used during the standard clinical workflow for cardiac interventions. However, prior work [10] has shown that registering a 4D ultrasound sequence to a single, static CT image will

result in high target registration errors (TRE) at cardiac phases other than that represented by the initial CT scan, because of intra-cycle cardiac morphology changes. To overcome this problem without introducing extra radiation dose to the patient, we propose a solution that would allow a high-resolution 4D synthetic CT dataset be derived from a single 3D CT being iteratively deformed to create a dynamic 4D sequence using 4D ultrasound data as a target. These pre-operatively generated images would be employed to provide a high quality 4D anatomical context through visualization of some or all structural components spatially co-registered (and ECG-synchronized) to the patient using standard intra-operative imaging, such as 2D/3D ultrasound. With these real-time registration techniques, an augmented reality framework can be developed and integrated into navigation platforms to provide critical information to surgeons at the time of intervention.

Much work has been performed towards estimating cardiac motion in ultrasound and MRI images by using non-rigid registration [11–14], with most of the reports suggesting that the estimated motion can be used for the assessment of both cardiac motion and mechanics. In this paper, we introduce a new concept that attempts to combine the motion estimation obtained from dynamic ultrasound images with a static CT image, to generate a synthetic dynamic CT dataset. These synthetic CT images can take advantage of the higher temporal resolution of the ultrasound images upon which they are modeled. By introducing these synthetic CT images into a navigation system, we anticipate improved model-to-patient registration and more intuitive visualization of therapeutic targets for beating heart surgeries.

Validation was performed by comparing the synthetic CT images to ground truth dynamic CT images. Quantitiative metrics were obtained by computing the Dice Similarity Coeffcients (DSC) and Root Mean Square (RMS) errors for the entire left ventricle.

## 2.2 Methods

### 2.2.1 Non-local Means Filtering for Ultrasound Images

In an effort to improve the smoothness of the deformation fields obtained from non-rigid registrations between ultrasound images, a restoration step is first applied on the ultrasound images. However, restoration of ultrasound images is known to be very challenging, because speckle, as an inherent characteristic of ultrasound images, is tissue-dependent and cannot be easily modeled. The original patch-based nonlocal recovery paradigm was proposed by Buades et al. [15] The general assumption behind this approach is that for those points in an image representing the same feature, similarity should not only be observed in intensities of the pixels, but also in the patterns surrounding them. In 2009, Coupé et al. [16] adopted this idea and proposed a nonlocal means based speckle filter to perform speckle reduction, and reported competitive results on both synthetic and patient data. In this chapter, we use this method to smooth the ultrasound images before the non-rigid registration.

Suppose we have an 3D image $\Omega$ with each point in the image being denoted as $p_i(x_i, y_i, z_i)$ and the intensity of $p_i$ is denoted as $I(p_i)$. A cubic neighbourhood area centred at $p_i$ with a length of $2r_d+1$ is defined as $N(p_i) := \left\{ p_j(x_j, y_j, z_j) \;\middle|\; |x_j - x_i| \le r_d,\ |y_j - y_i| \le r_d,\ |z_j - z_i| \le r_d \right\}$ and a cubic search area centred at $p_i$ with a length of $2r_s + 1$ is defined with the same manner as $S(p_i) := \left\{ p_j(x_j, y_j, z_j) \;\middle|\; |x_j - x_i| \le r_s,\ |y_j - y_i| \le r_s,\ |z_j - z_i| \le r_s \right\}$.

Then, for each point $p_j$ in the search area $S(pi)$, the non-local means filter compare the neighbourhood $N(p_j)$ to $N(p_i)$ and compute a weight term $w(p_j, p_i)$ as

$$w(p_j, p_i) = \frac{1}{Z_i} \exp - \frac{\left\| I\left(N(p_j)\right) - I\left(N(p_i)\right) \right\|^2}{h^2}, \tag{2.1}$$

where $Z_i$ is a normalization constant that ensures the sum of the weights equals to unity, $h$ is the parameter controlling the decay of the exponential function, and $\left\| I\left(N(p_j)\right) - I\left(N(p_i)\right) \right\|$ is the $L_2$-norm between the intensity vector $I\left(N(p_j)\right)$ and $I\left(N(p_i)\right)$ convolved with a Gaussian kernel.

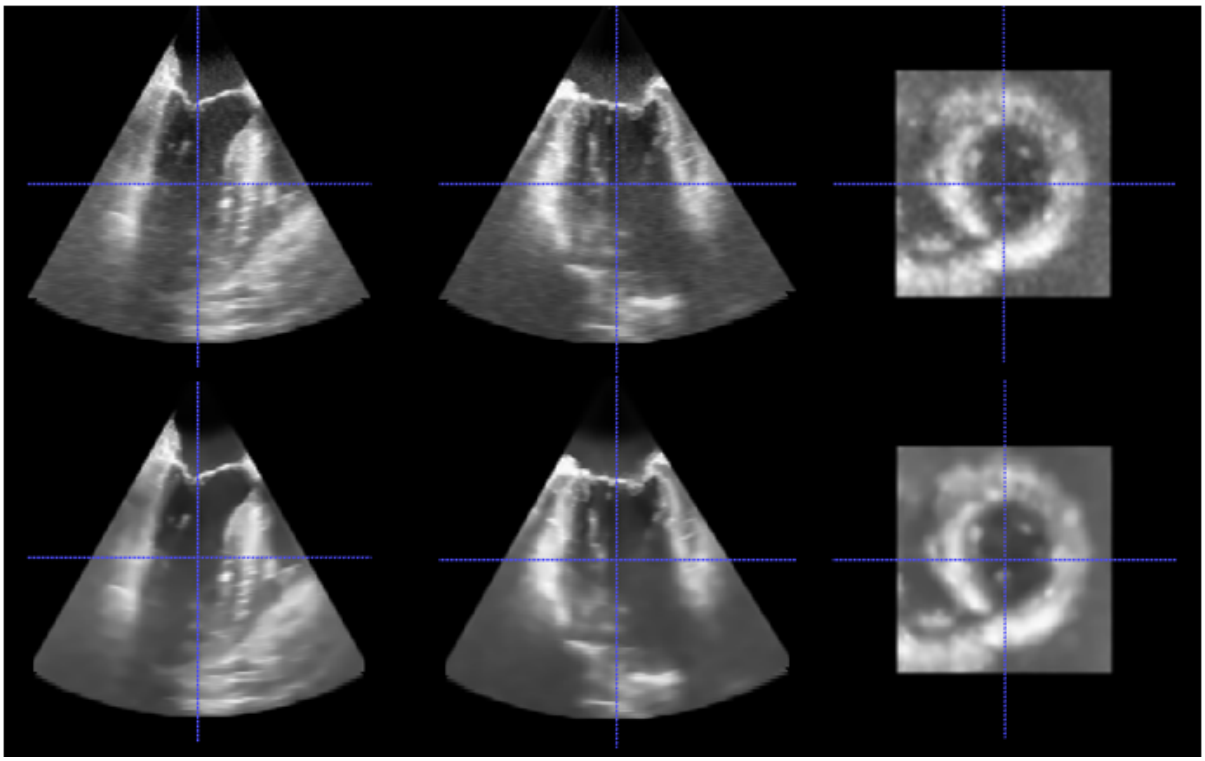

Figure 2.1: An example of ultrasound images smoothed by nonlocal means based filtering. First row: original TEE image. Second row: nonlocal means smooth image. Speckle is greatly reduced, while anatomical features are mainly retained in the smoothed images.

The filtered intensity value $I'(p_i)$ is then computed as a weighted sum of all the points in the search area $S(p_i)$. That is

$$I'(p_i) = \sum_{p_j \in S(p_j)} w(p_j, p_i) I(p_j), \tag{2.2}$$

Since the nonlocal means methods compare patches around pixels instead of pixels themselves, the computational complexity becomes a common drawback of those methods. To perform such a method on a $n^3$ volume with a search volume size $m^3$ and a patch size $p^3$, the computational complexity can be $O(n^3 m^3 p^3)$. However, since the method described in [16] treats each voxel independently, we were able to parallelize the method with a GPU implementation and greatly reduced the computation time. One example of an ultrasound image, filtered using nonlocal means with search volume size $9^3$ and patch size $7^3$ , is shown in Figure 2.1.

### 2.2.2 Fast Free Form (F3D) Registration Approach

The F3D approach [17] is an efficient non-rigid registration approach based on the well known Free Form Deformation (FFD) algorithm [18]. Compared to the elastic deformation model based algorithms, e.g. Demons [19], and optical flow based algorithms [20], the advantages of the FFD based approach are that it does not require linear relationship of tissue intensities between images, can deal with large image deformations, which is important for cardiac motion analysis, and provides smooth deformation fields.

The F3D approach uses a transformation model $T$ that consists of a global affine transformation $T_{global}$ and a local B-spline based transformation $T_{local}$. The global transformation can be written as

$$T_{global}(x,y,z) = \begin{pmatrix} a_{11} & a_{12} & a_{13} \\ a_{21} & a_{22} & a_{23} \\ a_{31} & a_{32} & a_{33} \end{pmatrix} \begin{pmatrix} x \\ y \\ z \end{pmatrix} + \begin{pmatrix} t_1 \\ t_2 \\ t_3 \end{pmatrix}, \tag{2.3}$$

while the local transformation is achieved by defining and manipulating a mesh of control points $\phi(x,y,z)$ overlaid on the image domain to compute B-spline curves that indicates the transformation of each individual voxel (Equations 2.4).

$$T_{local}(x,y,z) = \sum_{l=0}^{3}\sum_{m=0}^{3}\sum_{n=0}^{3} B_l(u)B_m(v)B_n(w)\phi_{i+l,j+m,k+n}, \tag{2.4}$$

where $i = \lfloor x/n_x \rfloor - 1$, $j = \lfloor y/n_y \rfloor - 1$, $k = \lfloor z/n_z \rfloor - 1$, $u = x/n_x - \lfloor x/n_x \rfloor$, $v = y/n_y - \lfloor y/n_y \rfloor$, $w = z/n_z - \lfloor z/n_z \rfloor$ and $B_p, p := l, m, .n$ are the $p$th basis function of the B-spline [21] (Equation 2.5).

$$
\begin{aligned}
B_0(u) &= (1-u)^3/6 \\
B_1(u) &= (3u^3 - 6u^2 + 4)/6 \\
B_2(u) &= (-3u^3 + 3u^2 + 3U + 1)/6 \\
B_3(u) &= u^3/6
\end{aligned}
\tag{2.5}
$$

The cost function used to find the optimized transformation contains an image similarity term $C_{similarity}$ and a deformation field smoothness term $C_{smooth}$ as shown below:

$$
C(T) = C_{similarity}(I_{fixed}, T(I_{moving})) + \lambda C_{smooth}(T), \tag{2.6}
$$

where the similarity term is defined as the measurement of the similarity metric, in this chapter the normalized mutual information [22], between the transformed image $T(I_{moving})$ and the fixed image $I_{fixed}$. The smoothness term itself is defined as

$$
C_{smooth} = \frac{1}{V}\int_0^X \int_0^Y \int_0^Z \left[\left(\frac{\partial^2 T}{\partial x^2}\right)^2 + \left(\frac{\partial^2 T}{\partial y^2}\right)^2 + \left(\frac{\partial^2 T}{\partial z^2}\right)^2 + 2\left(\frac{\partial^2 T}{\partial x \partial y}\right)^2 + 2\left(\frac{\partial^2 T}{\partial x \partial z}\right)^2 + 2\left(\frac{\partial^2 T}{\partial y \partial z}\right)^2\right], \tag{2.7}
$$

where $V$ is the volume of the image. The parameter $\lambda$ determines the weight of the smoothness term, which is manually tuned as the bending energy (see Table 2.1) in this project for tracking large deformation as well as maintaining smooth deformation fields.

The optimization procedure is performed by a gradient descent approach. To improve the computational efficiency, a multi-resolution strategy [23] is used and a parallel implementation [17] is developed for the local transformation optimization.

### 2.2.3 Generating Synthetic CT Images

For the generation of a synthetic CT (synCT) series, we require a 3D ultrasound sequence (usually TEE), that covers at least one complete cardiac cycle, and a single static CT image

from the same patient. For the purpose of mitral valve repair, we suggest that the CT images cover the entire heart and that the TEE images are acquired as a mid-esophageal (ME) 4-chamber or 2-chamber view, that at least contains the entire left ventricle and the mitral valve.

### Temporal Matching of Ultrasound and CT Image Series

First, one ultrasound image, at the same or closest cardiac phase to that of the CT volume, is selected from the 4D US sequence to act as the reference image to be registered to the CT (see Figure 2.2). Since a prospectively gated CT scan requires that the user first selects a particular cardiac phase (e.g. mid-diastole) for data acquisition, the cardiac phase of the static CT image is usually known. The proper phase information of the TEE images can be obtained via ECG or image-based gating. This temporal alignment is important to ensure similarity of the heart motion in the reference and CT image.

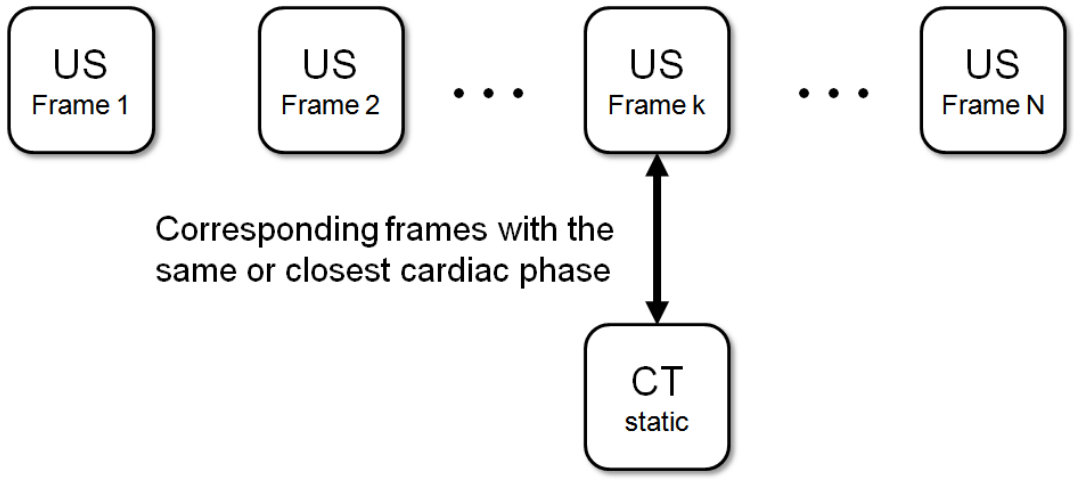


Figure 2.2: Finding the US Image with the corresponding cardiac phase as the static CT image

### Initial Rigid Registration

The reference US image is then rigidly registered to the CT image for initialization. In this study, this step is performed by employing an iterative closest point (ICP) algorithm [24] using surfaces of the left ventricles (LV) from both modalities and subsequent rapid image-based

registration step for robustness [22]. The 4D US series is then resampled using linear interpolation into the CT images reference frame via the transformation obtained from this initial registration.

### Obtaining Deformation Fields of the Heart Motion

The third step is to perform non-rigid registration between the 4DUS image frames to obtain the image deformations that represent the cardiac motion (see Figure 2.3). For this purpose we employ a GPU-accelerated Fast Free-Form (F3D) multi-level deformable registration [17] approach with normalized mutual information (NMI) as the similarity metric. Deformable registration is performed sequentially between adjacent images starting from the reference image. Here, the reference image is used as the floating image, while the following frame in the sequence is the target image for the initial registration. This image becomes the new floating image and its subsequent image becomes the new target image until all deformations between US frames are obtained. This process results in a series of deformations that describe the heart motion throughout one complete cardiac cycle [13].

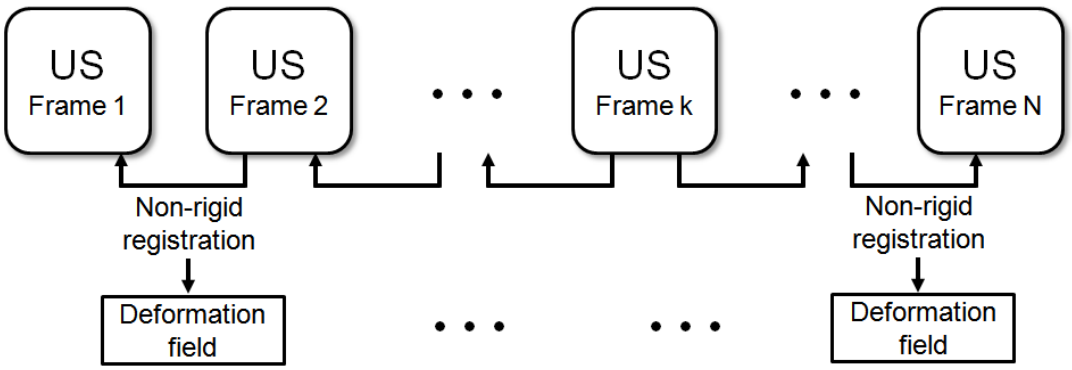


Figure 2.3: Performing non-rigid registration between US images to obtain deformation fields

### Generation of A Synthetic Dynamic CT Series

The obtained deformations are iteratively applied to the static CT image and its deformed descendants to create a sequence of synCT images that with the cardiac motion derived from

the TEE images (see Figure 2.4).

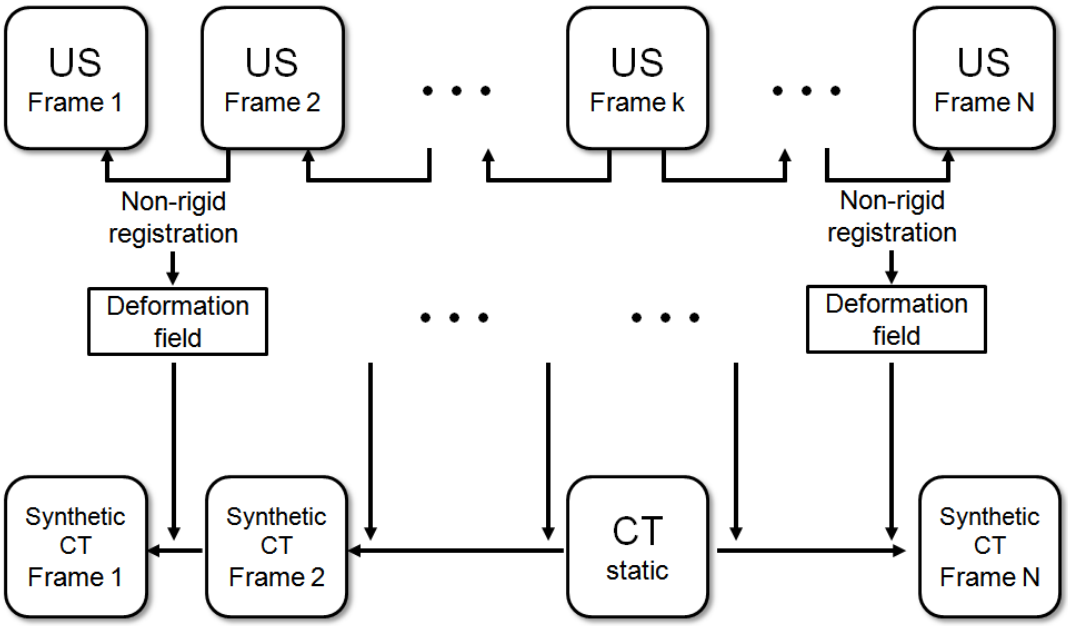


Figure 2.4: Applying obtained deformation fields to the static CT image to generate synCT images

## 2.3 Experiments

### 2.3.1 Image Data Acquisition

Images employed in this study were collected retrospectively under a protocol approved by the the Research Ethics Board of Western University, London, ON. Image data of patients (N = 10) undergoing valve repair were collected and subsequently anonymized before being prepared for processing. Each dataset contains a series of dynamic CT images obtained from retrospectively gated CT scans and reconstructed as ten frames per cardiac cycle with the first frame in the sequence at mid-diastole. Additionally, patient-specific pre-operative 4D TEE images of 2-chamber or 4-chamber views was acquired at 25Hz. The dimensions and voxel spacing of the dynamic CT is about $512\times512\times150$ voxels at $0.4\times0.4\times1.3(mm)$, while that of the TEE images is about $200\times200\times180$ voxels at $0.8\times0.8\times0.7(mm)$. CT images were acquired

on a GE Lightspeed 7-VCT scanner (GE Heathcare, Waukesha, WI, USA) and the ultrasound images on a Philips iE33 xMATRIX Echocardiography System (Philips Healthcare, Andover, MA, USA) with a X7-2t probe. The 4D TEE series was acquired to cover at least an entire cardiac cycle. All datasets fulfilled these requirements and none had to be excluded.

### 2.3.2 Validation Metrics Employed

The Dice Similarity Coefficient (DSC) is a measure of mean region overlap between region ($R_A$) and the reference region ($R_B$), using the formula

$$DSC = \frac{2(R_A \cap R_B)}{R_A + R_B} \tag{2.8}$$

Further a root-mean-squared error (RMSE) between surfaces A and B is defined as

$$RMSE = \sqrt{\frac{\sum_{i=1}^{N}(a_i - b_i)^2}{N}} \tag{2.9}$$

where $a_i \in A$ and $b_i \equiv \arg\min_{b_k \in B} \|b_k - a_i\|$. The RMSE serves as a distance-based metric.

### 2.3.3 Validation of Generation of Synthetic CT Series

To validate the suitability of the synthetically generated CT images the first CT frame of each dynamic CT (dynCT) series was chosen as the reference image from which a synCT sequence was constructed. An anatomical region important to the navigation task is manually segmented by an expert user from both the synCT and its corresponding ground truth dynCT series. The DSC and RMSE measures are calculated to determine the accuracy of the proposed method in generating proper motion of cardiac anatomical structures. The blood pool of the LV was chosen as the region to be validated because of its common involvement in navigation tasks in intra-cardiac image-guided interventions and its vicinity to the aortic and mitral valve. In addition, it was entirely visible in the 4D TEE series throughout the cardiac cycle. Since synCT and dynCT images have different frame rates, for each dynCT image, a synCT image with the

closest cardiac phase to it was selected for comparison. We assume the synCT images present the same cardiac phase as the corresponding TEE images, so the selection was performed with the same approach described in section 2.2.3.

### 2.3.4 Parameter Tuning

All the parameters were manually tuned to achieve good and stable accuracy for all the patients. The tuning was based on the five of the patient datasets. The values used for the parameters in this paper are listed below:

Table 2.1: Parameters and their values used in F3D Registration

| | |
|---|---|
| Number of level in the pyramidal approach | 9 |
| Control point spacing in the last level | 2.5 mm |
| Bending energy coefficient | 0.005/1 |

As mentioned previously, we use a multi-resolution pyramidal approach that employs a small number of control points with large spacing to analysis global deformation first and then iteratively increases the number of control points to track local detailed deformation. In each iteration, new control points are added to the centre of two existing control points along each axis, which means the new control point spacing is exactly half of that in the previous iteration. The number of level in the table indicates the number of iterations performed in this multi-resolution approach. The control point spacing in the last level determines the smallest level of deformation that can be tracked. The bending energy coefficient is defined in the cost function (Equation 2.6) and determines the trade-off between deformation and smoothness.

## 2.4 Results

### 2.4.1 Visual Results

Figure 2.5 shows one example set of synthetic CT images covering one complete cardiac cycle compared to its corresponding real dynamic CT images. It can be seen that the left ventricle first contracts and then dilates. The deformation of the left atrium can also be observed, although this is not as obvious. The right ventricle and right atrium do not show much deformation, because the TEE images we used did not cover these regions, and so no motion information can be obtained from the TEE images for those two areas. While this is a potential limitation of this approach, from a surgical perspective, one is only interested in the cardiac motion in the vicinity of the target, i.e. left ventricle together with the mitral valve, and the deformation of the right ventricle and right atriums not of major concern.

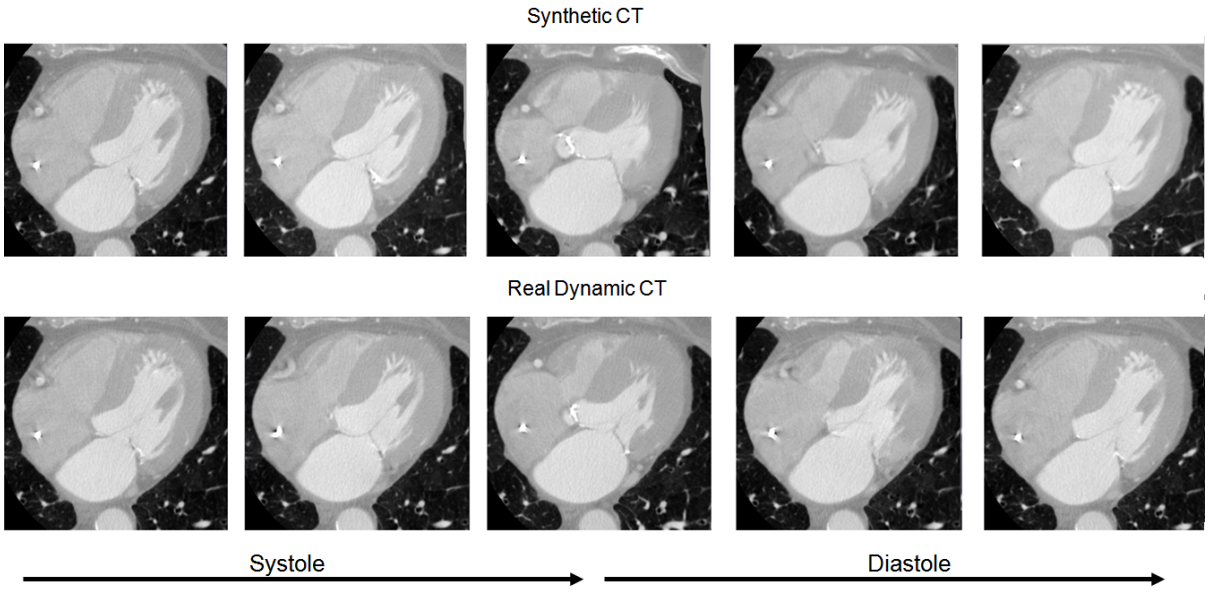


Figure 2.5: One example showing the comparison between the synthetic CT and the corresponding real dynamic CT covering one cardiac cycle

Figure 2.6 shows an example set of segmented LVs from dynCT and synCT images. It can be observed that the synCT images represent similar LV deformation as that in the dynCT images for most of the frames through the entire cardiac cycle. However, the deformation at

end-systole was underestimated (Numerical results in Section 2.4.2).

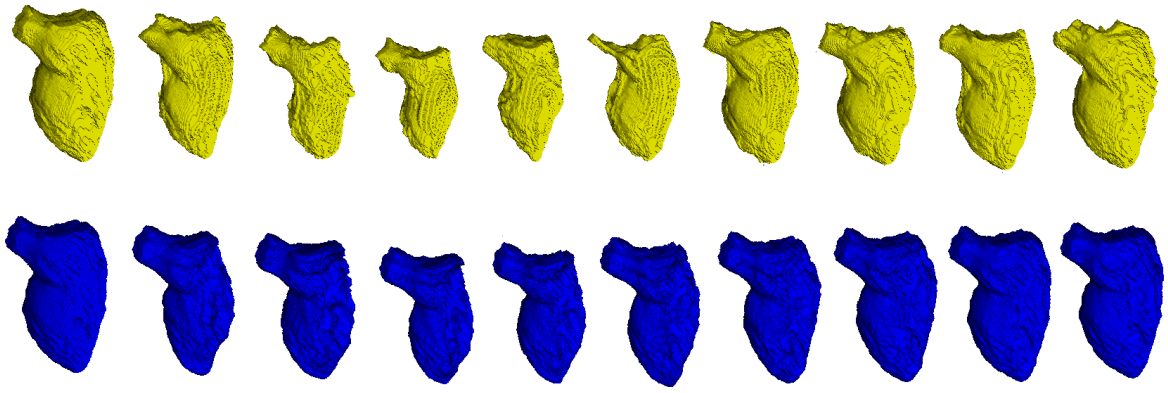

Figure 2.6: An example manually segmented LV from dynCT and synCT images, showing the contraction and dilation within one cardiac cycle. First row: surfaces from original dynCT images. Second row: surfaces from synCT images

### 2.4.2 Numerical Validation of LV Comparison

The numerical evaluation of suitability of the synCT images is performed by comparing them to the actual dynCT images generated from the retrospectively gated CT scans. Although our major purpose is not to generate pathologically "realistic" images that can be used for diagnosis, but rather images that are appropriate for navigation, we found it helpful to examine the regional correspondences between synthetic and real versions.

Table 2.2 and Table 2.3 show the DSC and the RMSE between the left ventricles of corresponding synthetic CT images and real dynamic images. The DSC shows the overlap of the entire left ventricle volume, whereas the RMSE shows the surface distance between the walls of the left ventricles.

The overall DSC for all the patients is 0.83±0.05 with the overall RMSE being 2.99±0.78mm. We also computed the mean DSC and RMSE for each patient and each cardiac phase (# of frames) respectively, demonstrating that for all but two of the patients, the mean DSCs are above 80%. With respect to the cardiac phases, it is apparent that the accuracy is better for the

Table 2.2: DSC between synthetic and original CT images

| # of frames | 2 | 3 | 4 | 5 | 6 | 7 | 8 | 9 | 10 | Mean±Std |
|---|---|---|---|---|---|---|---|---|---|---|
| Patient 1 | 0.88 | 0.87 | 0.84 | 0.84 | 0.84 | 0.87 | 0.89 | 0.92 | 0.90 | 0.87± 0.03 |
| Patient 2 | 0.88 | 0.87 | 0.85 | 0.84 | 0.84 | 0.90 | 0.91 | 0.91 | 0.88 | 0.88± 0.03 |
| Patient 3 | 0.82 | 0.75 | 0.73 | 0.72 | 0.73 | 0.73 | 0.79 | 0.79 | 0.79 | 0.76± 0.04 |
| Patient 4 | 0.91 | 0.89 | 0.88 | 0.86 | 0.86 | 0.85 | 0.87 | 0.89 | 0.89 | 0.88± 0.02 |
| Patient 5 | 0.88 | 0.79 | 0.79 | 0.81 | 0.78 | 0.88 | 0.89 | 0.89 | 0.91 | 0.85± 0.05 |
| Patient 6 | 0.85 | 0.84 | 0.76 | 0.80 | 0.84 | 0.86 | 0.86 | 0.87 | 0.89 | 0.84± 0.04 |
| Patient 7 | 0.82 | 0.79 | 0.74 | 0.76 | 0.77 | 0.87 | 0.90 | 0.89 | 0.90 | 0.82± 0.06 |
| Patient 8 | 0.88 | 0.83 | 0.83 | 0.78 | 0.78 | 0.77 | 0.82 | 0.87 | 0.85 | 0.82± 0.04 |
| Patient 9 | 0.91 | 0.83 | 0.83 | 0.84 | 0.82 | 0.88 | 0.86 | 0.85 | 0.88 | 0.86± 0.03 |
| Patient 10 | 0.85 | 0.78 | 0.69 | 0.68 | 0.79 | 0.79 | 0.74 | 0.78 | 0.83 | 0.77± 0.06 |
| Mean | 0.87 | 0.82 | 0.79 | 0.79 | 0.81 | 0.84 | 0.85 | 0.87 | 0.87 | 0.83± 0.05 |
| ± Std | ± 0.03 | ± 0.05 | ± 0.06 | ± 0.06 | ± 0.04 | ± 0.06 | ± 0.05 | ± 0.05 | ± 0.04 | |

Table 2.3: RMSE between synthetic and original CT images (mm)

| # of frames | 2 | 3 | 4 | 5 | 6 | 7 | 8 | 9 | 10 | Mean±Std |
|---|---|---|---|---|---|---|---|---|---|---|
| Patient 1 | 2.62 | 2.41 | 3.04 | 3.13 | 2.62 | 2.86 | 2.78 | 1.90 | 2.10 | 2.61± 0.41 |
| Patient 2 | 2.57 | 2.39 | 2.79 | 3.20 | 2.57 | 2.14 | 2.41 | 2.57 | 3.14 | 2.64± 0.35 |
| Patient 3 | 2.80 | 4.47 | 4.64 | 4.36 | 4.45 | 4.86 | 3.55 | 3.61 | 3.53 | 4.03± 0.68 |
| Patient 4 | 2.09 | 2.60 | 2.91 | 3.47 | 3.30 | 3.74 | 3.46 | 2.66 | 2.82 | 3.01± 0.52 |
| Patient 5 | 2.19 | 3.12 | 4.47 | 3.43 | 4.10 | 2.24 | 2.17 | 2.08 | 1.59 | 2.82± 1.00 |
| Patient 6 | 3.06 | 3.10 | 4.61 | 3.69 | 2.95 | 2.72 | 2.79 | 2.74 | 2.75 | 3.16± 0.62 |
| Patient 7 | 3.20 | 3.81 | 4.80 | 4.42 | 4.20 | 2.48 | 2.10 | 2.27 | 2.29 | 3.28± 1.04 |
| Patient 8 | 2.55 | 3.11 | 2.72 | 3.91 | 4.09 | 4.36 | 3.42 | 2.64 | 2.71 | 3.28± 0.69 |
| Patient 9 | 1.77 | 3.20 | 2.80 | 2.64 | 3.04 | 2.20 | 2.77 | 2.85 | 2.31 | 2.62± 0.45 |
| Patient 10 | 1.83 | 2.35 | 3.44 | 3.50 | 2.13 | 1.96 | 2.47 | 2.44 | 2.04 | 2.46± 0.61 |
| Mean | 2.47 | 3.06 | 3.62 | 3.58 | 3.35 | 2.96 | 2.79 | 2.57 | 2.53 | 2.99± 0.78 |
| ±Std | ±0.49 | ±0.68 | ±0.89 | ±0.55 | ±0.81 | ±1.01 | ±0.53 | ±0.47 | ±0.57 | |

images in diastole than in systole. The results of the RMSE are basically consistent with those which can be interpreted from the DSCs. However, the size of the heart may affect the results somewhat. For example, the mean DSC of patient 10 was the second lowest among all the patients, but the RMSE of that patient was lower than for many of the others simply because the patient in question had a relatively small heart.

For further investigation of the synthetic CT images, we also computed the two dimensional slice-by-slice DSC from the mitral valve plane down to the apex. Such an investigation can tell us whether the accuracy of the synthetic CT is consistent over the whole left ventricle. Three graphs are presented in Figure 2.7. The first shows the best result among all the patients, in which the DSC remained high over the entire left ventricle for all the frames. The second demonstrates the worst result among all the patients, in which the DSC decreased rapidly when

approaching the apex for frame 4 and frame 5 (systolic phase). The third graph shows the average DSC of all the patients. Since the physical size of the left ventricle varies for each patient, the average computation was performed on slices that were at the same portion point along the long axis from the mitral valve plane to the apex. The graph demonstrates that despite the worst case with very low DSC for systolic frames, the average DSC remains good (mostly over 80%) for all the patients and all the cardiac phases. It also shows that the accuracy of systole frames was slightly lower than those in diastole.

### 2.4.3 Computational Efficiency

The computational efficiency was measured on a desktop computer with an Intel© Xeon© dual core CPU at 3.47 GHz and NVIDIA GeForce© 690 graphics card and CUDA© 4.2 programming interface [NVIDIA Corp, Santa Clara, CA, USA].

The CPU based implementation of the non-local means filter took about 2 hours to filter one ultrasound volume, whereas the GPU based implementation took only 3 minutes.

Similarly, the F3D registration took 10-12 minutes to perform one registration with a CPU based implementation, whereas it took only 30 seconds with a GPU based implementation.

## 2.5 Discussion

### 2.5.1 Field of View

One limitation of this approach is that the synthetic CT images can only deform the anatomical structures that are presented in the TEE images, whereas the structures outside the imaging region of the TEE scan cannot be deformed. For example, the right ventricles, right atria, and part of the left atria did not get deformed correctly in the tests. However, as for the mitral valve repair application, it is appropriate to show only the left ventricle and the mitral valve area, since these are the actual regions of interest to the interventionists, whereas the right chambers

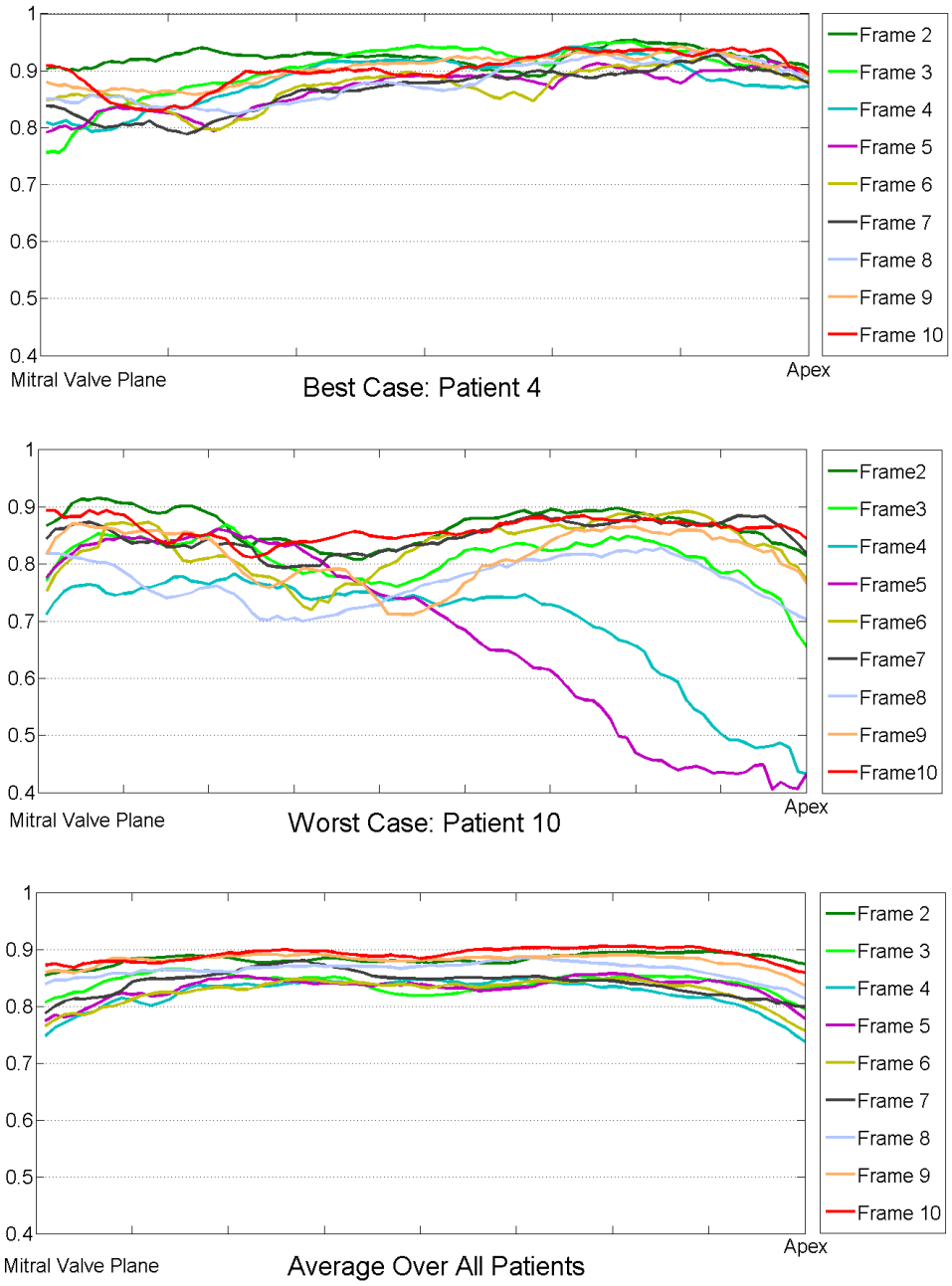


Figure 2.7: Slice-by-Slice DSC Results along the longitudinal axis (Each colored line represents a different cardiac frame.)

are not the major concern. As for other applications, the users can adjust the TEE views when performing the scans to ensure that the structures of interest are within the imaging region. It is also possible to include the deformation of the entire heart in the synthetic CT images by using ultrasound image mosaicing approaches [25] that can generate images covering a large field of

view.

### 2.5.2 Overall Accuracy of the Results

The reported average RMSE between the synCT and dynCT images with respect to the surface of LV was about 2.99±0.78mm. This error comprises the registration errors between TEE images, the potential differences in the representation of the same structure between CT and ultrasound images, the temporal distances between the corresponding synCT and dynCT images, and the variation in manual segmentations. Although there is no literature reporting errors on exactly the same issue, we compared it to some related studies. For example, Linte et al. [26] attempted to register intra-op US images to pre-op MRI images for navigation purpose; Mansi et al. [27] performed non-rigid registration between cardiac cine-MR images using iLogDemons approach; King et al. [28] validated the registration among 3D US images with 4-chamber views; Huang et al. [29] performed US-MR registrations for guidance of cardiac intervention as well; Sun et al. [30] attempted to register intra-op 3D intra-cardiac echo (ICE) images to pre-op CT images; and Wierzbicki et al. [13] aimed to build cardiac models based on cine MRI images. The comparison is listed in Table 2.4 showing the studies, modalities used, the region of interest (ROI), and the reported RMSE. It can be observed that although the RMSE we reported between synCT and dynCT is not the lowest reported in the literature, it is within a reasonable range compared to the RMSE of other studies. The lowest RMSE was achieved in Wierzbicki's study in which he performed non-rigid registration between MRI images from the same cardiac cycle, which means the RMSE only resulted from the registration error without any impact from inter-modality variation or imperfect temporal alignment, the two important sources of error in our application.

### 2.5.3 Causes for Inaccuracy in Synthetic CT at Systole

The validation of the synthetic CT images against the actual images demonstrates that the accuracy of the synthetic images may yield lower values for systolic images for some patients,

Table 2.4: Comparison of RMSE of related works

| Study | Modality | ROI | RMSE |
|---|---|---|---|
| Linte et al. | MRI-US | LV | 5.2 mm |
| Manis et al. | Cine-MR | LV | 2.3-3.5 mm |
| King et al. | 3D US | 4 chambers | 2.6-4.2 mm |
| Huang et al. | US-MR | 5 landmarks | 2.0 mm |
| Sun et al. | ICE-CT | LA+LV | 4.4 mm |
| Wierzbicki et al. | Cine-MR | Whole heart | 1.1 mm |
| SynCT generation | Syn-Dyn CT | LV | 3.0 mm |

especially in the areas close to the apex. On investigation, we found this to be due to the nature of the TEE images themselves. Figure 2.8 shows one example of the problem. The images represent a small time interval centred at the end-systole phase. The first row shows the last stage of the left ventricle contraction, whereas the second row shows the beginning of the dilation. It can be seen that a boundary of the inner wall of the left ventricle is clearly shown in the first image (indicated by the white arrow). However, when the left ventricle continues to contract, the boundary is missing from the images. This phenomenon lasts for a few frames until the left ventricle has dilated sufficiently and the boundary appears in the image again (the last images in the second row). Figure 2.9 shows another cause for missing boundaries. The three orthogonal slices shows that a segment of the boundary close to the apex was hidden in the shadow probably caused by the valve calcification.

The missing boundary causes insufficient deformation at the area where it occurred, since the intensity based registration approach cannot deal with a deformation if it is not present in the image. The missing boundary probably occurs when the boundary is close to parallel to the ultrasound beam, so that no reflection is generated at that surface.

While some model based registration methods [31–33] may be able to compensate for the missing boundary, they have two major limitations, which may prevent them from being practically used in a real application. First, they usually require a set of parameters to be pre-defined relating to the biomechanical behavior of the heart muscle. However, these parameters

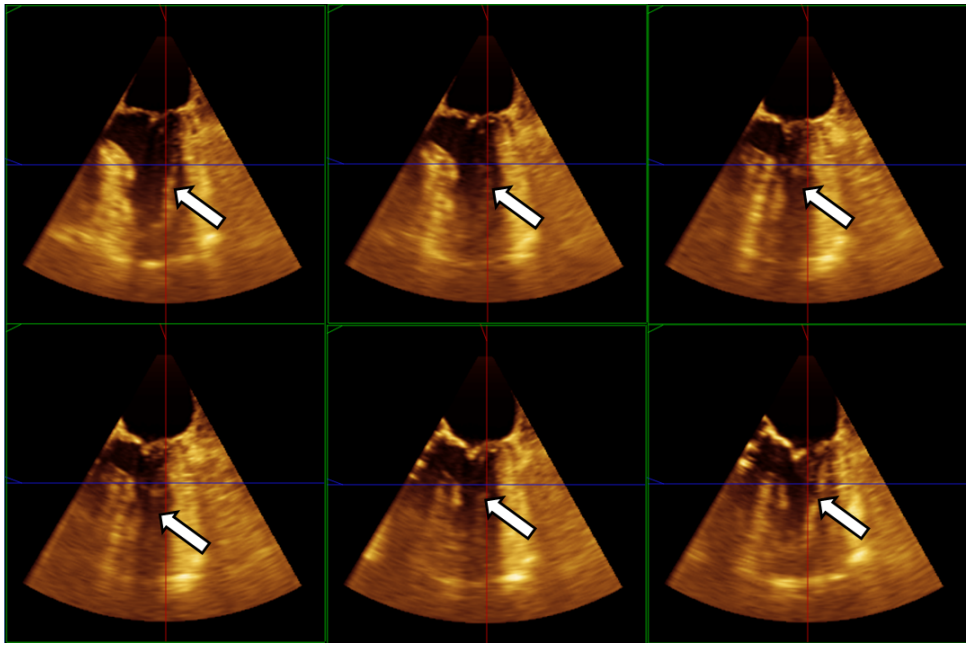

Figure 2.8: An illustration of the missing boundary phenomenon at systole

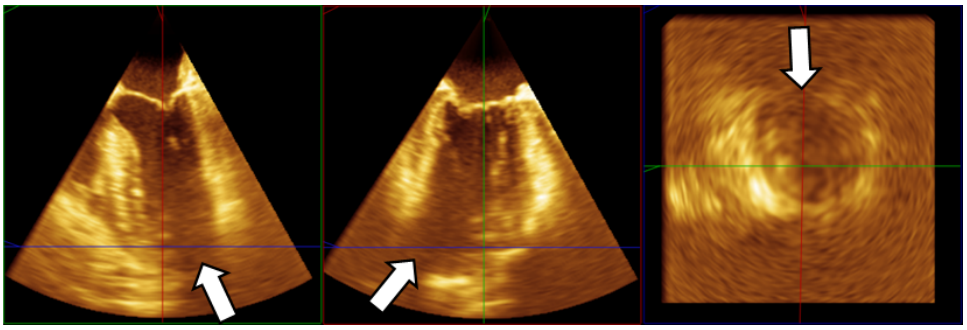

Figure 2.9: Missing boundary caused by shadow

are usually difficult to obtain for specific patients. Second, such models are usually defined based on data from healthy heart data, and may not be appropriate for pathological cases. We believe that contrast enhanced TEE images [34, 35] may be a potential solution for such a problem. With micro bubble contrast agents we could obtain strong reflections from the blood pool, which would make the surface between the blood and the myocardium clearer.

Some other possible yet minor causes for the inaccuracy are temporal difference between the corresponding images, difference in cardiac motion during the CT and TEE scans, and different appearance of the papillary muscles and trabeculae in the CT and TEE scans.

### 2.5.4 Visualization Options

For different guidance tasks the visualization of the images and models need to be adjusted to provide the most suitable display for the surgeon to perform the operation safely and efficiently. One of the advantage of the synCT images is that they allow multiple visualization options just as real CT images.

Figure 2.10 shows a few ways to visualize the synCT images. For example, the synCT image itself can be volume rendered to show a 3D presentation of the entire heart. When proper transfer function is applied [36], it is also possible to render selected anatomy or features. Anatomical models can be defined both pre- and intra-operatively and overlaid on the images through registration or tracking techniques. Direct fusion of the CT and ultrasound images can be another option.

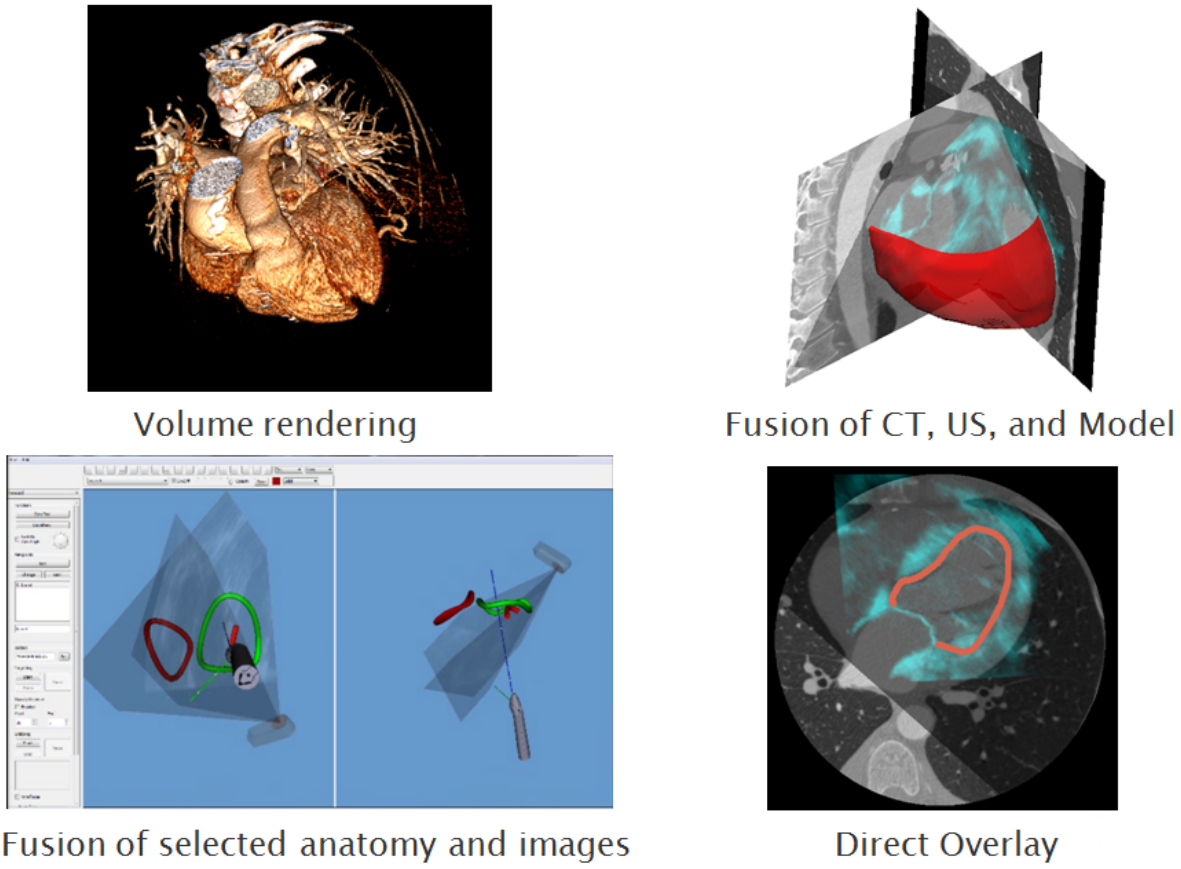


Figure 2.10: Visualization options

## 2.6 Conclusion & Future Work

This chapter introduces a novel approach that attempts to exploit the high temporal resolution of ultrasound imaging and high spatial resolution of CT imaging to generate a novel, high spatio-temporal resolution synthetic CT dataset. The synthetic CT images derived the anatomical presentation from the static CT image and the cardiac motion information from the 4D TEE images. Our validation experiments compared the synthetic CT dataset to the real dynamic CT images. Two metrics, DSC and RMSe, were used to measure the level of overlap and surface distances between the LV segmentations. The results showed that the synthetic CT images can provide very similar anatomical representations as the real images for the region of interest. The synthetic dataset is proposed to be used for the guidance of minimally invasive off-pump beating heart interventions. The advantage is that they can provide high quality 3D images with high temporal resolution (same as 3D TEE scans) for registration, feature tracking, and modelling purposes with no ionizing radiation dose applied to either the patients or the clinicians.

# Bibliography

[1] D. Doty, J. Flores, and J. Doty, "Cardiac valve operations using a partial sternotomy (lower half) technique," *Journal of cardiac surgery*, vol. 15, no. 1, pp. 35–42, 2000.

[2] T. A. Vassiliades, P. C. Block, L. H. Cohn, D. H. Adams, J. S. Borer, T. Feldman, D. R. Holmes, W. K. Laskey, B. W. Lytle, M. J. Mack, and D. O. Williams, "The clinical development of percutaneous heart valve technology.," *The Journal of thoracic and cardiovascular surgery*, vol. 129, pp. 970–6, May 2005.

[3] T. M. Peters, "Image-guidance for surgical procedures," *Physics in medicine and biology*, vol. 51, pp. R505–40, July 2006.

[4] E. R. Mcveigh, M. A. Guttman, P. Kellman, A. N. Raval, R. J. Lederman, and C. B. A. N. R, "Real-time, Interactive MRI for Cardiovascular Interventions," *Acad Radiol*, vol. 12, no. 9, pp. 1121–1127, 2005.

[5] F. G. Sommer, R. A. Filly, and M. J. Minton, "Acoustic Shadowing Due to Refractive and Reflective Effects," *American Journal of Roentgenology*, vol. 132, no. 6, pp. 973–977, 1979.

[6] W. P. Shuman, K. R. Branch, J. M. May, L. M. Mitsumori, D. W. Lockhart, T. J. Dubinsky, B. H. Warren, and J. H. Caldwell, "Prospective versus Retrospective ECG Gating for 64-Detector CT of the Coronary Arteries : Comparison of Image Quality and Patient Radiation Dose," *Radiology*, vol. 248, no. 2, pp. 431–437, 2008.

[7] N. Hirai, J. Horiguchi, C. Fujioka, M. Kiguchi, H. Yamamoto, N. Matsuura, T. Kitagawa, H. Teragawa, N. Kohno, and K. Ito, "Prospective versus Retrospective ECG-gated 64-Detector Coronary CT Angiography : Assessment of Image Quality, Stenosis, and Radiation Dose," *Radiology*, vol. 248, no. 2, pp. 424–430, 2008.

[8] C. A. Linte, J. Moore, C. Wedlake, D. Bainbridge, G. M. Guiraudon, D. L. Jones, and T. M. Peters, "Inside the beating heart: an in vivo feasibility study on fusing pre- and intra-operative imaging for minimally invasive therapy.," *International journal of computer assisted radiology and surgery*, vol. 4, pp. 113–23, Mar. 2009.

[9] C. a. Linte, A. Wiles, J. Moore, C. Wedlake, and T. M. Peters, "Virtual reality-enhanced ultrasound guidance for atrial ablation: in vitro epicardial study.," *Medical image computing and computer-assisted intervention : MICCAI ... International Conference on Medical Image Computing and Computer-Assisted Intervention*, vol. 11, pp. 644–51, Jan. 2008.

[10] F. Li, P. Lang, M. Rajchl, E. C. S. Chen, G. Guiraudon, and T. M. Peters, "Towards real-time 3D US-CT registration on the beating heart for guidance of minimally invasive cardiac interventions," in *Proc. SPIE 8316, Medical Imaging 2012* (D. R. Holmes III and K. H. Wong, eds.), vol. 8316, p. 831615, Feb. 2012.

[11] M. J. Ledesma-Carbayo, J. Kybic, M. Desco, A. Santos, M. Sühling, P. Hunziker, and M. Unser, "Spatio-temporal nonrigid registration for ultrasound cardiac motion estimation," *IEEE transactions on medical imaging*, vol. 24, pp. 1113–26, Sept. 2005.

[12] W. Shi, X. Zhuang, H. Wang, S. Duckett, D. V. N. Luong, C. Tobon-gomez, K. Tung, P. J. Edwards, K. S. Rhode, R. S. Razavi, S. Ourselin, and D. Rueckert, "A Comprehensive Cardiac Motion Estimation Framework Using Both Untagged and 3-D Tagged MR Images Based on Nonrigid Registration," *IEEE transactions on medical imaging*, vol. 31, no. 6, pp. 1263–1275, 2012.

[13] M. Wierzbicki, M. Drangova, G. Guiraudon, and T. Peters, "Validation of dynamic heart models obtained using non-linear registration for virtual reality training, planning, and guidance of minimally invasive cardiac surgeries.," *Medical image analysis*, vol. 8, pp. 387–401, Sept. 2004.

[14] H. Sundar, H. Litt, and D. Shen, "Estimating Myocardial Motion by 4D Image Warping," *Pattern Recognitioin*, vol. 42, no. 11, pp. 2514–2526, 2010.

[15] a. Buades, B. Coll, and J. M. Morel, "A Review of Image Denoising Algorithms, with a New One," *Multiscale Modeling & Simulation*, vol. 4, pp. 490–530, Jan. 2005.

[16] P. Coupé, P. Hellier, C. Kervrann, and C. Barillot, "Nonlocal means-based speckle filtering for ultrasound images.," *IEEE transactions on image processing : a publication of the IEEE Signal Processing Society*, vol. 18, pp. 2221–9, Oct. 2009.

[17] M. Modat, G. R. Ridgway, Z. a. Taylor, M. Lehmann, J. Barnes, D. J. Hawkes, N. C. Fox, and S. Ourselin, "Fast free-form deformation using graphics processing units.," *Computer methods and programs in biomedicine*, vol. 98, pp. 278–84, June 2010.

[18] D. Rueckert, L. I. Sonoda, C. Hayes, D. L. Hill, M. O. Leach, and D. J. Hawkes, "Non-rigid registration using free-form deformations: application to breast MR images.," *IEEE transactions on medical imaging*, vol. 18, pp. 712–21, Aug. 1999.

[19] P. Muyan-Ozcelik, J. D. Owens, J. Xia, and S. S. Samant, "Fast Deformable Registration on the GPU: A CUDA Implementation of Demons," *2008 International Conference on Computational Sciences and Its Applications*, pp. 223–233, June 2008.

[20] R. Kumar, J. C. Asmuth, K. Hanna, J. Bergen, C. Hulka, D. B. Kopans, R. Weisskoff, and R. Moore, "Application of 3D registration for detecting lesions in magnetic resonance breast scans," in *SPIE Medical Imaging, 1996*, vol. 2710, pp. 646–656.

[21] S. Lee, G. Wolberg, K.-Y. Chwa, and S. Y. Shin, "Image metamorphosis with scattered feature constraints," *IEEE Transactions on Visualization and Computer Graphics*, vol. 2, no. 4, pp. 337–354, 1996.

[22] J. P. W. Pluim, J. B. A. Maintz, and M. a. Viergever, "Mutual-information-based regis-

tration of medical images: a survey," *IEEE transactions on medical imaging*, vol. 22, pp. 986–1004, Aug. 2003.

[23] C. Studholme, D. L. Hill, and D. J. Hawkes, "Automated three-dimensional registration of magnetic resonance and positron emission tomography brain images by multiresolution optimization of voxel similarity measures.," *Medical physics*, vol. 24, pp. 25–35, Jan. 1997.

[24] P. J. Besl and N. D. McKay, "A Method for Registration of 3-D Shapes," *IEEE Transaction on Pattern Analysis and Machine Intelligence*, vol. 14, no. 2, pp. 229–256, 1992.

[25] O. Kutter, W. Wein, and N. Navab, "Multi-modal registration based ultrasound mosaicing," *Medical image computing and computer-assisted intervention : MICCAI ... International Conference on Medical Image Computing and Computer-Assisted Intervention*, vol. 12, pp. 763–70, Jan. 2009.

[26] C. Linte, M. Wierzbicki, J. Moore, G. Guiraudon, D. L. Jones, and T. M. Peters, "On enhancing planning and navigation of beating-heart mitral valve surgery using pre-operative cardiac models.," *Conference proceedings : ... Annual International Conference of the IEEE Engineering in Medicine and Biology Society. IEEE Engineering in Medicine and Biology Society. Conference*, vol. 2007, pp. 475–8, Jan. 2007.

[27] T. Mansi, X. Pennec, M. Sermesant, H. Delingette, and N. Ayache, "iLogDemons: A Demons-Based Registration Algorithm forTracking Incompressible Elastic Biological Tissues," *International Journal of Computer Vision*, vol. 92, pp. 92–111, Nov. 2010.

[28] A. P. King, Y. L. Ma, C. Yao, C. Jansen, R. Razavi, K. S. Rhode, and G. P. Penney, "Image-to-physical registration for image-guided interventions using 3-D ultrasound and an ultrasound imaging model.," *Information processing in medical imaging : proceedings of the ... conference*, vol. 21, pp. 188–201, Jan. 2009.

[29] X. Huang, J. Ren, G. Guiraudon, D. Boughner, and T. M. Peters, "Rapid dynamic image registration of the beating heart for diagnosis and surgical navigation," *IEEE transactions on medical imaging*, vol. 28, pp. 1802–14, Nov. 2009.

[30] Y. Sun, S. Kadoury, Y. Li, M. John, J. Resnick, G. Plambeck, R. Liao, F. Sauer, and C. Xu, "Image guidance of intracardiac ultrasound with fusion of pre-operative images," *Medical image computing and computer-assisted intervention : MICCAI ... International Conference on Medical Image Computing and Computer-Assisted Intervention*, vol. 10, pp. 60–7, Jan. 2007.

[31] A. J. Sinusas, X. Papademetris, R. T. Constable, D. P. Dione, M. D. Slade, P. Shi, and J. S. Duncan, "Quantification of 3-D regional myocardial deformation: shape-based analysis of magnetic resonance images.," *American journal of physiology. Heart and circulatory physiology*, vol. 281, pp. H698–714, Aug. 2001.

[32] A. I. Veress, G. T. Gullberg, and J. A. Weiss, "Measurement of Strain in the Left Ventricle during Diastole with cine-MRI and Deformable Image Registration," *Journal of Biomechanical Engineering*, vol. 127, p. 1195, July 2005.

[33] N. S. Phatak, S. a. Maas, A. I. Veress, N. a. Pack, E. V. R. Di Bella, and J. a. Weiss, "Strain measurement in the left ventricle during systole with deformable image registration.," *Medical image analysis*, vol. 13, pp. 354–61, Apr. 2009.

[34] M. McCulloch, C. Gresser, S. Moos, J. Odabashian, S. Jasper, J. Bednarz, P. Burgess, D. Carney, V. Moore, E. Sisk, A. Waggoner, S. Witt, and D. Adams, "Ultrasound contrast physics: a series on contrast echocardiography, article 3," *Journal of the American Society of Echocardiography*, vol. 13, pp. 959–967, Oct. 2000.

[35] J. R. Lindner, "Microbubbles in medical imaging: current applications and future directions.," *Nature reviews. Drug discovery*, vol. 3, pp. 527–32, June 2004.

[36] J. S. H. Baxter, T. M. Peters, and E. C. S. Chen, "A unified framework for voxel classification and triangulation," in *SPIE Medical Imaging: Visualization, Image-Guided Procedures, and Modeling*, 2011.

# Chapter 3

# Ultrasound Guidance for Beating Heart Mitral Valve Repair Augmented by Synthetic Dynamic CT

This chapter is adapted from the papers:

- Feng Li, Pencilla Lang, Martin Rajchl, Elvis C.S. Chen, Gerard Guiraudon, Terry M. Peters, Towards Real-time 3D US-CT Registration on the Beating Heart for Guidance of Minimally Invasive Cardiac Interventions, SPIE Medical Imaging Conference, San Diego, Feb. 4-9, 2012

- Feng P. Li, Martin Rajchl, James A. White, Aashish Goela, and Terry M. Peters, Towards CT Enhanced Ultrasound Guid- ance for Off-pump Beating Heart Mitral Valve Repair. In: MIAR/AE-CAI 2013.

- Feng P. Li, Martin Rajchl, James A. White, Aashish Goela, and Terry M. Peters, Ultrasound Guidance for Beating Heart Mitral Valve Repair Augmented by Synthetic Dynamic CT, IEEE Transaction on Medical Imaging (submitted)

## 3.1 Introduction

The mitral valve provides unidirectional control of blood flow between the left atrium and the left ventricle. In approximately 2% of people the mitral valve fails to close sufficiently and leads to clinically significant regurgitation warranting surgical intervention [1, 2]. Conventional mitral valve repair can be accomplished through open heart surgery, a procedure that requires cardiopulmonary bypass. Such an approach has been associated with appreciable risk and morbidity, such as renal injury and stroke [3–5]. In an attempt to deliver equivalent therapy with reduced morbidity, minimally invasive off-pump beating heart (BH) mitral valve repair (MVR) has recently emerged and is rapidly gaining clinical interest [6–8]. However, due to the lack of direct visualization of both the surgical tools and tissue targets, these procedures are inherently dependent upon intra-operative image guidance systems to support such visualization.

### 3.1.1 Overcoming Inherent Limitations of Intra-operative Imaging

The guidance system should be able to display both the dynamic cardiac anatomy and motion, employ a low cost but intuitive platform, and have minimal impact on clinical workflow. Currently, the most commonly used intra-operative imaging modalities for off-pump BH MVR are 2D X-ray fluoroscopy and 2D or 3D TEE [9, 10]. However, due to the complexity of the task and limitations of imaging techniques, no single modality is considered ideal for the guidance of the complete procedure [11].

#### X-ray Fluoroscopy

X-ray fluoroscopy is widely used in interventional procedures and can provide real-time intra-operative imaging with good representation of surgical tools, particularly wires and catheters, and of intra-vascular or chamber contrast injections. However, 2D projectional images limit the capacity of the imaging system to provide real-time spatial registration within a 3-dimensional

environment. A lack of soft-tissue contrast prevents visualization of relevant tissue targets. Finally, prolonged use leads to high radiation exposure, raising concern for the safety of patients and the interventional team.

**Transesophageal Echocardiogram (TEE)**

TEE can provide real-time intra-operative images of high temporal and spatial resolution, allowing excellent representation of rapid cardiac motion, especially that of the mitral leaflets. In addition, the visualization of other relevant intracardiac structures is excellent with no associated concern of radiation exposure. However, 2D and biplane TEE provide only planar images, making it difficult to maintain both the surgical tool and the anatomical targets in the same imaging plane. 3D TEE can overcome this limitation to some degree, but at the cost of decreased temporal and spatial resolution and a restricted FOV. Furthermore, the signal-to-noise ratio of TEE is less than that which can be achieved using tomographic imaging techniques, such as MRI or CT.

**Interventional MRI**

The intra-procedural use of MRI, typically termed interventional MRI, can display cardiac anatomy and motion dynamically with improved signal to noise and excellent soft tissue characterization. However, development of these techniques has been clinically hampered by the requirement to develop and demonstrate safety of non-ferromagnetic tools, and to create specialized MRI-based tools for the tracking of catheters or devices in real time. These systems also prevent the simultaneous use of magnetic tracking systems, are not available in most institutions, and are of high capital and operational cost.

To compensate for these limitations, many authors have suggested fusing pre-operative and intra-operative imaging to take advantage of the high image quality, large field of view, and predefined annotations [12–15]. Linte et al. [16] proposed combining high resolution pre-operative tomographic images with intra-operative ultrasound, both of which are independently

performed in standard clinical practice. Huang et al. [17] proposed a registration approach which introduced the possibility of performing registration between ultrasound and CT/MRI images in real time. However, although retrospectively gated (multi-phase) CT imaging that provides dynamic information of cardiac motion would be desired for this purpose, concerns regarding radiation exposure have led to only static, single phase CT imaging being used in routine clinical practice [18, 19].

### 3.1.2 Current Clinically Available Systems for BH MVR

Several commercially available techniques have been developed and are currently under clinical trials (details in Section 1.4.4). The NeoChord© procedure (NeoChord, Inc., MN, USA) is designed to repair flailing leaflets by attaching artificial chordae between the leaflets and the apex to limit the motion of the leaflets [9, 10]. Another approach is the MitraClip© (Abbott Laboratories, IL, USA), a percutaneous mitral valve repair system that delivers a clip that grasps the two leaflets together to create a double orifice valve to reduce regurgitation [9, 20]. The Mitralign© procedure (Mitralign Inc. MA, USA) aims to perform percutaneous mitral annuloplasty by deploying pledgets on the mitral annulus and pulling them together to decrease the circumference of the mitral annulus [21]. Finally, the MONARC© device (Edwards Lifesciences, CA, USA) uses a different approach to perform annuloplasty by implanting a curved device in coronary sinus to reduce the spetal-lateral diameter of the mitral annulus [22]. All current clinically available BH MVR systems rely on ultrasound guidance for intra-operative imaging, due to its real-time capabilities, low-cost and high availability.

### 3.1.3 Contributions

In this study, we propose a generic guidance system for BH MVR that can potentially address the stated limitations of current clinical systems [11, 12] and provide improved visualization of target anatomy under intra-operative TEE guidance.

The proposed system is able to enhance intra-operative ultrasound images with information

about the target anatomy generated from pre-operative dynamic CT (dynCT) images in real-time. Because of the limited clinical availability of dynamic CT imaging, again due to its increased radiation dose, we examine the accuracy of using a single pre-operative static CT image to provide a series of synthetic CT (synCT) images through non-rigid registration of 4D TEE images obtained from the same patient.

Finally, we study the accuracy of the system to visualize anatomic targets using both dynCT and synCT image datasets and demonstrate that there is no significant difference in their ability to enhance intra-operative imaging for this clinical application.

## 3.2 Methods

### 3.2.1 Overall Workflow

The suggested clinical workflow for using dynCT-enhanced TEE guidance is illustrated in Figure 3.1. The overall workflow can be broken down into three stages at which parts of the proposed pipeline are executed [23]:

#### Pre-operative Stage

In this stage, dynCT images are either acquired by performing a retrospectively gated CT scan or synCT images are generated from a static CT and a TEE series from the same patient using the proposed method in Section 2.2.3. The CT image series is used to extract the target anatomy and are subsequently transferred to the guidance system prior to surgery.

#### Peri-operative Stage

An initial rigid registration is performed between a peri-operatively acquired 3D US volume and a CT image at the same or closest cardiac phase using feature based registration. Features, such as the inner walls of the left ventricle, are rapidly semi-automatically segmented using the

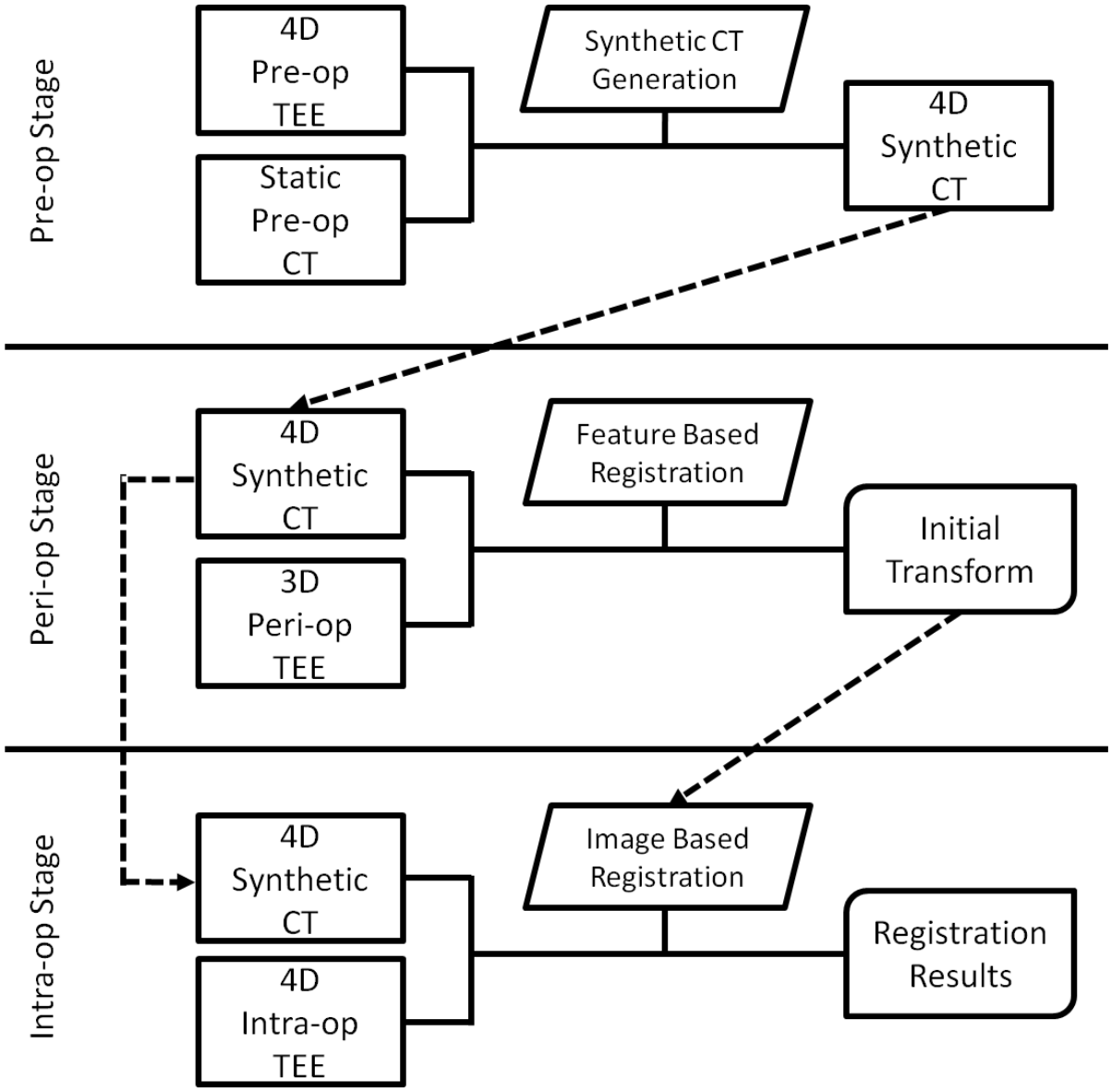


Figure 3.1: Overall Workflow

approach described by Rajchl et al. [24]. The resulting registration transform is then saved and employed as an initialization for the intra-operative CT to ultrasound registration.

**Intra-operative stage**

Here, CT images are registered to the intra-operatively acquired TEE images using a rapid GPU-based algorithm [25]. The registered images can be visualized differently (i.e. surface models, volume rendered, etc.) according to surgeon's preference. In this way, a visual linkage

can be provided between the intra-operative images, pre-operative image, anatomical models, and surgical tools (with the help of tool tracking) within the same guidance framework [26].

### 3.2.2 Generation of 4D Synthetic CT

The methodology employed to generate the synthetic dynamic CT images is to perform non-rigid registrations between ultrasound images within a single cardiac cycle to obtain patient specific heart motion maps, in the form of deformation fields, and to apply these deformation maps to CT images to provide synthetic animation (details in Section 2.2.3).

The procedure begins with selecting one ultrasound image, acquired at a cardiac phase close to the static CT image, as a reference. A rigid registration [25] is then performed between this image and the static CT image. This step begins with semi-automatically segmenting the inner wall of the left ventricle [27] from both the static CT image and the reference ultrasound image, and using the iterative closest point (ICP) method to align the surfaces [28]. The alignment is then refined by a mutual information based registration [29] resulting in an optimized transform. All the other ultrasound images in the 4D sequence are then rigidly registered to the reference image as initialization for the later non-rigid transform.

After the initial rigid registration step, non-rigid registrations are performed among the 3D ultrasound images in the 4D sequence and the resulting deformation fields are recorded. This can be achieved either by registering the reference image directly to every image in the sequence, or by performing a registration between adjacent frames. The deformation fields obtained from the non-rigid registration are used as cardiac motion maps and applied to the static CT image to generate a synthetic dynamic CT sequence. By performing the approach for each frame, we generate an entire sequence of synthetic dynamic CT images with the same temporal resolution as the dynamic ultrasound images. For this operation we employed the multi-resolution fast free-form (F3D) deformation registration method of Modat et al. [30] because of its capability of handling the morphological deformation due to cardiac motion and providing relatively smooth deformation fields.

### 3.2.3 GPU-based Intra-operative Real-time Registration

The dynCT or synCT images can now be employed to enhance an intra-operative guidance system. For navigation, they must be registered to the intra-operative TEE images in real-time (In this context we refer to real-time as the ability to process multiple frames within one second). The proposed intra-operative registration contains two components: temporal and spatial registration.

#### Temporal Registration

A time point in the cardiac cycle is chosen (here mid-diastole) to temporally match the dynCT or synCT series to the intra-operative 4D US. Similar to the method employed for generation of the synCT, each frame in the CT series is matched with its corresponding 4DUS frame, which is determined by finding the nearest neighbour in time (cardiac phase).

#### Spatial Registration

A rigid registration method, using normalized mutual information (NMI) as the similarity metric with Powell's conjugate direction method [31, 32] as the underlying optimizer, is employed to register each CT frame to its corresponding US frame, as determined by the temporal registration procedure. Since both images series to be registered are specific to the patient, deformations are assumed to be identical in corresponding frames, which is the rationale for using a rigid approach as a trade-off between efficiency and accuracy. A flowchart depicting the employed registration pipeline can be found in Figure 3.2.

***Initialization:*** While the proposed optimization method guarantees that local optima are found, a proper initialization in the peri-operative stage can guarantee quick convergence to the correct optimum. This initialization can be achieved via registration of landmarks (i.e. features, manually defined in the LV of a frame) or via LV-surface based registration with the ICP algorithm, as used in here (Figure 3.3). Rapid LV segmentations were obtained peri-operatively by using a fast interactive segmentation technique [27].

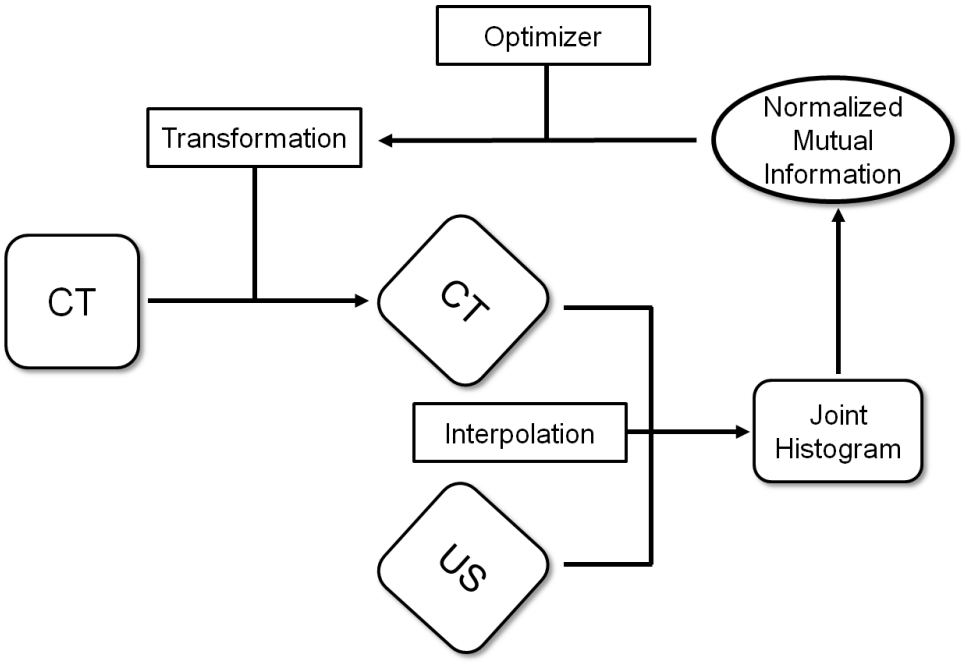


Figure 3.2: Intra-operative registration pipeline

***Linear interpolation and rigid transformation:*** The rigid transformation contains six parameters, three for rotation and three for translation. Let $\alpha, \beta, \gamma$ be the rotation angle and $t_1$, $t_2$, $t_3$ be the translation along $x$, $y$, and $z$ axis respectively. A rigid transformation can be written as

$$x' = R(\alpha, \beta, \gamma)x + T, \tag{3.1}$$

where $x$ is the original coordinate, $x'$ is the transformed coordinate, $R(\alpha, \beta, \gamma)$ is the rotation matrix, and $T := (t_1, t_2, t_3)'$. The rotation matrix $R(\alpha, \beta, \gamma)$ is the production of three rotation matrices, which are

$$R_x := \begin{pmatrix} 1 & 0 & 0 \\ 0 & \cos\alpha & -\sin\alpha \\ 0 & \sin\alpha & \cos\alpha \end{pmatrix} R_y := \begin{pmatrix} \cos\beta & 0 & \sin\beta \\ 0 & 1 & 0 \\ -\sin\beta & 0 & \cos\beta \end{pmatrix} R_z := \begin{pmatrix} \cos\gamma & -\sin\gamma & 0 \\ \sin\gamma & \cos\gamma & 0 \\ 0 & 0 & 1 \end{pmatrix}. \tag{3.2}$$

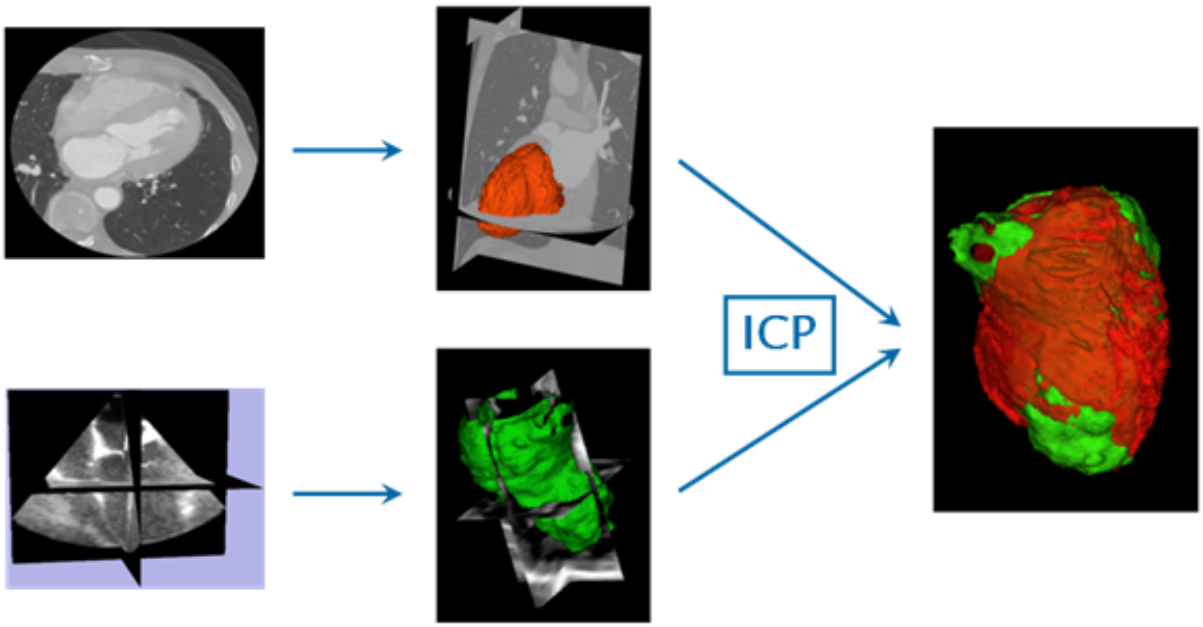


Figure 3.3: The initialization obtained through surface based registration

A tri-linear interpolation is then used to the matching the transformed floating CT image and the corresponding US frame. Suppose the coordinate of a transformed point $p$ is $(x, y, z)$ in the US image space and the lattice point below and above $p$ are denoted as $p_0(x_0, y_0, z_)$ and $p_1(x_1, y_1, z_1)$, we define

$$\begin{aligned} x_d &= (x - x_0)/(x_1 - x_0) \\ y_d &= (y - y_0)/(y_1 - y_0)\,, \\ z_d &= (z - z_0)/(z_1 - z_0) \end{aligned} \tag{3.3}$$

Then the interpolated intensity value of $p$ can be computed by performing the interpolation along $x$, $y$, and $z$ axis respectively. The equation used for interpolation along each axis is given below:

$$\begin{aligned} &\text{x axis:} \quad C_{j,k} = (1 - x_d)\, I_{i,j,k} + x_d\, I_{i+1,j,k} \quad (i = 0,\ j = 0, 1,\ k = 0, 1) \\ &\text{y axis:} \quad C_k = (1 - y_d)\, C_{j,k} + y_d\, C_{j+1,k} \quad (j = 0,\ k = 0, 1) \\ &\text{z axis:} \quad I_p = (1 - z_d)\, C_k + z_d\, C_{k+1} \quad (k = 0) \end{aligned} \quad , \tag{3.4}$$

where $I$ indicates the intensity value.

Both the transformation and interpolation components are inherently parallel operations and implemented simultaneously using GPGPU. In heuristic testing, we observed an approximately 50-fold increase computation speed for these two steps over sequential computation on a single CPU thread.

***Parallelized mutual information implementation:*** (Normalized) mutual information is a very common similarity metric used for multi-modality registration [29]. If we consider two digital images, $A$ and $B$, as two random variables, the mutual information of the two images can be defined as

$$I(A, B) = H(A) + H(B) - H(A, B), \tag{3.5}$$

while the normalized mutual information can be written as

$$I(A, B) = \frac{H(A) + H(B)}{H(A, B)}, \tag{3.6}$$

where $H$ defines the entropy of the random variable and

$$\begin{aligned} H(A) &= -\sum_{a \in A} p(a) \log p(a) \\ H(A, B) &= -\sum_{a \in A} \sum_{b \in B} p(a, b) \log p(a, b) \end{aligned} \tag{3.7}$$

The computation of the similarity metric is parallelized using the concept General-Purpose Programming on Graphics Processing Units (GPGPU) [33–35] for a substantial increase in computation speed. Since the computation of the mutual information, specifically histogram construction, is a naturally sequential procedure, race conditions are expected in parallelized implementations [36]. This implementation mitigates this situation using the MapReduce paradigm [37] (see Figure3.4), that is, by partitioning the image into parallel sub-images with independently stored histograms, which are then summed together. For an additional increase in computation speed of the mutual information, the intra-operative 4D US images are sub-

jected to a thresholding procedure and only high intensity voxels in TEE images are used to compute the mutual information (Figure 3.5). The rationale for this step is that it greatly speeds up the computation of the mutual information metric by only using about 10% of all voxels in the image and additionally biases the registration towards the myocardial anatomy, which is particularly desired in this application.

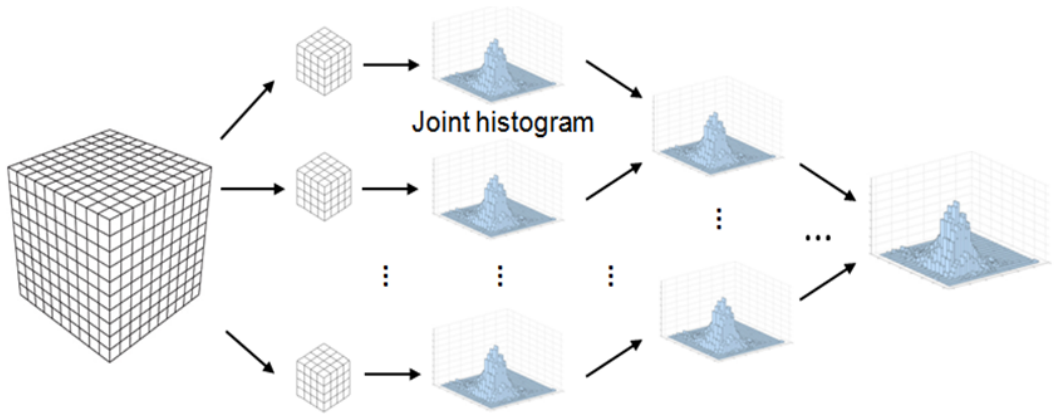


Figure 3.4: MapReduce approach to the computation of the joint histogram in the proposed GPGPU implementation of the mutual information

## 3.3 Experiments

### 3.3.1 Image Data and Patient Population

All data used in the experiments were collected retrospectively under a protocol approved by the Research Ethics Board of Western University, London, ON.

Image data of patients (N = 10) undergoing valve repair were collected and subsequently anonymized before being prepared for processing. Each dataset contained a series of retrospectively gated cardiac CT scans using a Lightspeed 7-VCT scanner (GE Heathcare, Waukesha, WI, USA) with $512 \times 512 \times 150$ voxels at $0.4 \times 0.4 \times 1.3$ mm resolution at 10 single frames per cardiac cycle, totaling 100 single CT frames (10 frames per patient).

Additionally, a 3D TEE time series of two-chamber or 4-chamber views with approximately

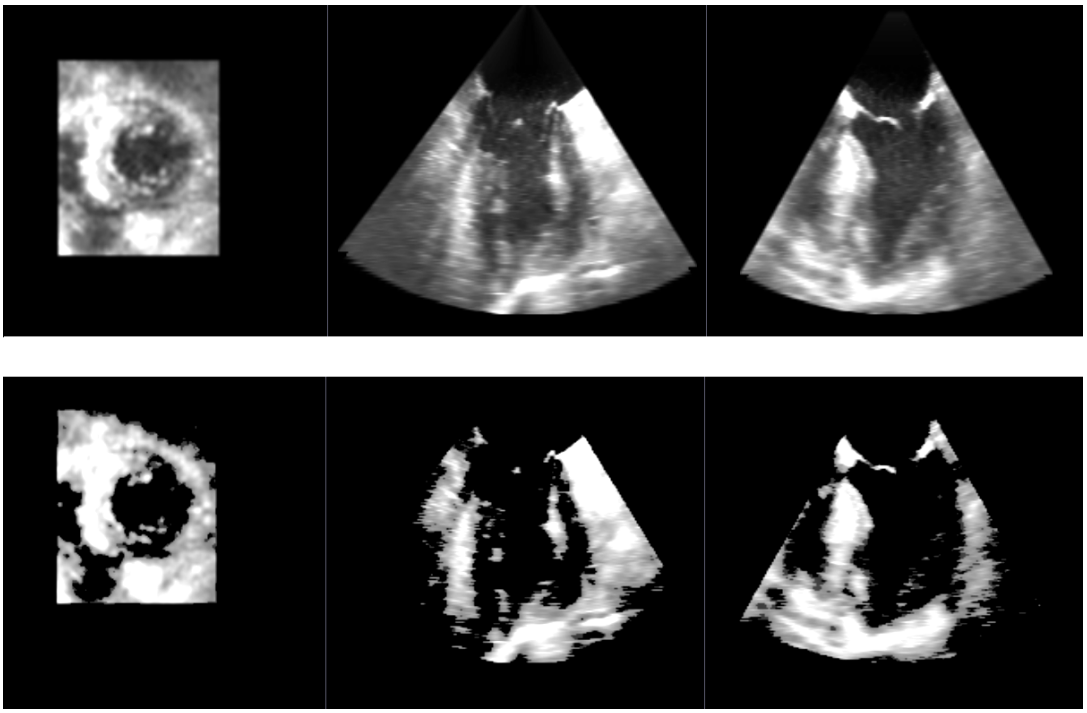

Figure 3.5: Example of a thresholded intra-operative 4D TEE frame. Top row represents three orthogonal slices through the volume, while the bottom row shows the result of discarding all values less than 35% to facilitate faster computations of the parallelized mutual information

$200 \times 200 \times 180$ voxels at a resolution of $0.8 \times 0.8 \times 0.7$ mm was acquired at around 25Hz using an Philips iE33 xMATRIX Echocardiography System (Philips Healthcare, Andover, MA, USA) with a X7-2t probe. The 4D US series was acquired to cover at least an entire cardiac cycle.

All datasets fulfilled these requirements and none had to be excluded.

### 3.3.2 Intra-operative Registration Accuracy

Both the original dynCT and generated synCT series are subjected to the proposed intra-operative registration pipeline and the resulting mean accuracy over time reported using RMSE on the mitral valve annulus (MVA), the region that defines the target area in the navigation. The entire MVA was manually segmented from synCT, dynCT, and TEE images. The target registration error (TRE) was measured by computing the mean distance between corresponding points on the MVAs from both CT and TEE images. Note that the TEE images are considered

to represent the true anatomy of the mitral valve during the procedure. Comparisons were performed between the results using dynCT and synCT series to investigate whether the synCT series can provide similar or equivalent registration accuracy to the dynCT series when the latter is not available.

### 3.3.3 Run Times

The computational efficiency was evaluated on a desktop computer with an Intel© Xeon© dual-core 3.47 GHz CPU (Intel Corporation, Santa Clara, CA, USA) and an NVIDIA© Tesla C2075 graphic card (Nvidia Corporation, Santa Clara, CA, USA). The average computation time for one registration is calculated over the entire dataset using the same parameter settings.

### 3.3.4 Parameter Tuning

All the parameters were manually tuned to achieve good and stable accuracy for all the patients. The tuning was based on the five of the patient datasets. The values used for the parameters in this paper are listed in Table 3.1.

Table 3.1: Parameters and their values used in TEE-CT Registration

| | |
|---|---|
| Threshold applied on TEE images | 0.35/1 |
| Bin number for joint histogram | 50×50 |
| Translation to rotation ratio | 1000 |
| Step length in Powell's method | 0.0003 |
| Convergence criteria for NMI | 0.01 |

## 3.4 Results

### 3.4.1 Validation of Real-time Registration

The validation is performed for two purposes: accessing the CT-US registration accuracy and examing if it differs between synthetic and real CT images. As previously stated, the purpose of generating the synthetic CT sequence is to provide dynamic CT images to the guidance system without additional patient radiation dose. If the comparison demonstrates equivalent results, we can conclude that that the synthetic CT images have the potential to replace actual dynamic CT images in a guidance application.

For each patient, the registration was performed independently between the real dynamic CT images and the TEE images, and between the synthetic CT images and the TEE images. The TEE images used here are different from those employed in the generation of synthetic CT images. To validate the accuracy of the registration, we manually segmented the mitral annulus from both CT and TEE images as our targets, because the centre of the mitral annulus defines the destination where the cardiac surgeons want to move the tools to during the navigation stage.

Table 3.2 presents the overall target registration error (TRE) with respect to the manually segmented mitral annulus ring models. The mean TRE and the standard deviation were quite similar to the synthetic and real dynamic CT images. Figure 3.6 shows one of the registration results, where TEE images are presented in yellow and overlaid on the CT images. The first row shows the results with real dynamic CT images, whereas the second row displays the results with synthetic CT images. The red points indicated the MVA from the CT images while the MVA from the TEE images is displayed in green.

We also compared the TRE results phase by phase throughout an entire cardiac cycle. One cardiac cycle was divided into ten phases with reference to the real dynamic CT images. Synthetic CT images with the corresponding phases were then selected for comparison. Figure 3.7 shows the result of this comparison, in which we observe that there was also no obvious trend

Table 3.2: Comparison of the TRE (MVA as target) with Synthetic and Real Dynamic CT images

| Synthetic CT | | Dynamic CT | |
|---|---|---|---|
| Mean (mm) | 2.74 | Mean (mm) | 2.68 |
| Std (mm) | 0.93 | Std (mm) | 0.94 |

or difference between the results with synthetic and real CT images. We also computed the confidence interval of the TRE differences between the results using synthetic and real CT images, which was $[-0.35, 0.55]$mm with 95% confidence ($\alpha = 0.05$). This means that if we replace real CT with synthetic CT in our registration application, the difference in TRE can be expected to be smaller than half a millimetre on average.

### 3.4.2 Computational Efficiency

The overall computational run time was 317.3±88.3ms for each registration with about one million sample points after the thresholding operation used during registration. This is fast enough for performing one registration per cardiac cycle, while it is not fast enough for ten registrations per cardiac cycle. Discussions about the efficiency and a possible solution is addressed in section 3.5.3.

The comparison between the computational efficiency of a CPU based implementation and a GPU based implementation showed that the latter was about 15 times faster. Figure 3.8 shows the comparison on one of the dataset.

## 3.5 Discussion

### 3.5.1 Overall Efficacy of the Approach

By introducing synthetic dynamic CT images, we are able to use high spatio-temporal resolution dynamic images as a major component of our mixed-reality guidance system for mini-

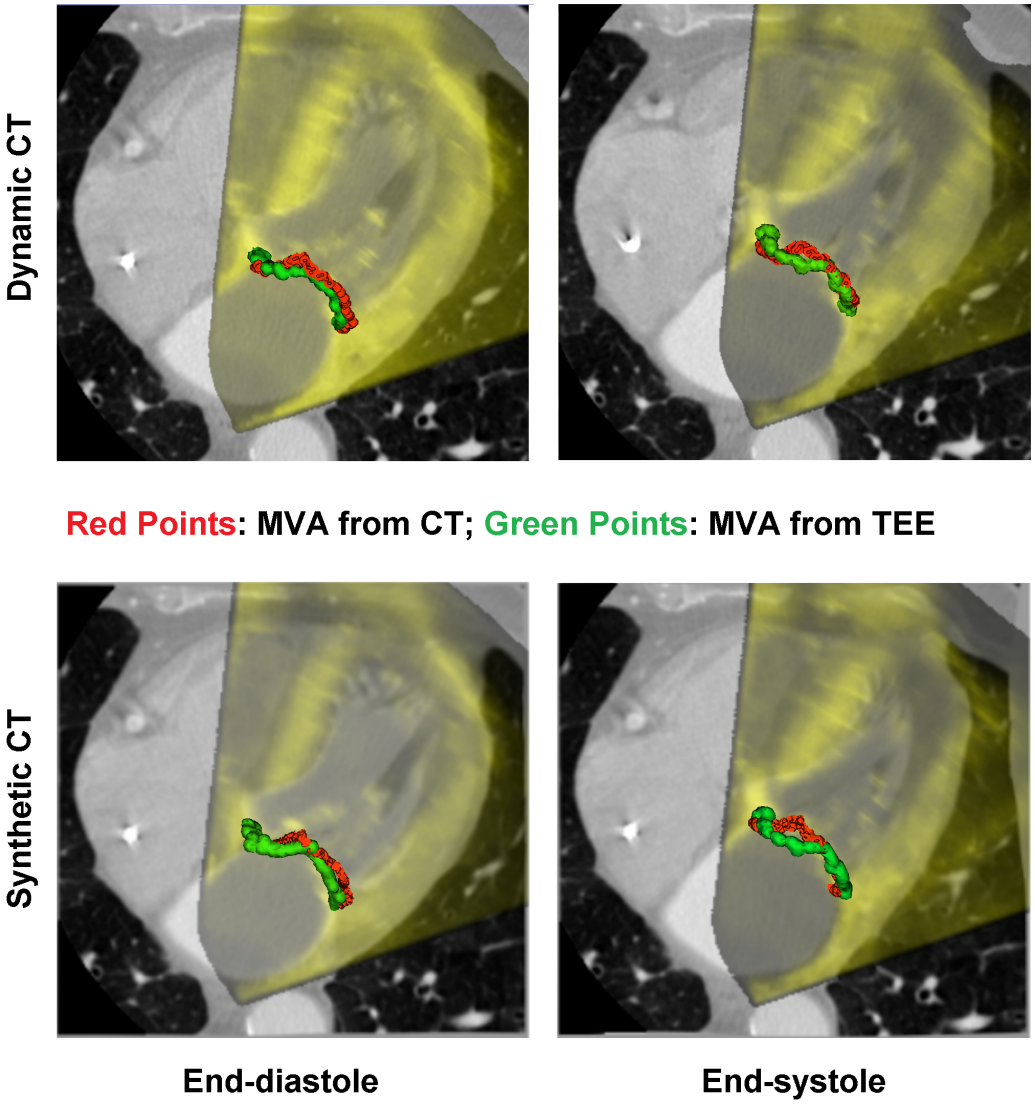


Figure 3.6: An Example of the Registration Results

mally invasive off-pump beating heart mitral valve repair. Compared to retrospectively gated CT scans, the generation of the synthetic CT images can significantly reduce the radiation dose applied to the patients, whereas the registration accuracy is maintained with respect to the MVA.

The approach uses only the modalities that are commonly available and are already used as standard of care, which adds no extra workflow in image acquisition.

Compared to performing non-rigid registration intra-operatively, which is still very difficult to achieve as a real-time application, the idea of generating synthetic CT images pre-operatively

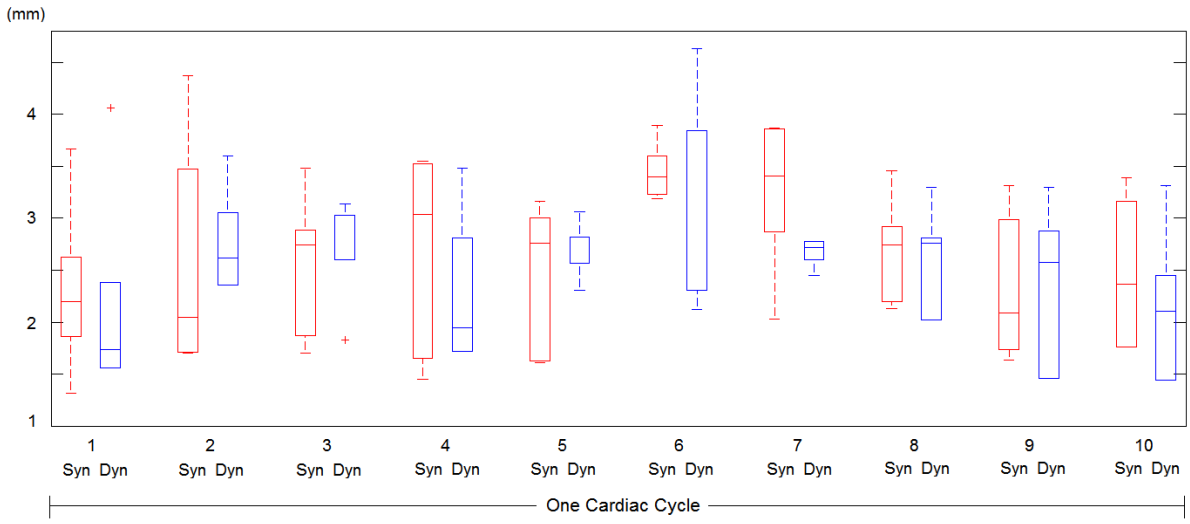


Figure 3.7: Comparison between the Phase-by-Phase TRE Results with Synthetic and Real Dynamic CT images

divides a difficult task into two relatively simple tasks. The synthetic CT generation places the most computationally intensive tasks, i.e. the non-rigid registration that deals with the heart deformation, at the pre-operative stage, which eliminates the real-time requirement.

The mutual information based rigid registration approach is used intra-operatively to perform the CT-TEE registration. Although it is not the most accurate registration approach, the accuracy is considered to be sufficient for navigation purposes, and most importantly, it is able to be performed in real time.

Furthermore, just as for real dynamic CT images, the synthetic images also provide the opportunity of generating user defined segmentations, annotations and mesh models that may be integrated into the intra-operative guidance, volume-rendering them with various transfer functions or even fusing them with intra-operative images.

### 3.5.2 Overall Accuracy of the Registration Results

In the validation of real-time CT-TEE registration, we used the MVA as the target for our TRE validation. The resulting TRE error is about 2.7±0.9 mm for both synCT and dynCT images. As for the synthetic CT generation, this error is a combination of registration error, imperfect

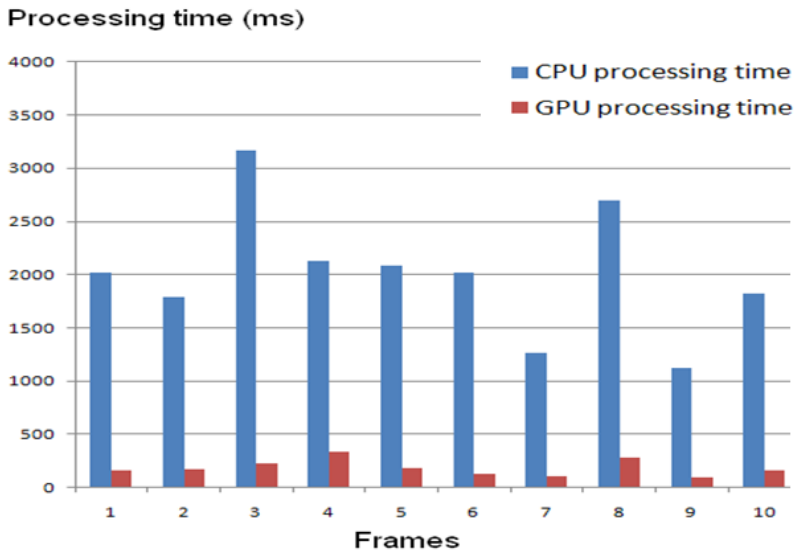


Figure 3.8: The comparison of processing time between GPU and CPU implementations

temporal alignment, inter-modality variation, and manual segmentation variation.

The most similar validation in terms of MVA tracking was reported in the studies of Schneider et al. [38, 39], in which the MVA was segmented from 3D US images. The segmentation errors against manual segmentation in those two papers were 1.81±0.78 mm and 1.67±0.63 mm. However, they also reported that the inter-expert variation in manual segmentation was from 1.63±0.76 mm to 1.99±1.15 mm.

Since we have made several trade-offs between accuracy and efficiency, it is not surprising that the TRE errors in our study are higher than those reported by Schneider. For example, the transformation was restricted to be rigid for the sake of speed, whereas a non-rigid deformation can easily achieve lower TRE error. However, our approach is able to perform several registrations within one second which makes it available for intra-op applications that require real-time updates, whereas Schneiders approach takes 30-90 seconds for a single segmentation.

In our experience, a TRE of 3-4 mm is within the tolerance of inaccuracy in the navigation stage of off-pump BH MVR. In this sense, the advantage of our approach is being able to integrate pre-op images to intra-op applications in real-time with the required accuracy.

### 3.5.3 Computational Efficiency

The performance test showed that the registration approach discussed in this paper was able to perform 3-5 registrations per second, which was still lower than the image acquisition rate for TEE. Although the efficiency can be improved to ten frames per cardiac cycle by decreasing the number of sample points used for registration, the registration accuracy suffers as a result. In other words, with a relatively small number of sample points the registration may still give correct results for some of the frames, but for others the errors may be in the order of centimeters. This situation is unacceptable for a real time clinical application, since robustness is one of the major concerns.

Another option for overcoming the limitation in efficiency is to perform a single registration for one frame and applying the resulting transformation to all of the individual CT-US frame pairs within the cardiac cycle. This approach is based on the assumption that in an ideal world, where CT and TEE images represent exactly the same heart motion, the corresponding CT and TEE frames are temporally perfectly aligned, and that they represent exactly the same structure and deformation. We also assume that the registration approach delivers optimal results, and the relative position between the TEE probe and the heart is completely fixed. In this scenario, the rigid transformation between the CT and TEE images should be identical for all the frames. In the real world, imperfections in the above factors can result in slightly different registration results for each frame, which is why we perform registration for each frame in the validation section. However, if the TRE errors associated with using identical transformations for all the frames in one cardiac cycle are still within the tolerance of the navigation application, it is reasonable to use this approach as a trade-off between accuracy and feasibility, for a highly time-critical application. To investigate the accuracy of this approach, we employed the same datasets as used in the results section, registered the first pair of CT-US frames, applied the resulting transformations to each of the other nine frames, and compared the results to those obtained when we performed ten separate registrations per cardiac cycle. Figure 3.9 shows the results of this comparison, in which the left image displays the comparison between the

one-transformation-applied-to-all-frames approach (green) and the one-registration-per-frame approach (blue), with real dynamic CT images, whereas the right image shows the same type of comparison (results of the one-transformation-per-frame approach in red) with synthetic CT images. It is seen that applying identical transformations to all the frames led to worse registration accuracy than that obtained when using a single transform (with a p-value of $< .05$), but that the differences in TREs were only about 1-2 mm. If this level of errors is still tolerable for the navigation application, then this approach may be considered as an option for implementing a real time application and avoiding the need for additional hardware acceleration.

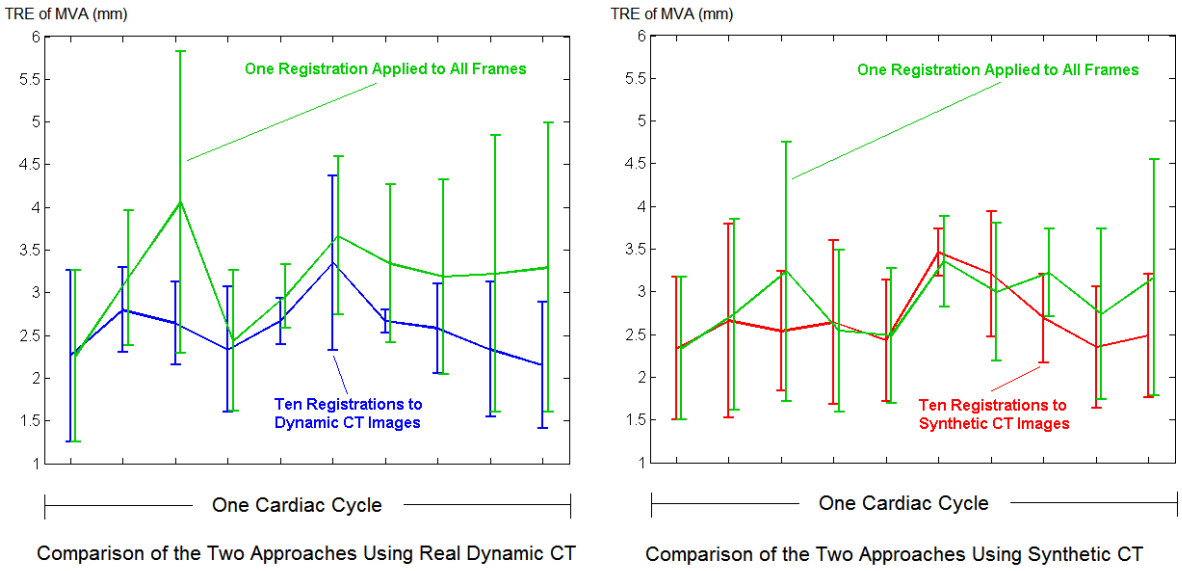


Figure 3.9: Comparison of the registration accuracy between one-registration-applied-to-all-frames approach and one-registration-per-frame approach using both real dynamic and synthetic CT images

For comparison, Figure 3.10 shows the registration accuracy, if all the TEE images are registered to a static CT image, which can be considered as the lower bound of accuracy.

## 3.6 Conclusion

In this chapter, we introduced an approach to support guidance of minimally invasive off-pump beating heart mitral valve repair that employs both TEE images and dynamic CT images. The

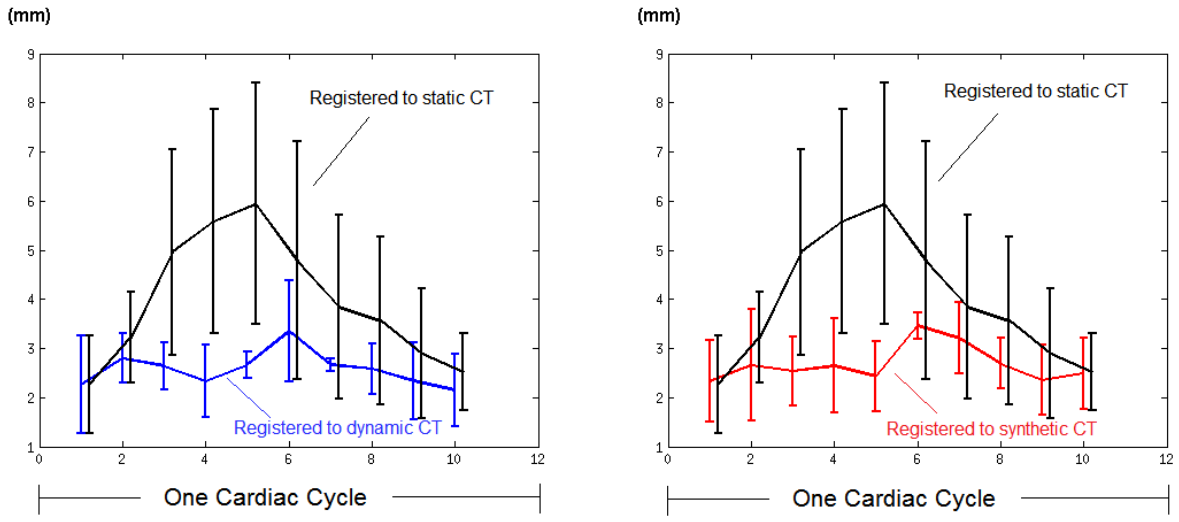


Figure 3.10: An illustration of the registration accuracy, if all TEE images are registered to a static CT image

dynamic CT images are registered to the intra-operative TEE images in real time through a GPU accelerated rigid registration approach. We demonstrated such an approach can provide good registration accuracy (TRE: ~3mm) and consequently accurate MVA tracking results. To avoid ionizing radiation dose, we attempted to use the synthetic CT images described in Chapter 2 to replace real dynamic CT images. Validation experiments have compared the registration accuracy using synthetic CT to that using real dynamic CT. The TRE was measured by computing the distances between the manually segmented MVAs. The results demonstrated that the synthetic CT images can provide similar registration accuracy in the CT-TEE registration applications to that can be achieved using real dynamic CT images. The registration algorithm was accelerated by a parallelized GPU implementation, which allows it to perform 3-5 registrations per second. Future work may include testing this approach in animal studies, investigating optimal visualization options, and measuring the impact on clinical outcomes.

# Bibliography

[1] L. A. Freed, D. Levy, R. A. Levine, M. G. Larson, J. C. Evans, D. L. Fuller, B. Lehman, and E. J. Benjamin, "Prevelence and Clinical Outcome of Mitral Valve Prolapse," *The New England Journal of Medicine*, vol. 341, no. 1, pp. 1–7, 1999.

[2] E. Hayek, C. N. Gring, and B. P. Griffin, "Mitral valve prolapse," *Lancet*, vol. 365, no. 9458, pp. 507–18, 2005.

[3] T. Gardner, P. Horneffer, T. Manolio, T. Pearson, V. Gott, W. Baumgartner, A. Borkon, L. Watkins Jr., and B. Reitz, "Stroke following coronary artery bypass grafting: a ten-year study," *Annual Thoracic Surgery*, vol. 40, no. 6, pp. 574–581, 1985.

[4] S. Slogoff, G. Reul, A. Keats, G. Curry, M. Crum, B. Elmquist, N. Giesecke, J. Jistel, L. Rogers, and J. Soderberg, "Role of perfusion pressure and flow in major organ dysfunction after cardiopulmonary bypass," *Annual Thoracic Surgery*, vol. 50, no. 6, pp. 911–918, 1990.

[5] M. F. Newman, J. P. Mathew, H. P. Grocott, G. B. Mackensen, T. Monk, K. a. Welsh-Bohmer, J. a. Blumenthal, D. T. Laskowitz, and D. B. Mark, "Central nervous system injury associated with cardiac surgery.," *Lancet*, vol. 368, pp. 694–703, Aug. 2006.

[6] G. M. Guiraudon, D. L. Jones, D. Bainbridge, and T. M. Peters, "Mitral valve implantation using off-pump closed beating intracardiac surgery: a feasibility study.," *Interactive cardiovascular and thoracic surgery*, vol. 6, pp. 603–7, Oct. 2007.

[7] S. W. Downing, W. A. Herzog, J. S. McLaughlin, and T. P. Gilbert, "Beating-heart mitral valve surgery: Preliminary model and methodology," *The Journal of Thoracic and Cardiovascular Surgery*, vol. 123, pp. 1141–1146, June 2002.

[8] Y. Suematsu, G. R. Marx, J. a. Stoll, P. E. DuPont, R. O. Cleveland, R. D. Howe, J. K. Triedman, T. Mihaljevic, B. N. Mora, B. J. Savord, I. S. Salgo, and P. J. del Nido,

"Three-dimensional echocardiography-guided beating-heart surgery without cardiopulmonary bypass: a feasibility study.," *The Journal of thoracic and cardiovascular surgery*, vol. 128, pp. 579–87, Oct. 2004.

[9] E. Altiok, M. Becker, S. Hamada, S. Reith, N. Marx, and R. Hoffmann, "Optimized guidance of percutaneous edge-to edge repair of the mitral valve using real-time 3-D transesophageal echocardiography," *Clinical research in cardiology : official journal of the German Cardiac Society*, vol. 100, pp. 675–81, Aug. 2011.

[10] N. Wunderlich, J. Franke, N. Wilson, and H. Sievert, "3D Echo Guidance for Structural Heart Interventions," *Interventional Cardiology Review*, vol. 4, no. 1, pp. 16–20, 2009.

[11] J. T. Moore, M. W. A. Chu, B. Kiaii, D. Bainbridge, G. Guiraudon, C. Wedlake, M. Currie, M. Rajchl, R. V. Patel, and T. M. Peters, "A navigation platform for guidance of beating heart transapical mitral valve repair.," *IEEE transactions on bio-medical engineering*, vol. 60, pp. 1034–40, Apr. 2013.

[12] M. W. Chu, J. Moore, T. M. Peters, D. Bainbridge, D. McCarty, G. M. Guiraudon, C. Wedlake, P. Lang, M. Rajchl, M. E. Currie, R. C. Daly, and B. Kiaii, "Augmented reality image guidance improves navigation for beating heart mitral valve repair," *Innovations*, vol. 7, no. 4, pp. 274–281, 2012.

[13] D. Bainbridge, D. L. Jones, G. M. Guiraudon, and T. M. Peters, "Ultrasound image and augmented reality guidance for off-pump, closed, beating, intracardiac surgery.," *Artificial organs*, vol. 32, pp. 840–5, Nov. 2008.

[14] R. Bauernschmitt, M. Feuerstein, J. Traub, E. U. Schirmbeck, G. Klinker, and R. Lange, "Optimal port placement and enhanced guidance in robotically assisted cardiac surgery.," *Surgical endoscopy*, vol. 21, pp. 684–7, Apr. 2007.

[15] S. De Buck, F. Maes, J. Ector, J. Bogaert, S. Dymarkowski, H. Heidbüchel, and P. Suetens,

"An augmented reality system for patient-specific guidance of cardiac catheter ablation procedures.," *IEEE transactions on medical imaging*, vol. 24, pp. 1512–24, Nov. 2005.

[16] C. A. Linte, J. Moore, C. Wedlake, D. Bainbridge, G. M. Guiraudon, D. L. Jones, and T. M. Peters, "Inside the beating heart: an in vivo feasibility study on fusing pre- and intra-operative imaging for minimally invasive therapy.," *International journal of computer assisted radiology and surgery*, vol. 4, pp. 113–23, Mar. 2009.

[17] X. Huang, J. Ren, G. Guiraudon, D. Boughner, and T. M. Peters, "Rapid dynamic image registration of the beating heart for diagnosis and surgical navigation," *IEEE transactions on medical imaging*, vol. 28, pp. 1802–14, Nov. 2009.

[18] W. P. Shuman, K. R. Branch, J. M. May, L. M. Mitsumori, D. W. Lockhart, T. J. Dubinsky, B. H. Warren, and J. H. Caldwell, "Prospective versus Retrospective ECG Gating for 64-Detector CT of the Coronary Arteries : Comparison of Image Quality and Patient Radiation Dose," *Radiology*, vol. 248, no. 2, pp. 431–437, 2008.

[19] N. Hirai, J. Horiguchi, C. Fujioka, M. Kiguchi, H. Yamamoto, N. Matsuura, T. Kitagawa, H. Teragawa, N. Kohno, and K. Ito, "Prospective versus Retrospective ECG-gated 64-Detector Coronary CT Angiography : Assessment of Image Quality, Stenosis, and Radiation Dose," *Radiology*, vol. 248, no. 2, pp. 424–430, 2008.

[20] "http://www.abbottvascular.com/int/mitraclip.html#overview."

[21] "http://www.mitralign.com/,"

[22] J. Harnek, J. G. Webb, K.-H. Kuck, C. Tschope, A. Vahanian, C. E. Buller, S. K. James, C. P. Tiefenbacher, and G. W. Stone, "Transcatheter implantation of the MONARC coronary sinus device for mitral regurgitation: 1-year results from the EVOLUTION phase I study (Clinical Evaluation of the Edwards Lifesciences Percutaneous Mitral Annuloplasty System for the Treatment of Mitral R," *JACC. Cardiovascular interventions*, vol. 4, pp. 115–22, Jan. 2011.

[23] F. P. Li, M. Rajchl, J. A. White, A. Goela, and T. M. Peters, "Towards CT Enhanced Ultrasound Guidance for Off-pump Beating Heart Mitral Valve Repair," in *Augmented Reality Environments for Medical Imaging and Computer-Assisted Interventions Lecture Notes in Computer Science, Volume 8090*, pp. 136–143, 2013.

[24] M. Rajchl, J. Yuan, J. White, E. Ukwatta, J. Stirrat, C. Nambakhsh, F. Li, and T. Peters, "Interactive Hierarchical Max-Flow Segmentation of Scar Tissue from Late-Enhancement Cardiac MR Images.," *IEEE transactions on medical imaging*, vol. 33, pp. 159–172, Sept. 2013.

[25] F. Li, P. Lang, M. Rajchl, E. C. S. Chen, G. Guiraudon, and T. M. Peters, "Towards real-time 3D US-CT registration on the beating heart for guidance of minimally invasive cardiac interventions," in *Proc. SPIE 8316, Medical Imaging 2012* (D. R. Holmes III and K. H. Wong, eds.), vol. 8316, p. 831615, Feb. 2012.

[26] P. Lang, M. Rajchl, F. Li, and T. M. Peters, "Towards Model-Enhanced Real-Time Ultrasound Guided Cardiac Interventions," in *Proc. 2011 International Conference on Intelligent Computation and Bio-Medical Instrumentation*, pp. 89–92, Ieee, Dec. 2011.

[27] M. Rajchl, J. Yuan, E. Ukwatta, and T. M. Peters, "Fast Interactive Multi-region Cardiac Segmentation with Linearly Ordered Labels," in *2012 9th IEEE International Symposium on Biomedical Imaging (ISBI)*, pp. 1409–1412, 2012.

[28] P. J. Besl and N. D. McKay, "A Method for Registration of 3-D Shapes," *IEEE Transaction on Pattern Analysis and Machine Intelligence*, vol. 14, no. 2, pp. 229–256, 1992.

[29] J. P. W. Pluim, J. B. A. Maintz, and M. a. Viergever, "Mutual-information-based registration of medical images: a survey," *IEEE transactions on medical imaging*, vol. 22, pp. 986–1004, Aug. 2003.

[30] M. Modat, G. R. Ridgway, Z. a. Taylor, M. Lehmann, J. Barnes, D. J. Hawkes, N. C. Fox,

and S. Ourselin, "Fast free-form deformation using graphics processing units.," *Computer methods and programs in biomedicine*, vol. 98, pp. 278–84, June 2010.

[31] M. J. D. Powell, "An efficient method for finding the minimum of a function of several variables without calculating derivatives," *The computer journal*, vol. 7, no. 2, pp. 155–162, 1964.

[32] R. Shams, P. Sadeghi, R. Kennedy, and R. Hartley, "Parallel computation of mutual information on the GPU with application to real-time registration of 3D medical images," *Computer Methods and Programs in Biomedicine*, vol. 99, no. 2, pp. 133–146, 2009.

[33] J. Fung and S. Mann, "Using Multiple Graphics Cards as a General Purpose Parallel Computer : Applications to Computer Vision," in *Proceedings of the 17th International Conference on Pattern Recognition*, vol. 00, pp. 2–5, 2004.

[34] D. Tarditi and J. Oglesby, "Accelerator : Using Data Parallelism to Program GPUs for General-Purpose Uses," in *Proceedings of the 12th international conference on Architectural support for programming languages and operating systems*, pp. 325–335, 2006.

[35] R. Shams, P. Sadeghi, R. A. Kennedy, and R. I. Hartley, "A Survey of Medical Image Registration on Multicore and the GPU," *IEEE Signal Processing Magzine*, no. March, pp. 50–60, 2010.

[36] S. Unger, "Hazards, critical races, and metastability," *IEEE Transactions on Computers*, vol. 44, pp. 754–768, June 1995.

[37] C. Ranger, R. Raghuraman, A. Penmetsa, G. Bradski, and C. Kozyrakis, "Evaluating MapReduce for Multi-core and Multiprocessor Systems," *2007 IEEE 13th International Symposium on High Performance Computer Architecture*, pp. 13–24, 2007.

[38] R. J. Schneider, D. P. Perrin, N. V. Vasilyev, G. R. Marx, P. J. del Nido, and R. D. Howe,

"Mitral annulus segmentation from 3D ultrasound using graph cuts," *IEEE transactions on medical imaging*, vol. 29, pp. 1676–87, Sept. 2010.

[39] R. J. Schneider, D. P. Perrin, N. V. Vasilyev, G. R. Marx, P. J. del Nido, and R. D. Howe, "Mitral annulus segmentation from four-dimensional ultrasound using a valve state predictor and constrained optical flow," *Medical image analysis*, vol. 16, pp. 497–504, Feb. 2012.

# Chapter 4

# A Mitral Annulus Tracking Approach for Navigation of Off-pump Beating Heart Mitral Valve Repair

This chapter is adapted from the papers:

- Feng P. Li, Martin Rajchl, John Moore, Terry M. Peters, Ultrasound based mitral valve annulus tracking for off-pump beating heart mitral valve repair, SPIE Medical Imaging, 2014

- Feng P. Li, Martin Rajchl, John Moore, and Terry M. Peters, A Mitral Annulus Tracking Approach for Navigation of Off-pump Beating Heart Mitral Valve Repair, Medical Physics (submitted)

# 4.1 Introduction

## 4.1.1 Clinical Background

Mitral regurgitation (MR) is a common heart disorder in which the mitral valve does not close properly when the left ventricle contracts, and a portion of the oxygenated blood regurgitates from the left ventricle back to the left atrium, which reduces the amount of blood pumped out to the body [1]. This phenomenon is associated with symptoms including heart murmur, shortness of breath, fatigue, and heart palpitations. The most common cause of severe non-ischemic MR is mitral valve prolapse [2], which means one or both of the leaflets prolapse upward into the left atrium when the heart contracts. Its prevalence in North America is about 2-3% of the population [3].

Surgical options to treat mitral regurgitation are to repair or replace the mitral valve. The choice between repair and replacement is based on many factors including patient's general health, the condition of the valve, and expected benefits of the surgery. However, in recent years surgeons have begun to favor repair over replacement in most cases due to better survival rate and development of related techniques [4, 5].

Conventional mitral valve repair (MVR) was usually performed via open-heart surgery together with the use of a heart lung machine. A sternotomy is performed to gain the visual and surgical access to the patients heart, which is arrested during the procedure with the heart-lung machine temporarily taking over the function of the heart. This procedure can be associated with severe trauma and side effects to the patients, which makes it unsuitable for patients with co-morbidities such as previous heart surgery or renal dysfunction [6–8]. Aiming to reduce the trauma and side effects associated with the large incisions and the usage of heart lung machines, many techniques have been developed to perform minimally invasive off-pump beating heart mitral valve repair [9], whereby the procedure is performed through small incisions, and the heart remains beating during the procedure, with the blood flowing through the heart as normal. This technique can greatly reduce the trauma and side effects and potentially reduce

the recovery and hospitalization time. However, one important limitation of this technique is that the surgeons have direct visual access to neither the surgical targets nor the tools, which greatly increases their cognitive load. For this reason, improved image guidance capabilities are essential for minimally invasive intracardiac surgeries.

### 4.1.2 Existing Techniques for Minimally Invasive Off-pump Beating Heart MVR

Several commercially available techniques have been developed in the past few years to perform minimally invasive off-pump beating heart MVR. For example, NeoChord©DS1000 (NeoChord, Inc., MN, USA) [5, 10] is designed to perform transapical mitral valve repair by implanting artificial chordae to flailing leaflets to restore normal valvular function. MitraClip© (Abbott Laboratories, IL, USA) [11, 12] is a percutaneous mitral valve repair system that uses a clip grasping both leaflets to create a double orifice valve that can lead to better valve closure and less regurgitation. Mitralign© (Mitralign Inc. MA, USA) [13] aims to perform percutaneous mitral annuloplasty by attaching plegdgets delivered by wires to the mitral annulus and pulling the plegdgets together to reduce annulus size. Finally, the MONARC© device (Edwards Lifesciences, CA, USA) uses a different approach to perform annuloplasty by implanting a curved device in the coronary sinus to reduce the spetal-lateral diameter of the mitral annulus [14]. The latter two systems are specific to functional MR (caused by enlarged ventricles and/or annuli). While the NeoChord and Mitraclip procedures can be used to treat both functional and degenerative MR (prolapsed or flail leaflets), the NeoChord approach has been primarily used to treat degenerative MR while the MitraClip is employed primarily for functional MR.

### 4.1.3 Image Guidance for Minimally Invasive Off-pump Beating Heart MVR

Lack of direct visual access to the surgical targets and tools is a limitation of minimally invasive off-pump intracardiac procedures. This limitation precludes the intuitive understanding of the surgical field and anatomy available during open heart surgeries. To solve this problem, image guidance becomes essential in minimally invasive procedures as visual assistance that shows the necessary information about the targets and tools for the surgeons to perform the operations [15, 16]. The two most commonly used imaging modalities in cardiac procedures are X-ray fluoroscopy and echocardiography.

Although the percutaneous approaches may use X-ray fluoroscopy to guide the catheters to the heart, all the procedures mentioned above use intra-operative (intra-op) echocardiography, typically TEE, for intra-cardiac guidance, due to its capability of real-time imaging, zero ionizing radiation dose, good soft tissue contrast, low cost, and high availability [17, 18]. Using NeoChord as an example, the procedure is guided with real time 2D single plane, 2D bi-plane, and 3D TEE scans at different stages, depending on the task and corresponding imaging requirements. When the tool is approaching from the apex of the heart to the mitral valve area, it is guided by 2D single/bi-plane scans since 3D imaging lacks sufficient spatial resolution to properly identify the tool. When the tool is close to the mitral valve, the echocardiographer switches the scan mode to 3D to confirm the position of the tool tip (2D imaging lacks the sense of spatial awareness provided by 3D imaging). The imaging mode is then typically reverted to 2D because of its superior temporal and spatial resolution, to guide the procedure of grasping the leaflets. The MitaClip procedure also uses the same concept of switching between different scanning modes for guidance at different stages [19, 20].

However, ultrasound guidance introduces several problems. For 2D modes, both single plane and bi-plane, it is difficult to differentiate the tool tip from a cross-section of the shaft, because both appear as elliptical shapes in the images. It is also very hard to maintain both the tool tip and the surgical target in the imaging plane simultaneously. 3D TEE can overcome

this limitation to some extent, but at the cost of decreased temporal and spatial resolution in a restricted field of view (FOV). For the NeoChord procedure, it is also hard to differentiate the tool tip from trabeculae and papillary muscles, when it is close to the apex at the beginning of the procedure.

Our previous work has demonstrated that by integrating virtual models showing the position, orientation, and trajectory of the surgical tools, and the targets in the guidance system, the safety and efficiency of navigation can be significantly improved [21]. In that work, an MVA model was manually defined immediately before the beginning of the procedure, by selecting four MVA points, two points on each plane, in the bi-plane ultrasound images and generating a cubic spline based on the four points. By visualizing both the MVA model the surgical tool model that is continuously updated based on the magnetic tracking information in the same guidance platform, the navigation task is accomplished by moving the tip of the tool model to the centre of the MVA model. However, one limitation of this work was that the MVA model was stationary during the procedure, and experience has shown that other than periodic motion related to the cardiac motion within one cardiac cycle, the MVA can also shift by one or two centimeters during the procedure, due to tool manipulation and changes in patient positioning. A stationary model is not sufficient for accurate navigation when such a situation occurs, especially for the NeoChord procedure which typically requires the attachment of multiple chordae. Although it is possible to pause the operation and re-define the new position of the MVA manually, it is very time-consuming and can be a distraction for the surgeons.

### 4.1.4 Contributions

In this paper, we introduce an approach to automatically track the MVA and render it at a desired cardiac phase in near real-time, based on both the TEE images and the magnetic tracking information of the TEE probe. The validation of the approach was performed both on a dynamic heart phantom and on retrospectively on images from a porcine study.

## 4.2 Method

### 4.2.1 Overall System Setup

The guidance system comprises three major components: the TEE, the magnetic tracking system including the sensors to be attached to the surgical tools, and the guidance software platform. Figure 4.1 shows the general workflow of the system and how each component interacts with the others.

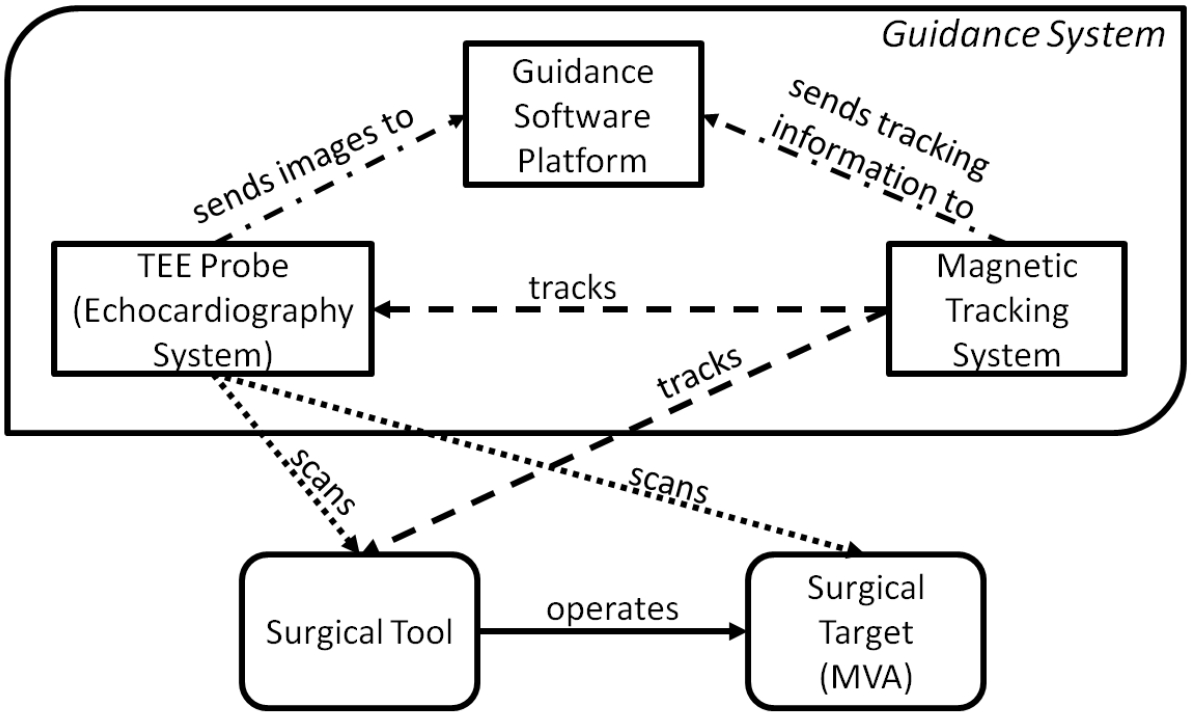


Figure 4.1: Overall system setup showing how each component interacts with the others

The TEE probe is inserted into the patients esophagus to scan the surgical targets (i.e. MVA) together with its surrounding tissues and the surgical tools. The obtained images are continuously transferred to the guidance software platform in real time. The echocardiography system we use in this project is the Phillips iE33 ultrasound system and the X7-2t probe. This system allows the echocardiographer to choose from three scanning modes: single plane 2D,

bi-plane 2D, and live 3D. For the navigation task in the NeoChord procedure, we use the bi-plane mode, which is also used in the current guidance solution for the NeoChord procedure, and we recommend positioning the two planes orthogonal to each other with one showing the Mid-esophageal (ME) four chamber view and the other showing the ME two chamber view.

The magnetic tracking system tracks the position and orientation of the surgical tools and the TEE probe and continuously sends the tracking information to the guidance software. We use the Aurora© system from the Northern Digital Inc. (NDI) as the magnetic tracking system (MTS) in this project. A flat table-top magnetic field generator is placed between the subject and the operating table, and the position of the generator should ensure that the operating field is adequately covered by the magnetic field. A 6 Degree-of-freedom (DoF) magnetic sensor (3 DoF of translation and 3 DoF of rotation) is attached to the side of the transducer, and another 6 DoF sensor is integrated into the NeoChord tool. With proper calibration, those two sensors provide information about the position and orientation of the tools and the probe with reference to the field generator. A 5 DoF sensor is attached to the moving part of the NeoChord tool to track the open-and-close movement of the jaw.

The guidance software platform has four major functions. First, it continuously collects the TEE images and the tool tracking information in real time, synchronizes them, and stores them in memory. It then visualizes the TEE images and the tools in one common coordinate frame, with real time updates based on the tracking information and the pre-defined tool models. Next, it allows the user to define a few, typically four, MVA points, and generates a virtual MVA spline model immediately before the procedure starts. Finally, it tracks the movement of the MVA and updates its new position during the procedure (Figure 4.2).

### 4.2.2 Mitral Valve Tracking Based on TEE Image Data

Our MVA tracking approach can be divided into three parts: image based gating, predictive re-initialization, and registration based MVA tracking. Figure 4.3 shows the overall workflow of the MVA tracking approach.

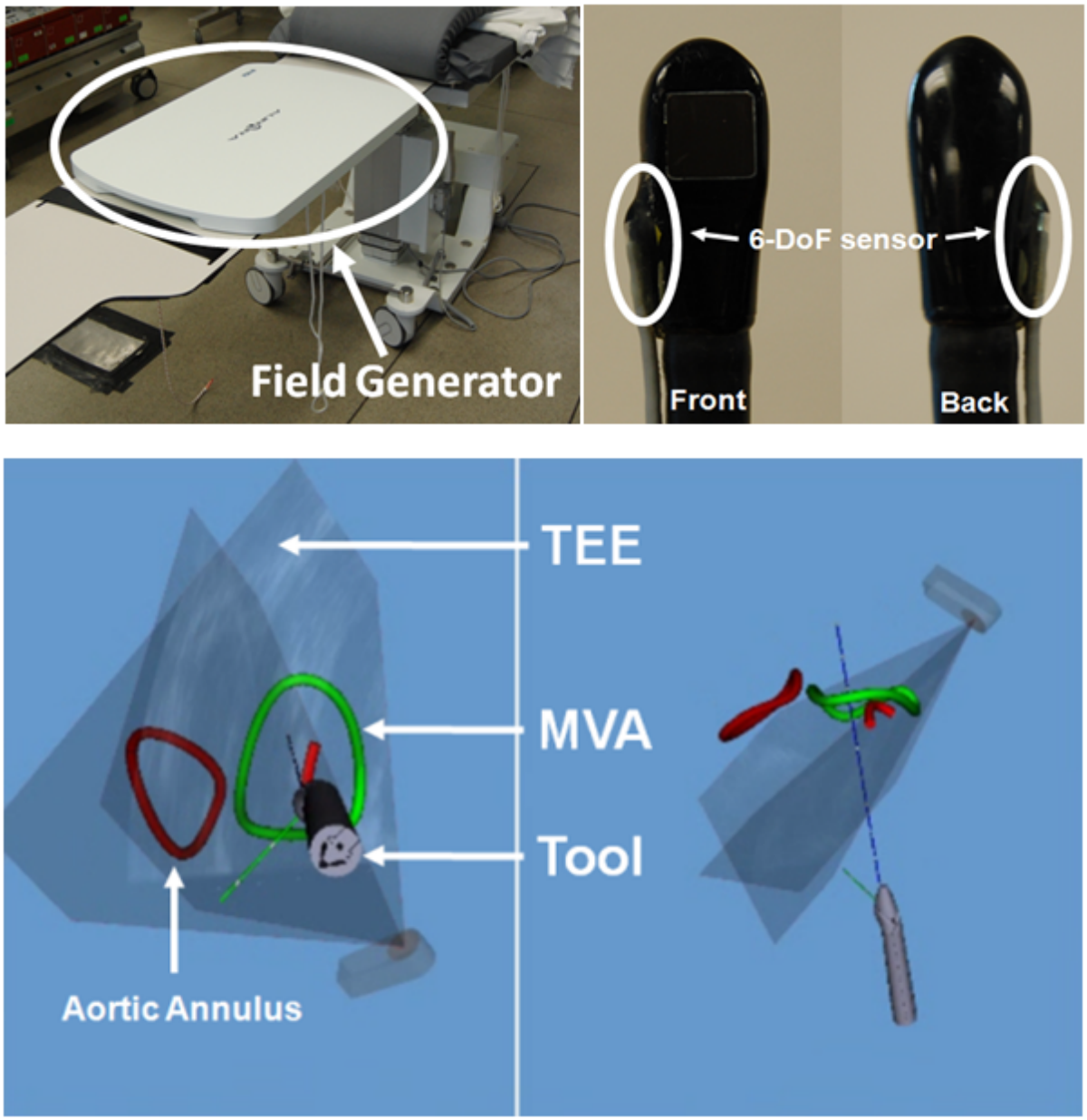


Figure 4.2: Overall system setup. Left: Magnetic field generator. Middle: TEE probe with an attached 6-DoF magnetic sensor. Right: Screen capture of the augmented virtuality guidance system.

### Initialization

In the initialization stage, which occurs immediately after apical access is secured, the user is asked to define two MVA points on each plane of the biplane image (four MVA points in total). An MVA model is computed as a cubic spline with the four MVA points as control points, as

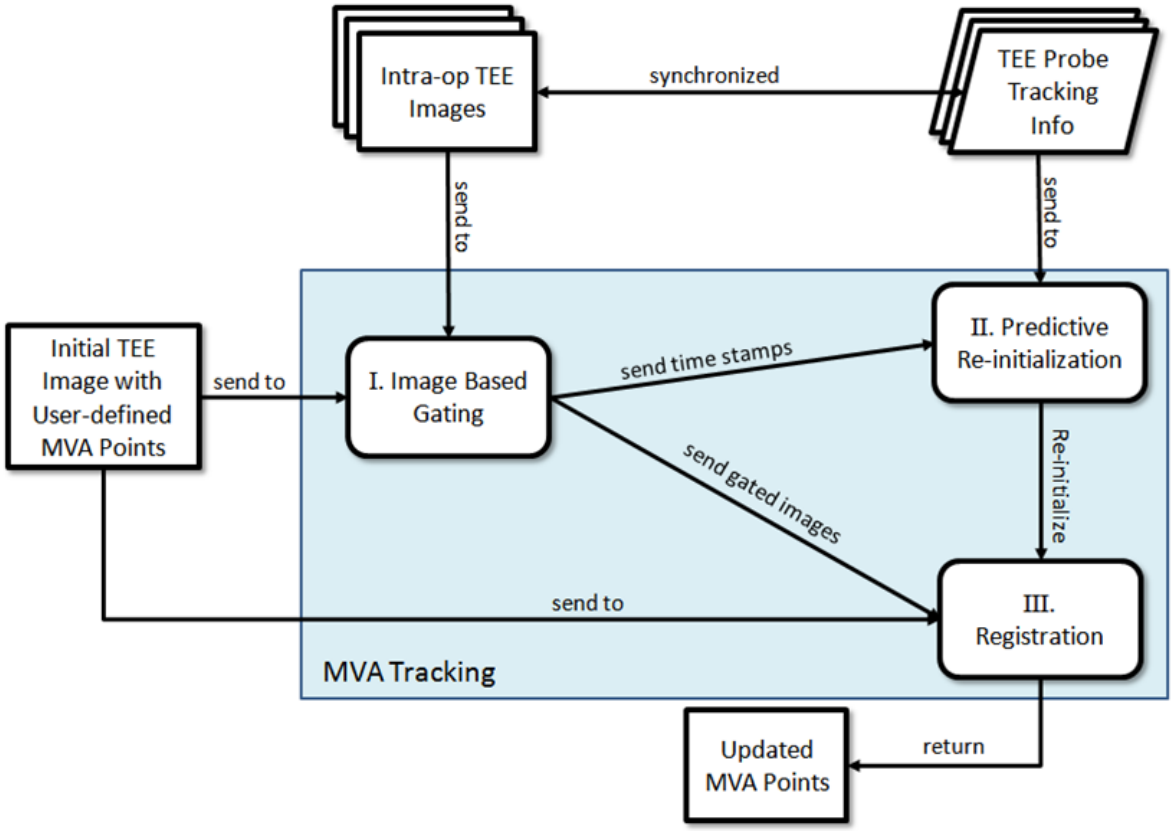


Figure 4.3: Overall workflow of the MVA tracking approach

described in previous work by our group [21]. The initial image together with the four MVA points is transferred to the mitral valve tracking module for the image based gating component and the registration component to use.

### Image Based Gating

The mitral valve undergoes constant cyclical motion over the course of the cardiac cycle. From systole to diastole it can move more than 10mm [22, 23]. In our experience, rendering this motion is actually a distraction for the surgeon, and it is preferable to render only one phase of the cardiac cycle. However, as mentioned previously the MVA can also shift location during the surgical intervention, and it is this motion we are interested in tracking and displaying to the surgical team. Image based gating is necessary to effectively filter out the natural MVA motion of the cardiac cycle, leaving only the anatomical shift caused by the intervention itself. During

the procedure the intra-operative (intra-op) TEE images are continuously transferred from the echocardiography system to the guidance software. The major task of the image based gating component is to identify the images that represent the same cardiac phase as the initial image from all the incoming images. This is achieved by comparing each intra-operative image to the initial image, compute the sum of absolute differences (SAD) similarity between them, and find the images that lead to a minimum.

The similarity is computed based on small patches rather than the entire images for computational efficiency. For the initial image, four patches are extracted, with each centred at the user-defined MVA points. Figure 4.4 shows one example of extracting a square-shaped patch with a width of 101 pixels from a TEE image. The centre of the patch coincides with the user-defined MVA points. These four patches are stored in the software throughout the whole procedure and all the patches extracted from the intra-op images are compared to them.

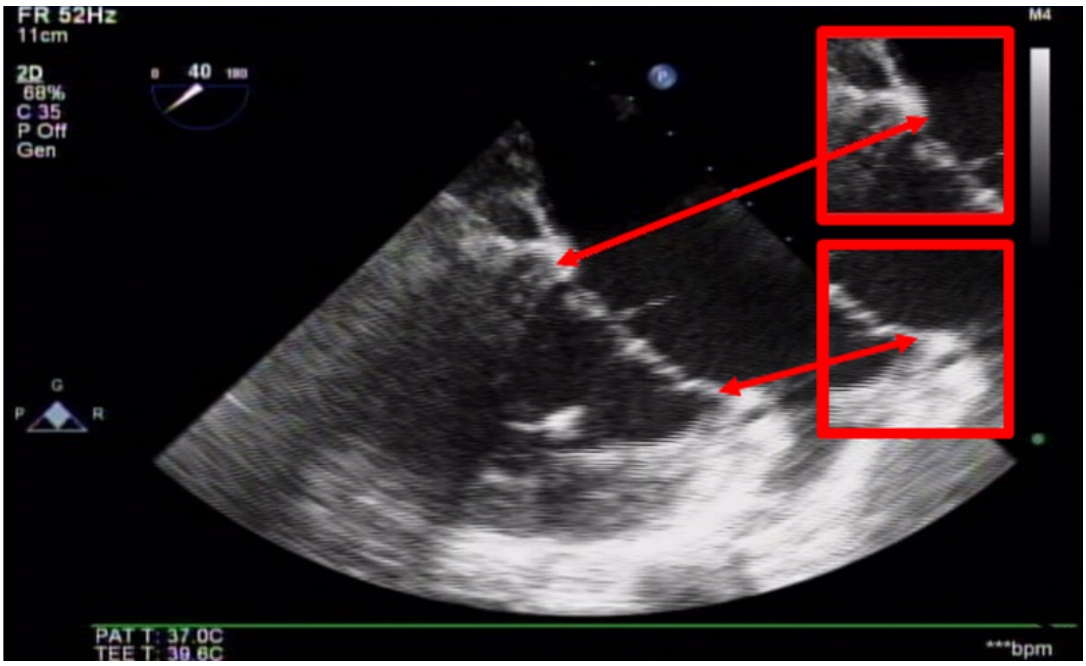


Figure 4.4: An example of extracting two square patches from a TEE image. The patches are centred at the user-defined MVA point.

During the procedure, for every intra-op image, four patches are extracted at the same image coordinates as the initial patches, and these patches are stored in four separate queues in

the memory. The length of the queues can be adjusted according to the heart rate and cover at least two complete cardiac cycles. When a queue reaches its maximum length, the oldest patch is eliminated to receive new images. For each patch in a queue we compute the SAD of the grayscale value between itself and its corresponding initial patch. The SAD metric is chosen here because this is a relatively simple intra-modality application and it can be very efficiently parallelized and executed on a graphic processing unit (GPU). Let the initial four patches be denoted as $P_{k,0}(x, y)$, $k = 1, 2, 3, 4$ and the subsequent patches as $P_{k,i}(x, y)$, $k = 1, 2, 3, 4$, where $i = 1, 2, 3, 4, .....$ indicates the time stamp. Then, we have

$$SAD_{k,i} = \sum_{x,y} |P_{k,0}(x, y) - P_{k,i}(x, y)| \tag{4.1}$$

where $P_{k,i}$ is the patch of the k-th MVA point with time stamp $i$ and $x, y$ is the image coordinate of each pixel in the patch with respect to the origin of the whole image. The SADs are also stored in four queues which correspond to the patch queues. A minimum detection function is applied continuously on the SAD queues to detect the patches leading to an SAD minimum (Figure 4.5), i.e. the patches that are most similar to the initial patches. A low-pass filter is applied to filter out high frequency changes. Once a new minimum is detected, we consider that patch to be of the same cardiac phase as its corresponding initial patch. Its time stamp is be sent to the predictive re-initialization component to index the probe tracking information at that time point, and the relevant patch itself is sent to the registration component for MVA point tracking.

### 4.2.3 Predictive Re-initialization

Since the location of the TEE probe is often adjusted during the surgical procedure, our MVA tracking algorithm must be able to adapt to both new MVA locations in the image plane, and variations in the actual MVA anatomy being displayed. To accommodate this, we use a predictive model to re-initialize the start point for our MVA patch registrations. As the intra-op

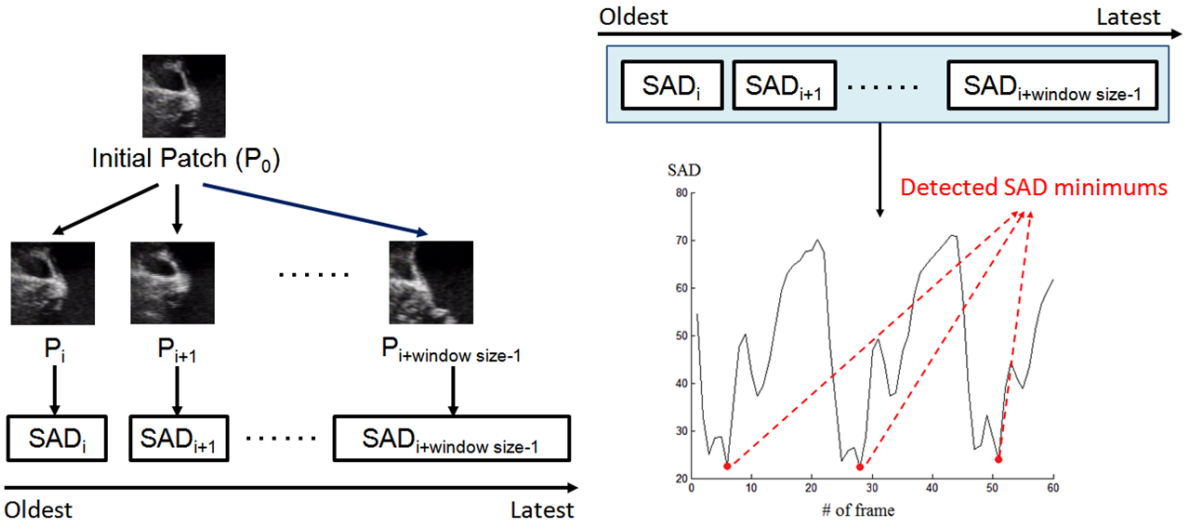


Figure 4.5: Flowchart of computing SAD values between the initial patch and the patch queue and detecting minimums in the SAD queue

images are continuously transferred to the image based gating component, their synchronized probe tracking data are simultaneously transferred to the predictive re-initialization component. The probe tracking information, together with the TEE calibration transform, can be used to compute the position and orientation of the imaging planes in the physical (magnetic tracker) space. This leads to the transform converting the image coordinate of each pixel in the TEE image to the physical coordinate with respect to the table-top field generator and vice versa.

The probe tracking information in the form of 2D-3D transforms is stored by the predictive re-initialization component in a queue with the same length as the patch queue and the SAD queue. Each time an image patch is added to the patch queue, its corresponding 2D-3D transform is added to the transform queue. In this manner, it is easy to retrieve both a patch and its transform from the two queues by using the same queue index.

The 2D-3D transforms are used to predict the position (image coordinate) of the MVA points in a TEE image, based on the last updated MVA model. The prediction is then used as an initialization in the registration component. Once the image based gating module sends a time stamp of a patch in the form of a queue index, to the predictive re-initialization component, the latter finds the corresponding 2D-3D transform. Here, we assume the position of the MVA has

not changed significantly since the last update. We can then compute the points of intersection in physical space between the latest MVA model and the imaging planes, as referenced by the time stamp, and convert the results to 2D image coordinates by using the 2D-3D transform (Figure 4.6). The converted 2D image coordinates are used as a prediction of the new MVA position.

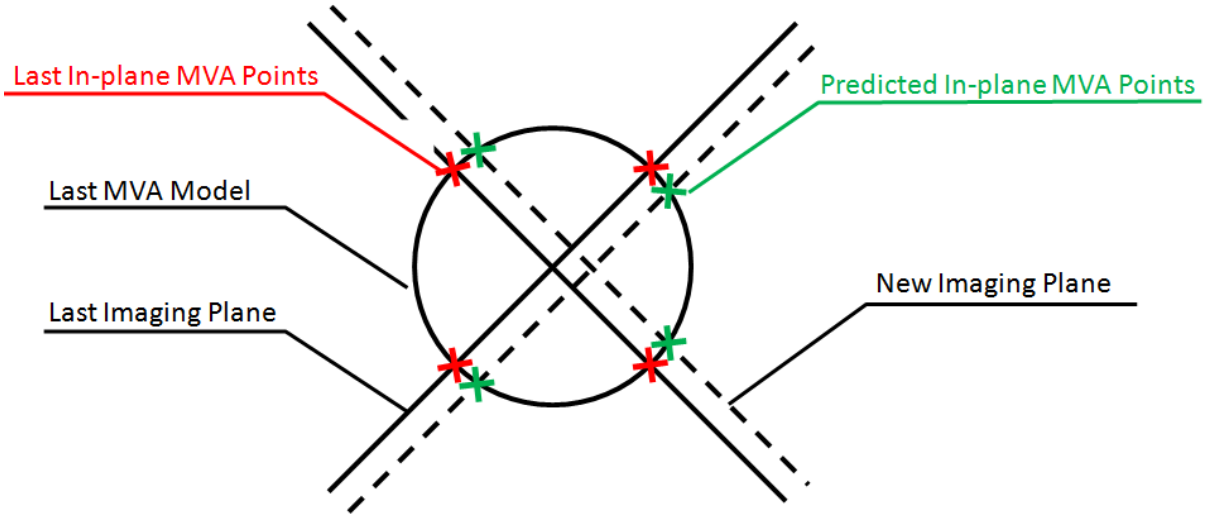


Figure 4.6: An illustration of predicting the position of in-plane MVA points based on the last MVA model and the new imaging plane

### 4.2.4 Registration for MVA tracking

The registration component updates the position of the MVA points by registering the patches to the initial image. The update occurs once the gating component detects a new minimum for each patch, i.e. once per cardiac cycle. The similarity metric used here is also SAD. With the initial image as the fixed image, and the patch as the moving image, the registration is performed by using a brute force approach to search every possible location in the translation space within a user-defined search area to ensure a global minimum. This minimization problem can be described as

$$(m,n) = \arg\min_{m,n\in S} \sum_{x,y\in P} |I_0(x,y) - P_i(x+m, y+n)| \tag{4.2}$$

where $S$ defines the search space, $I_0$ is the initial image, $x, y$ is the coordinate of a pixel in image coordinates. After the registration, we assume that the MVA point in the patch coincides with the MVA point in the initial image. By applying the inverse transform to the MVA point in the initial image, we can obtain the new image coordinates of the MVA point, which are then used to update the MVA spline model.

The brute force search approach for such a problem can be very time consuming, if it is implemented as a single thread application. However, GPU chips with the capability of general purpose computing have provided an opportunity to perform massively parallel computations in a very efficient manner [24], which is exactly what the brute force search approach can benefit from. There are two levels of parallelization that can be performed in this problem. First, for each set of search parameters, i.e. $(m_j, n_j)$, a SAD similarity can be computed (Figure 4.7b). Since the computations of the SADs based on different parameter sets are mutually independent, in theory all these computations could be performed simultaneously, whereas the procedure of finding the minimal SAD can be performed by a hierarchical approach called MapReduce [25]. In addition, for the SAD computation itself, the first step is to compute the absolute difference (AD) between each pair of pixels (Figure 4.7a), which can also be performed independently and simultaneously. The procedure of summing all the ADs to obtain an SAD can be performed by the MapReduce approach as well.

As mentioned earlier, we are able to update the four MVA hinge points in approximately 60 ms. Since our goal is to render the annular ring at only one cardiac phase (end diastole), this speed is more than adequate to track any shift in target anatomy.

## 4.3 Experiments

### 4.3.1 Phantom Study

A custom-built phantom, consisting of a left ventricle, mitral and aortic valves, a pneumatic actuator assembly and an atrial reservoir, was employed to validate our MVA tracking in a con-

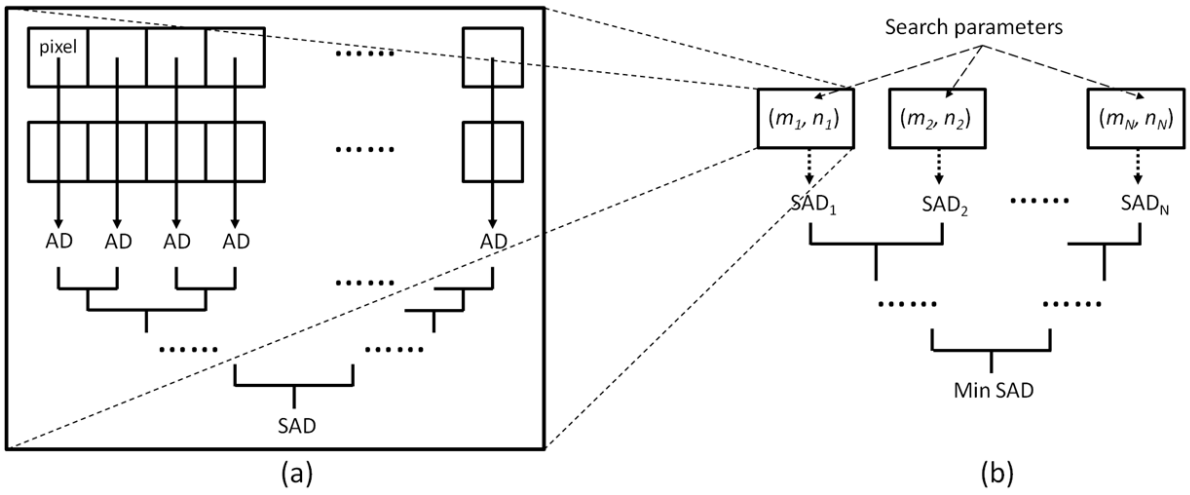


Figure 4.7: An example of parallelization for finding the minimal SAD

trolled environment. The silicone model of the left ventricle has papillary muscles and chordae tendinae controlling the mitral valve. The anterior and posterior leaflets of the mitral valve has also made from silicone, with nylon chordae embedded into the silicone for support. The length from anterior to posterior commissure is 35mm, and 25mm in the perpendicular plane (across the P2 to A2 leaflets). A microcontroller manages the pneumatic cylinders permitting a variety of contraction behaviors and rates (Figure 4.8).

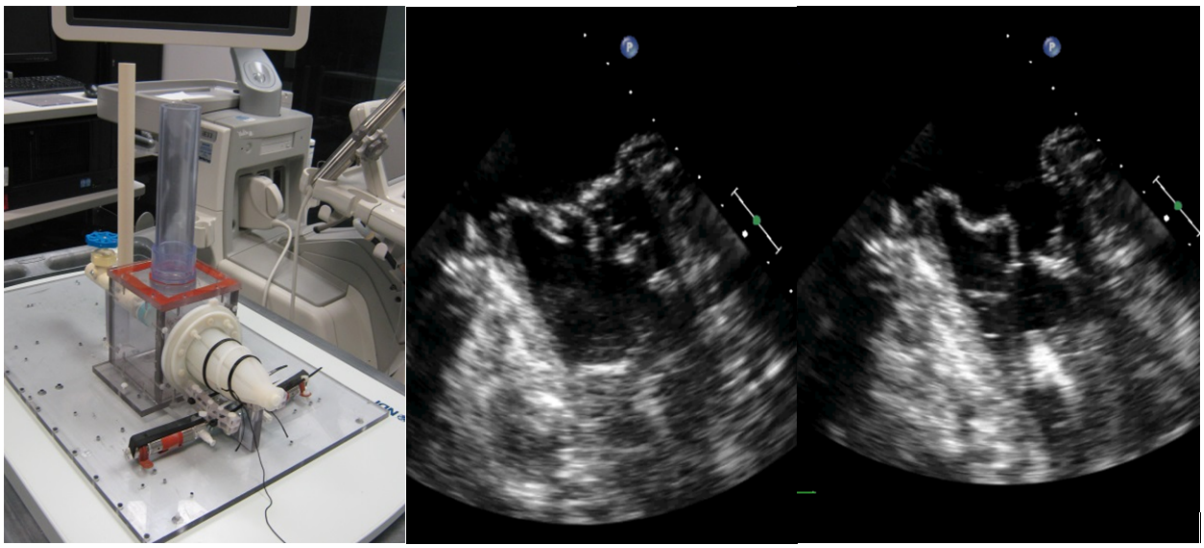

Figure 4.8: Left: LV phantom used in validation studies. Middle: LV two chamber long axis view at systole. Right: same view at diastole.

The phantom was used to simulate heart shift by translating the whole phantom in a controlled manner. Ground truth measurements of heart shift were obtained by tracking the phantom itself. In the experiments, the phantom was repeatedly translated by controlled distances (1, 2, and 3cm) within the horizontal plane relative to the tabletop field generator. A 6-DoF magnetic sensor attached to the wall of the phantom recorded the positions of the phantom before and after the translation. As the MVA in the phantom is rigidly secured to the frame, we assume the translation of the MVA to be the same as that of the phantom. The TEE probe was positioned in the atrial reservoir to mimic a long-axis two chamber TEE view, and was moved with approximately the same motion as the phantom itself. The virtual MVA model was manually defined before each translation and tracked by our tracking approach thereafter. The positions of the four control points of the MVA model were recorded before and after the translation. The accuracy of our tracking approach was determined by measuring the translation of the MVA model and then comparing it to that recorded by the 6-DoF sensor. The phantom heart rate was pre-set to 30 beats per minute.

### 4.3.2 Retrospective Study on Animal Data

We retrospectively analyzed our algorithm on 5 sets of 2D single plane TEE images with a total of 6676 images and 2 sets of bi-plane images with 706 images. These images were recorded during porcine validation studies of our augmented virtuality image guidance platform [21] and in many cases included the surgical tool in the image plane. Although 2D images, in which only two MVA points can be identified, do not provide enough information to form an MVA ring, we used them to validate the in-plane tracking accuracy.

The validation was performed by running the algorithm through each data set and recording the index of each frame that was detected by the image-based cardiac phase tracking approach. The coordinates of all the tracked MVA points were updated using the registration approach described in Section 4.2.4. We then retrospectively displayed these recorded frames on the screen (without displaying the positions of the automatically detected mitral annulus points)

and asked experienced users to manually identify the mitral annulus. The Euclidean distances between the automatically tracked MVA points and their manually defined counterparts were then computed.

Here, manually identified MVA points were used as the ground truth for validating the accuracy of our MVA tracking approach in the study on animal images. However, since there is an element of subjectivity in this form of manual identification, it is reasonable to assume that the results will vary, if multiple users are asked to identify the MVA points on the same images. This inter-operator variability should be considered as a limitation for any validation that relies on manual segmentation as ground truth.

To investigate this problem, we asked five experts to identify the MVA points on selected images, both in single plane and bi-plane modes. The average positions of the MVA points were computed for each image over all the users and the Euclidean distances were computed between user's segmentation and the average.

## 4.4 Results

### 4.4.1 Accuracy from Phantom Study

The MVA model was manually defined before each controlled translation of the phantom, and tracked by our approach thereafter. The coordinates of the four MVA points were recorded before and after the translations. The centre of the MVA model was computed based on the coordinates of the four MVA points. For each test, we estimated the true position of the MVA centre after the translation based on the information recorded by the 6-DoF sensor and compared this with the centre of the tracked MVA. The translation errors along each axis, with the long axis of the ventricle parallel to the long axis of the field generator, are listed in Table 4.1. The comparison of the tracked MVA and the estimated MVA (based on sensor translation) is also illustrated in Figure 4.9. The differences between those MVAs increase gradually along with the increments of the translation distances.

Table 4.1: MVA Centre Translation Error (mm) According to 6DoF Sensor

| Phantom translation | #Test | X-axis error | Y-axis error | Z-axis error |
|---|---|---|---|---|
| 10.00 | 1 | 2.18 | 0.18 | 1.35 |
| | 2 | 1.81 | 0.02 | 0.98 |
| | 3 | 1.41 | 0.43 | 0.61 |
| | 4 | 0.51 | 0.40 | 1.69 |
| | 5 | 0.20 | 0.05 | 2.05 |
| | Mean±std | 1.22±0.84 | 0.22±0.19 | 1.34±0.57 |
| 20.00 | 6 | 2.28 | 0.73 | 3.82 |
| | 7 | 1.54 | 1.26 | 3.41 |
| | 8 | 0.93 | 1.16 | 2.86 |
| | 9 | 0.73 | 1.20 | 3.15 |
| | 10 | 1.27 | 1.07 | 3.33 |
| | Mean±std | 1.35±0.60 | 1.08±0.21 | 3.31±0.35 |
| 30.00 | 11 | 1.11 | 2.54 | 4.13 |
| | 12 | 1.76 | 1.96 | 3.76 |
| | 13 | 1.28 | 2.24 | 3.72 |
| | 14 | 1.37 | 2.28 | 3.90 |
| | 15 | 0.93 | 2.24 | 3.91 |
| | Mean±std | 1.29±0.31 | 2.25±0.20 | 3.89±0.16 |
| | Overall mean±std | 1.29±0.58 | 1.18±0.88 | 2.85±1.19 |

### 4.4.2 Accuracy with Images from Animal Study

The Euclidean distances between the automatically tracked MVA points and their manually defined counterparts were recorded for both 2D single-plane and bi-plane images. Figure 4.10 shows two example images from the testing dataset and the MVA points are indicated by the red arrows. The NeoChord tool may be present in some of the images as shown in Figure 4.10b. Table 4.2 presents the validation results for both single plane and bi-plane images.

The inter-operator variation in manual segmentation were computed over the results of five users (N=5) and the results are listed in Table 4.3. Comparing the two results, our automatic tracking approach provides an accuracy of MVA position identification close to that which can be obtained by manual segmentation.

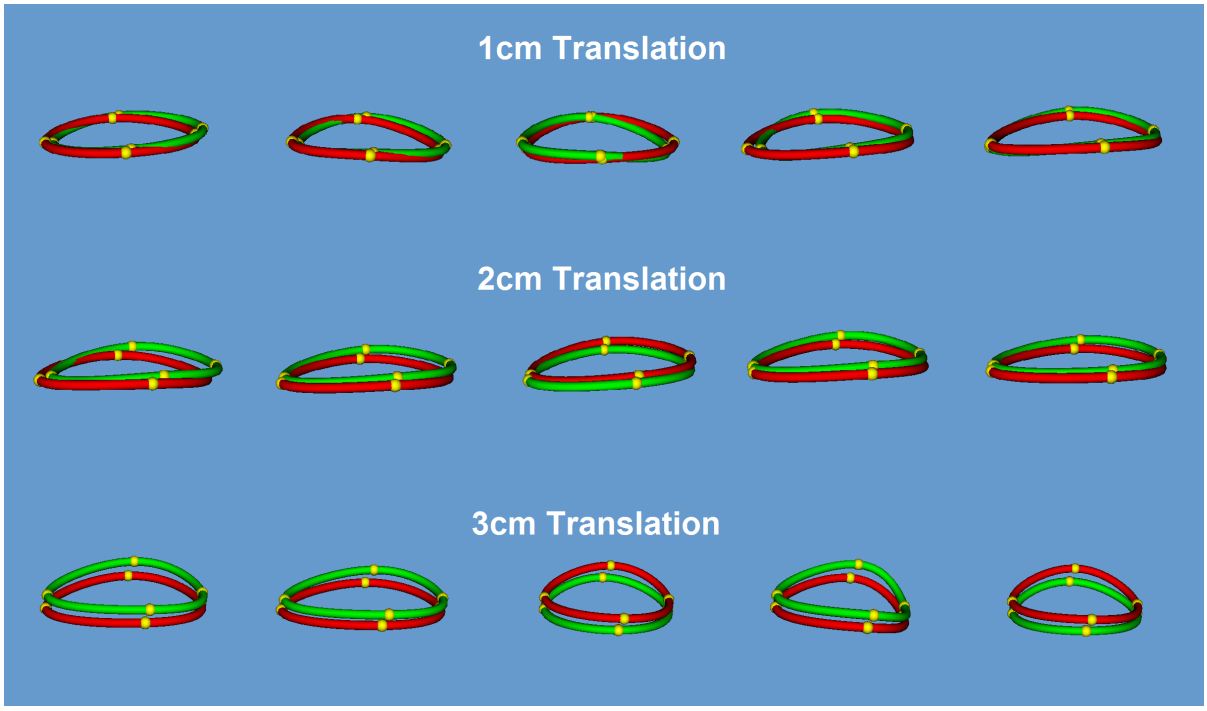


Figure 4.9: Comparison of the MVA model tracked by our approach (green) and the estimated MVA model based on the sensor translation (red). The yellow spheres denote the MVA points forming the splines. The diameter of the sphere is 2mm.

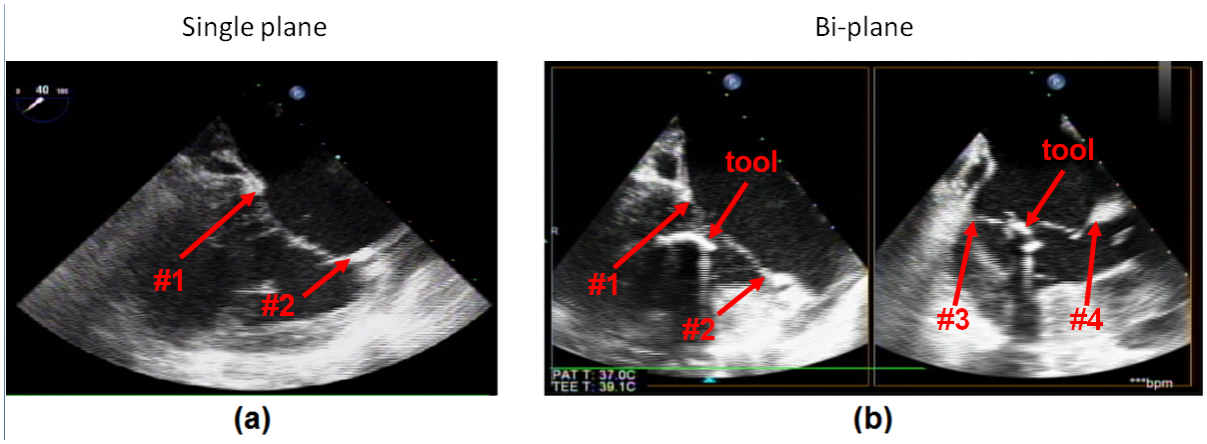


Figure 4.10: Example images of the test data showing the index of the tracked MVA points

### 4.4.3 Computational Efficiency

The computational efficiency was measurement on a desktop computer with an Intel© Xeon© CPU at 3.47 GHz and NVIDIA GeForce© 690 graphic card and CUDA© 4.2 programming interface [NVIDIA Corp, Santa Clara, CA, USA]. The registration of each point took 15±1

Table 4.2: MVA tracking accuracy of our approach

| RMS of 2D Single Plane | | | |
|---|---|---|---|
| Point | #1 (anterior) | #2 (posterior) | Overall |
| Mean±Std (mm) | 2.41±1.37 | 2.16±1.64 | 2.37±1.67 |

| RMS of 2D Bi-Plane | | | | | |
|---|---|---|---|---|---|
| Point | #1 (anterior) | #2 (posterior) | #3 (antero-lateral) | #4 (postero-medial) | Overall |
| Mean±Std(mm) | 1.89±1.26 | 1.52±0.61 | 4.06±1.92 | 1.93±0.68 | 2.3±1.55 |

Table 4.3: Inter-personal variation in manual MVA points definition

| RMS of 2D Single Plane | | | |
|---|---|---|---|
| Point | #1 (anterior) | #2 (posterior) | Overall |
| Mean±Std (mm) | 2.20±1.11 | 2.44±1.37 | 2.32±1.24 |

| RMS of 2D Bi-Plane | | | | | |
|---|---|---|---|---|---|
| Point | #1 (anterior) | #2 (posterior) | #3 (antero-lateral) | #4 (postero-medial) | Overall |
| Mean±Std(mm) | 1.58±0.80 | 1.37±0.71 | 2.07±1.29 | 1.89±1.61 | 1.73±1.18 |

ms, i.e. about 60 ms for four points. The standard deviation was very low, because the brute force approach was designed to search every possible point in the search space and the number of the points was constant for all image patches. This computational efficiency is sufficient for our goal of updating the MVA model once per cardiac cycle.

## 4.5 Discussion

### 4.5.1 Overall Accuracy

Both the phantom and the animal studies demonstrated similar MVA tracking accuracy using our approach, i.e. mean distance error in the range of 1-3 mm with a standard deviation of 1-2

mm. However, it is worth noting that the reported errors in the two studies were impacted by different factors.

In the phantom study, the true translation of the MVA was computed based on the position change of the 6-DoF magnetic sensor, so there is no manual segmentation variation involved in the MVA tracking error. The inaccuracy in the phantom study came from five major sources.

1. The inaccuracy of our image based tracking approach itself.

2. The magnetic tracking system with a 6-DoF sensor (used to tracking the phantom) and a table top field generator is reported to have an average RMS error of 0.80 mm in position [26] and this inaccuracy also applies to the tracked TEE probe to which a 6-DoF sensor is attached.

3. The calibration of the TEE probe. The calibration was performed using a Z-bar phantom which typically leads to a RMS error of 1-2 mm [27].

4. Since the relative position between the TEE probe and the MVA was not fixed, it was likely that the MVA points presented in the TEE images were not always the same physical points.

5. Although our phantom is designed to accurately mimic the valves of the left ventricle, the morphology is not an exact match.

In the retrospective study on animal images, the reported inaccuracy was in-plane error, and no magnetic tracking system or TEE probe calibration inaccuracy was involved. The two sources of inaccuracy were the image-based tracking approach itself and the inter-operator variation in manual segmentation.

The phantom study showed that the MVA tracking inaccuracy may increase as the total shift of the annulus increases. The accuracy was very good (approximately 2 mm) with a translation distance of 1cm, whereas it rose to almost 4 mm at a translation distance of 3cm. However, according to our clinical collaborators, the actual heart shift during a mini-thoracotomy apical

access NeoChord repair procedure is typically less than 2cm, which suggests that our approach can provide good tracking accuracy in most cases. An adjustment was also made in the software to freeze the MVA tracking when the tracked MVA moved far away from its original position, and re-initialization may need to be performed in such a situation.

### 4.5.2 Limitation of the Approach

The greatest limitation of this approach occurs when the feature points, i.e. the MVA points, are missing from the acquired image or disturbed by the tool. In the experiments we noted that the image based tracking approach may be affected by the tool presence in the image (Figure 4.11). Two problems can be seen in this image. First, since the tool is very close to the anterior MVA point, its presence is included in the image patch used for registration. However, such a feature is absent in the initial image patch, which leads to low registration accuracy. Second, the posterior MVA point is hidden in the shadow area below the tool. This phenomenon can last for a few cardiac cycles, which makes it impractical to accurately identify the position of the posterior MVA point for that period of time, even when using a Kalman filter or similar techniques that rely on input from the previous repeated patterns. In these situations, the image-based registration approach gives an arbitrary result, very often far away from the real position of the MVA point, because there is actually no MVA point shown in the image to be tracked.

Although these problems cannot be perfectly resolved by image-based approaches, we attempted to solve them with the help of the magnetic tracking system. As the position and orientation of the TEE probe and the surgical tool can be computed based on the tracking information, it is possible to estimate when such problems may occur and freeze the MVA tracking accordingly (the MVA model on the screen will be rendered with a different color). When the problem disappears, the MVA tracking begins to work again. However, the problem caused by the shadow of the tool may only occur with a porcine heart, due to its specific heart orientation and anatomy, and is extremely unlikely to occur in humans.

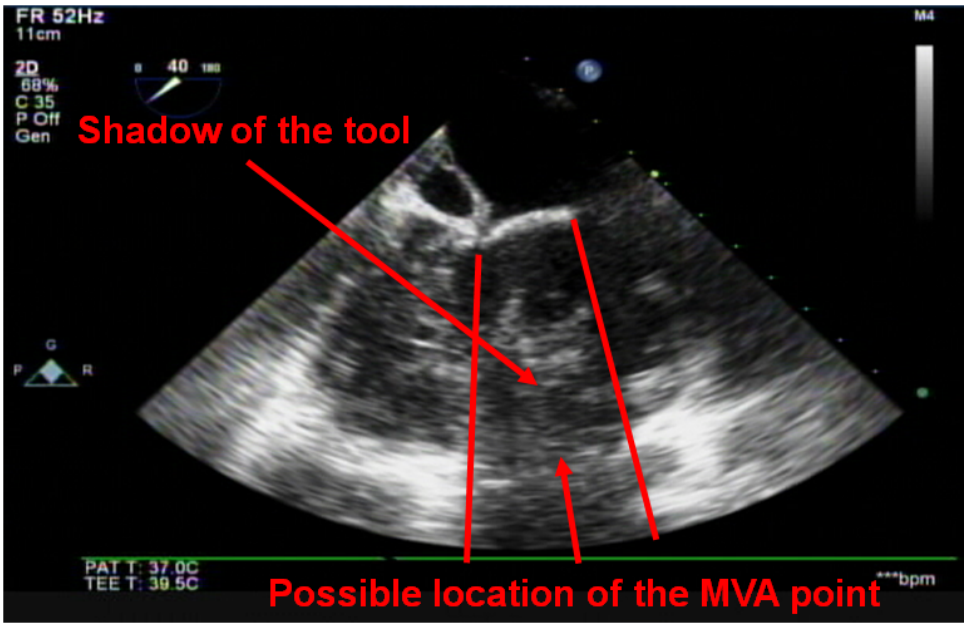


Figure 4.11: Problems caused by tool presence

Another possible problem occurs when the MVA is outside the field-of-view of the TEE probe. We used the same approach of estimating the occurrence of the problem with the magnetic tracking information and freezing the MVA tracking accordingly.

### 4.5.3 Navigation vs. Positioning

The difference between navigation and positioning in an image-guided procedure can be compared to that of driving a car to a destination with the help of a GPS and parking it with a backup camera. The main goal at the navigation stage is to get close to the destination safely through a shortest (either in time or distance) or safest path, whereas the positioning stage focuses on deploying a therapy with required accuracy. In the NeoChord procedure, navigation defines the procedure of moving the tool tip from the apex of the heart close to the centre of the MVA with tool tip in the left atrium, whereas positioning means grabbing the leaflets and placing the artificial chordae at the required position. The MVA tracking approach in this paper is designed for the navigation stage.

The motion of the MVA can be decomposed into two parts: the cyclical motion within each

cardiac cycle in which the MVA moves approximately 1cm along the left ventricular long-axis back and forth [28] and the heart shift caused by the tool manipulation and slight changes in patient position and pose. In our experience, the first type of motion is not of major concern during the navigation stage [21], whereas the second type of motion is that which we attempted to track with the approach in this paper.

## 4.6 Conclusion

In this paper we developed a rapid MVA tracking algorithm for use in the guidance of off-pump beating heart transapical mitral valve repair. This approach uses 2D biplane TEE images and was tested on a dynamic heart phantom and interventional porcine image data. Preliminary results regarding the accuracy and efficiency of this approach are quite promising.

While other systems exist for tracking the MVA, based on ultrasound image data [29, 30], implementing a system capable of functioning in near real time in a surgical environment adds a time-critical element to the process. Implemented on a standard desktop computer, our approach can track about 15 images per second with a low tracking RMS of approximately 2mm, which suggests that this approach can be readily implemented in the operating room.

Future work includes developing an automatic initialization approach based on an image altas, and further validating the approach with human data.

# Bibliography

[1] L. H. Ling, M. Enriquez-Sarano, J. B. Seward, J. Tajik, H. V. Schaff, K. R. Bailey, R. L. Frye, and A. J. Tajik, "Clinical Outcome of Mitral Regurgitation Due to Flail Leaflet," *The New England Journal of Medicine*, vol. 335, no. 19, pp. 1417–1423, 1996.

[2] E. Hayek, C. N. Gring, and B. P. Griffin, "Mitral valve prolapse," *Lancet*, vol. 365, no. 9458, pp. 507–18, 2005.

[3] L. A. Freed, D. Levy, R. A. Levine, M. G. Larson, J. C. Evans, D. L. Fuller, B. Lehman, and E. J. Benjamin, "Prevelence and Clinical Outcome of Mitral Valve Prolapse," *The New England Journal of Medicine*, vol. 341, no. 1, pp. 1–7, 1999.

[4] R. R. Moss, K. H. Humphries, M. Gao, C. R. Thompson, J. G. Abel, G. Fradet, and B. I. Munt, "Outcome of mitral valve repair or replacement: a comparison by propensity score analysis.," *Circulation*, vol. 108 Suppl, pp. II90–7, Sept. 2003.

[5] P. Bajona, W. E. Katz, R. C. Daly, K. J. Zehr, and G. Speziali, "Beating-heart, off-pump mitral valve repair by implantation of artificial chordae tendineae: an acute in vivo animal study.," *The Journal of thoracic and cardiovascular surgery*, vol. 137, pp. 188–93, Jan. 2009.

[6] I. Bahar, A. Akgul, M. A. Ozatik, K. M. Vural, A. E. Demirbag, M. Boran, and O. Tasdemir, "Acute renal failure following open heart surgery: risk factors and prognosis," *Perfusion*, vol. 20, pp. 317–322, Oct. 2005.

[7] R. Freeman, B. King, and M. H. Hambling, "Infective complications of open-heart surgery and the monitoring of infections by the NBT test," *Thorax*, vol. 28, pp. 617–621, Sept. 1973.

[8] M. K. Newman, J. L. Kirchner, B. Phillips-Bute, V. Gaver, H. Grocott, R. H. Johnes, D. B. Mark, J. G. Reves, and J. A. Blumenthal, "Longitudinal assessment of neurocognitive

function after coronary-artery bypass surgery," *The New England Journal of Medicine*, vol. 344, pp. 395–402, June 2001.

[9] A. Iribarne, R. Easterwood, E. Y. H. Chan, J. Yang, L. Soni, M. J. Russo, C. R. Smith, and M. Argenziano, "The golden age of minimally invasive cardiothoracic surgery: current and future perspectives," *Future Cardiology*, vol. 7, no. 3, pp. 333–346, 2011.

[10] "http://www.neochord.com/."

[11] T. Feldman, E. Foster, M. Qureshi, B. Whisenant, J. Williams, D. Glower, and L. Mauri, "TCT-788 The EVEREST II Randomized Controlled Trial (RCT): Three Year Outcomes," *Journal of the American College of Cardiology*, vol. 60, pp. B229–B230, Oct. 2012.

[12] "http://www.abbottvascular.com/int/mitraclip.html#overview."

[13] "http://www.mitralign.com/,"

[14] J. Harnek, J. G. Webb, K.-H. Kuck, C. Tschope, A. Vahanian, C. E. Buller, S. K. James, C. P. Tiefenbacher, and G. W. Stone, "Transcatheter implantation of the MONARC coronary sinus device for mitral regurgitation: 1-year results from the EVOLUTION phase I study (Clinical Evaluation of the Edwards Lifesciences Percutaneous Mitral Annuloplasty System for the Treatment of Mitral R," *JACC. Cardiovascular interventions*, vol. 4, pp. 115–22, Jan. 2011.

[15] C. A. Linte, J. White, R. Eagleson, G. M. Guiraudon, and T. M. Peters, "Virtual and augmented medical imaging environments: enabling technology for minimally invasive cardiac interventional guidance.," *IEEE reviews in biomedical engineering*, vol. 3, pp. 25–47, Jan. 2010.

[16] G. M. Guiraudon, D. L. Jones, D. Bainbridge, and T. M. Peters, "Mitral valve implanta-

tion using off-pump closed beating intracardiac surgery: a feasibility study.," *Interactive cardiovascular and thoracic surgery*, vol. 6, pp. 603–7, Oct. 2007.

[17] J. Ender and S. Sgouropoulou, "Value of transesophageal echocardiography (TEE) guidance in minimally invasive mitral valve surgery.," *Annals of cardiothoracic surgery*, vol. 2, pp. 796–802, Nov. 2013.

[18] N. C. Wunderlich and R. J. Siegel, "Peri-interventional echo assessment for the MitraClip procedure.," *European heart journal cardiovascular Imaging*, vol. 14, pp. 935–49, Oct. 2013.

[19] E. Altiok, M. Becker, S. Hamada, S. Reith, N. Marx, and R. Hoffmann, "Optimized guidance of percutaneous edge-to edge repair of the mitral valve using real-time 3-D transesophageal echocardiography," *Clinical research in cardiology : official journal of the German Cardiac Society*, vol. 100, pp. 675–81, Aug. 2011.

[20] R. A. Quaife, E. E. Salcedo, and J. D. Carroll, "Procedural guidance using advance imaging techniques for percutaneous edge-to-edge mitral valve repair.," *Current cardiology reports*, vol. 16, p. 452, Feb. 2014.

[21] J. T. Moore, M. W. A. Chu, B. Kiaii, D. Bainbridge, G. Guiraudon, C. Wedlake, M. Currie, M. Rajchl, R. V. Patel, and T. M. Peters, "A navigation platform for guidance of beating heart transapical mitral valve repair.," *IEEE transactions on bio-medical engineering*, vol. 60, pp. 1034–40, Apr. 2013.

[22] S. Saito, Y. Araki, A. Usui, T. Akita, H. Oshima, J. Yokote, and Y. Ueda, "Mitral valve motion assessed by high-speed video camera in isolated swine heart.," *European journal of cardio-thoracic surgery : official journal of the European Association for Cardio-thoracic Surgery*, vol. 30, pp. 584–91, Oct. 2006.

[23] D. W. Sohn, I. H. Chai, D. J. Lee, H. C. Kim, H. S. Kim, B. H. Oh, M. M. Lee, Y. B. Park, Y. S. Choi, J. D. Seo, and Y. W. Lee, "Assessment of mitral annulus velocity by

Doppler tissue imaging in the evaluation of left ventricular diastolic function.," *Journal of the American College of Cardiology*, vol. 30, pp. 474–80, Aug. 1997.

[24] F. Li, P. Lang, M. Rajchl, E. C. S. Chen, G. Guiraudon, and T. M. Peters, "Towards real-time 3D US-CT registration on the beating heart for guidance of minimally invasive cardiac interventions," in *Proc. SPIE 8316, Medical Imaging 2012* (D. R. Holmes III and K. H. Wong, eds.), vol. 8316, p. 831615, Feb. 2012.

[25] J. Dean and S. Ghemawat, "MapReduce : Simplified Data Processing on Large Clusters," *Magazine of Communications of the ACM*, vol. 51, no. 1, pp. 107–113, 2008.

[26] "http://www.ndigital.com/medical/products/aurora/#specifications-planer-field."

[27] M. Soehl, R. Walsh, A. Rankin, A. Lasso, and G. Fichtinger, "Tracked ultrasound calibration studies with a phantom made of LEGO bricks," in *Proc. SPIE 9036, Medical Imaging 2014: Image-Guided Procedures, Robotic Interventions, and Modeling*, 2014.

[28] S. Y. Hayashi, B. I. Lind, A. Seeberger, M. M. do Nascimento, B. J. Lindholm, and L.-A. Brodin, "Analysis of mitral annulus motion measurements derived from M-mode, anatomic M-mode, tissue Doppler displacement, and 2-dimensional strain imaging.," *Journal of the American Society of Echocardiography : official publication of the American Society of Echocardiography*, vol. 19, pp. 1092–101, Sept. 2006.

[29] R. J. Schneider, D. P. Perrin, N. V. Vasilyev, G. R. Marx, P. J. del Nido, and R. D. Howe, "Mitral annulus segmentation from 3D ultrasound using graph cuts," *IEEE transactions on medical imaging*, vol. 29, pp. 1676–87, Sept. 2010.

[30] R. J. Schneider, D. P. Perrin, N. V. Vasilyev, G. R. Marx, P. J. del Nido, and R. D. Howe, "Mitral annulus segmentation from four-dimensional ultrasound using a valve state predictor and constrained optical flow," *Medical image analysis*, vol. 16, pp. 497–504, Feb. 2012.

# Chapter 5

# Conclusions

## 5.1 Contributions

One of the principal challenges for developing guidance applications for off-pump beating heart procedures is that not only should such applications provide good accuracy in anatomy presentation, image registration, and feature tracking, but they must have the capability to perform image processing procedures rapidly to capture rapid cardiac motion as well [1, 2]. These two goals are usually competing with each other and trade-offs must be made between them. In this thesis, I developed several approaches to resolve this challenge.

Chapter 2 presents an approach to generate synthetic dynamic CT series based on a static CT image and a sequence of 3D US images. The synthetic CT images are generated by obtaining cardiac motion information in terms of image deformation fields and applying them to the static CT image to deform it into a sequence of dynamic CT images that represent the same cardiac motion as that shown in the US images. This approach can take advantage of high spatial resolution and image quality of the CT images and high temporal resolution of US images, whereas the generation procedure is completely virtual and does not require radiation dose to be applied to either the patients or the clinicians. The experiments compared the synthetic CT images to the real dynamic CT images obtained from retrospectively gated CT scans. The left

ventricle (LV) was chosen as the anatomical feature for comparison and manually segmented from corresponding synthetic and real dynamic CT images. Two metrics, DSC that measures level of overlap between real and synthetic LVs and RMS that measures the distances between the LV surfaces, were used for the comparison. The results demonstrated that the synthetic CT images can provide very similar anatomical representations as the real dynamic CT images for the region of interest (ROI), i.e. the LV. The ROI can be adjusted according to the procedural requirements. For example, for transcatheter aortic valve implantation (TAVI) procedure, the ROI can be trimmed to contain the aortic valve and part of the aortic arch [3]. Image mosaicing techniques [4] can also be applied here to provide a large field of view, if US sequences containing different ROIs are available.

Chapter 3 introduces a means of integrating pre-operative dynamic CT images to the intra-operative guidance system through real-time CT to US image registration. The dynamic CT images are used to provide a high quality 3D anatomical context for the guidance system, while the intra-operative US images are used for visualization of the real time cardiac anatomy and motion. The static CT image is not suitable in such applications because the target registration error can be greater than 1cm when the static image is registered to US images with non-corresponding cardiac phases. However, the retrospecitively gated CT scans that provide real dynamic CT images are associated with high radiation dose, which can be harmful to the patient. As discussed in Chapter 2, an approach was developed to generate synthetic dynamic CT images to replace the real ones in our guidance system in order to eliminate the radiation dose while providing similar registration results. The proposed CT-US registration approach uses the rigid transformation model and normalized mutual information as the similarity metric. To make the approach sufficiently rapid to capture the cardiac motion, I developed a parallelized implementation based on the GPGPU programming model. The experiments showed that good registration accuracy had been achieved for both real and synthetic CT images, which allowed the approach to be potentially used for feature tracking. The results using synthetic and real dynamic CT images were also compared, demonstrating that there was no significant difference

in terms of registration accuracy, which supported the concept of using synthetic CT images in the guidance system. The GPU based implementation allows registering 3-5 frames per seconds, which is sufficient for performing one registration per cardiac cycle.

Chapter 4 introduces an approach to track MVA points using bi-plane TEE images. There are two kinds of MVA motion during the operation, the normal periodic motion within one cardiac cycle and the shift caused by tool manipulation. This approach aims to track the latter. The tracking algorithm is based on both image processing techniques and information from a magnetic tracking system. Unlike the approach described in Chapter 3, this approach uses solely intra-operative images for feature tracking. We tested the approach with a dynamic heart phantom as well as on data collected from animal studies. The phantom study showed that the tracking accuracy was better than 2mm, when the MVA shift was smaller than 20mm, while it can be as low as 4mm, even when the shift was as large as 30mm. However, according to our clinical collaborators, the MVA shift in the NeoChord procedure with minithoractomy is usually smaller than 20mm. The experiment on the animal study data showed that the tracking accuracy is about 2mm in an actual animal study as well. We also measured the variation in manually defined MVA points, which was employed as the gold standard in the animal study. We asked five experienced users to identify the MVA points on the images and the results showed that the inter-user variation was about 2mm, very similar to the accuracy achieved by our tracking approach.

## 5.2 Clinical advantages

The approaches introduced in this thesis aim to resolve some of the major challenges of developing a clinically usable image guidance system for minimally invasive off pump beating heart mitral valve repair.

The first challenge comes from the limitations of the imaging techniques. As mentioned before, so far no one imaging modality can fulfil all the requirements, in terms of spatio-temporal

resolution, anatomy representation, FOV, feasibility in the OR, and safety, of a guidance system for beating heart interventions. With carefully chosen pre-operative and intra-operative imaging modalities, the techniques to fuse them together intra-operatively, and well designed visualization components, this thesis attempts to combine the advantages of different modalities together to provide a system that is rich in clinically relevant information as well as intuitive for the surgeons to interpret and to use.

The second challenge is related to rapid cardiac motion. The guidance system is responsible for showing both the cardiac anatomy and motion at the same time, with the capability of tracking certain anatomical features when required. This means that the image processing techniques must provide accurate results within a very limited time, usually shorter than one second. However, the requirements for accuracy and efficiency are usually competing with each other and have been an important barrier for many techniques to be translated to practical clinical applications. This thesis has put much effort in developing approaches that can provide good accuracy with sufficient efficiency with parallel computing techniques, which makes intra-operative applications possible. Detailed discussion about trade-offs between accuracy and efficiency can be found in the section 5.4.

The third challenge is related to clinical workflow. All the approaches in this thesis are designed to make minimal modifications to standard workflow. For example, all the imaging modalities suggested in thesis are already used as standard of care. The manual identification of anatomical features is performed only once immediately before the procedure starts and the associated workload is kept minimum.

## 5.3 Possible Extension to Use MRI Images

The approaches described in Chapter 2 and Chapter 3 suggest using CT (synthetic CT) as pre-operative images. This choice is made mainly under the consideration that CT is currently used in the standard of care and is widely available. However, MRI images can also be a good

option, when they are available. The image processing approaches in Chapter 2 and Chapter 3 can be easily adapted to use MRI images as well as generating synthetic dynamic MRI images.

## 5.4 Trade-offs between Accuracy and Efficiency

As mentioned in the previous chapters, trade-offs between the registration/tracking accuracy and efficiency were made to achieve applications capable of performing the required process in real time during the procedure, while still maintain desired accuracy. The trade-offs are listed below:

1. ***The non-rigid registration that tracks the cardiac motion is perform pre-operatively in terms of the generation of synthetic CT images rather than intra-operatively on the in vivo data.*** This approach is based on the assumption that the periodic cardiac motion does not change much between beats or between pre- and intra-operative stages. This assumption may not hold true when some pathology, such as arrhythmia or fibrillation, occurs. It would be ideal if real time non-rigid registration could be performed intra-operatively to track the motion exactly. However, no literature has reported the possibility of performing non-rigid registration in real time [5, 6]. The fastest GPU accelerated implementation in the current literature still needs about half a minute to perform one registration with 3D US data [7, 8]. We divided the registration process into two stages to deal with this problem. The time consuming non-rigid registration is move to the pre-operative stage in terms of synthetic CT generation, so that we don't need to worry about the computation time. In the intra-operative stage, we perform rigid CT-US registration, which is achieved in real time with our proposed approach. However, we hope in the future, with the development of new parallel computing hardware, real time non-rigid registration can become practical.

2. ***Rigid, rather than non-rigid, registration, is performed intra-operatively.*** Following the fist trade-off, we know that it is impossible to perform real time non-rigid registration

so far. We also know that rigid registration cannot deal with the image deformation caused by the cardiac motion [9]. Two compensations are performed to achieve good registration accuracy with rigid registration. First, synthetic dynamic CT images are generated using a high frame rate pre-operative US image sequence. For each image in the sequence, one synthetic CT image can be generated. This means that if the US sequence has a high frame rate (Full volume scan can provide 4D images at about 30Hz), the corresponding synthetic CT sequence will also have a high frame rate. Thus, we can create more images within a single cardiac cycle to be used for CT-US registration to reduce the potential deformation difference between the pre- and intra-operative images. Second, temporal alignment is performed between CT and US images to ensure the images to be registered present closest, if not the same, cardiac phases. The gating information of the US images can be obtained from the ECG signals, while that of the synthetic CT images is inherited from the corresponding US images.

3. ***Sample points, rather than the entire image, are used in the registration in Chapter 3.*** To further reduce the computation time, we use only sample points selected through thresholding for registration. This is based on the observation that points representing important anatomical features, such as leaflets and myocardium, are usually associated with high intensities [10]. We threshold the image and use only those points with high intensities for our registration, since this can accelerate the application and bias the registration to myocardium, which is actually what we want. The number of sample points must be optimized, because too few points may lead to unstable behaviour of the registration, whereas too many slow the computation.

4. ***The optimizer can only ensure local but not global optimal registration results.*** Optimizers use heuristic strategies to accelerate the process of finding an optimum. However, for non-convex optimization problems they can only ensure local optima. In Chapter 3, we perform a good initialization to align the images first, making sure the alignment

is very close to the global optimum, which reduces the number of iterations and time required by the optimization procedure, as well as increasing the chance of finding the global optimum. Chapter 4 presents a different methodology. Instead of using an optimizer, we perform brute force search within a small area using small image patches. Brute force search is usually not applicable for real life applications, because it requires all the possible parameter sets in the searching space are traversed, which is very time consuming. However, in Chapter 4 with a GPU based implementation, the brute force search can be achieved in real time. The trade-off is that to enable a real time brute force search, we have to limit the size of the search space. This approach works when the movement of the MVA is small and constrained, which is valid most of the time.

## 5.5 Comparison between the 3D and the 2D Approaches

Chapter 3 and 4 introduced two different methodologies for MVA tracking. The approach in Chapter 3 performs rapid registration between pre- and intra-operative 3D images. The anatomical feature of interest, MVA in this thesis, is first defined on the pre-operative images and then updated intra-operatively based on the registration results, aiming to represent the real time position of the feature. On the other hand, the approach in Chapter 4 performs feature tracking based on intra-operative bi-plane images. No 3D images are used in this approach. According to the experimental results, these two approaches provide very similar accuracy for MVA tracking, while the 2D approach is slightly faster in run time. However, the most important differences between the two approaches are the following:

### 5.5.1 Accessibility to Data

The 3D CT-US registration based approach requires the availability of real time 3D streaming US images. Our lab is one of the very few labs in the world that have the access to the programming interface of the 3D streaming data, which allows us to perform the related research projects. However, most of the research or clinical centres do not have the same accessibility.

This means that the 3D registration based approach cannot be easily translated into a widely available clinical application, unless the echocardiogram system providers are willing to promote the development and distribution of the programming interface of the 3D streaming data.

On the other hand, the 2D approach does not have such a limitation. Although the interface of obtaining 2D streaming data is also not available for now, a digital video grabber can be attached to the echocardiogram system to obtain screen captures and transfer them to a computer, which is how bi-plane images are obatined in this thesis.

### 5.5.2 Applicability

The 3D approach can be adopted when 3D streaming data and dynamic CT images are available. The dynamic CT images can be obtained from retrospectively gated CT scans or synthetically generated by the approach described in Chapter 2. Although this approach has only only been tested for MVA tracking in this thesis, it actually allows tracking multiple anatomical features simultaneously through one registration step as long as those features are pre-defined in the CT images. This is because that the CT-US registration approach we proposed in Chapter 3 is image based and does not rely on any *a priori* knowledge about the features. The CT images can also serve as high quality 3D anatomical context with different visualization options. However, this approach is not applicable when there are major differences between pre- and intra-operative cardiac motion. For example, arrhythmia and fibrillation occurrence during the procedure can cause such an approach to fail.

The 2D approach requires only 2D bi-plane streaming images, which are easily accessible. However, a shortage of 2D images is that as the scanning slice moves around, the anatomy presented in the images changes accordingly. This can become a serious problem for tracking MVA points when there is large change in the relative position between the US probe and the surgical target, since the intersection point between the scanning plane and the MVA can be centimetres away from the previous tracked point. The predictive re-initialization step was designed to deal with such a problem. When the predicted target point is far away from the

previous point, the tracking algorithm pauses the update of the MVA position and the display of the MVA model is frozen at the last updated position until the predicted points are close to the last updated positions again.

## 5.6 Ultrasound Guided Cardiac Intervention without X-ray Fluoroscopy

Fluoroscopy is a common imaging modality used for cardiac interventions. However, the associated ionizing radiation dose is always a concern for patients' and clinicians' health [11, 12]. The proposed guidance approaches in this thesis use only ultrasound as the intra-operative imaging modality with no X-ray fluoroscopy and has showed good potential for being translated into clinical application in the OR. This idea is already adopted by the NeoChord procedure [13], which is guided solely by the TEE images in the on-going clinical trial. With the techniques introduced in this thesis, US based guidance can become more accurate, more intuitive, and safer for cardiac interventions.

Currently, fluoroscopy is most frequently used in transcathether procedures for tracking the advancement of guide wires, especially in the navigation stage. For example, the MitraClip procedure uses fluoroscopy for guidance until the guide wire penetrates the atrial septal. Then it switches to use the 3D TEE scan for positioning task [14]. Recently, Translucent Medical ©(Translucent Medical Inc., Scotts Valley, CA) introduced guide wires with magnetic sensors attached to the tips. These guide wires can be tracked by a magnetic tracking system, which can potentially replace fluoroscopy in the guidance for transcatheter procedures. Thus, fluoroscopy may eventually be eliminated from the guidance system for cardiac interventions and US would become the principle imaging modality for such guidance systems.

## 5.7 Impact of GPU based Massive Parallel Computing on Guidance Systems

Other than accuracy, the requirement of rapid computation is one of the principal challenges for developing guidance applications for beating heart procedures due to the fast cardiac motion. The approaches developed in this thesis have demonstrated the feasibility of developing such applications using GPU based implementations to accelerate the registration and feature tracking procedures. The development of modern GPUs allows the user to perform general purpose parallel computing (only graphics related computing was allowed previously), which has a great impact on the image processing techniques, especially for 3D images. Previously, parallel computing could only be performed on super computers with multiple processors or on distributed systems that contain multiple computers on the network. Such computer systems are usually very expensive and have limited accessibility. The number of threads that can be generated is also very limited. However, an average GPU only costs a few hundred dollars, but is capable of generating millions of threads within one application. Many image processing algorithms required for real time guidance applications can be completely or partially parallelized, which makes GPU based implementation perfect for such algorithm to be accelerated to real time. It is foreseeable that GPUs will play an important role in real time interventional guidance systems in the near future.

## 5.8 Future Directions

### 5.8.1 Investigation on How Guidance Inaccuracy Affects the Deployment

One question that we would like to answer is how accurate the image guidance, especially registration, needs to be for a certain procedure and how the guidance inaccuracy affects the final deployment results. We have demonstrated that the answer can vary between different tasks, but we are also interested in having numerical answers to this question. Experiments

are under development to introduce synthetic registration/tracking errors in a simulated image guidance scenario to investigate how the surgeons may react to those errors and how these errors may affect the final deployment error.

### 5.8.2 Automated Initialization

Both the approaches in Chapters 3 and 4 require initialization immediately before the guidance starts. Current initialization approach demand manual input, which is slow. An improvement could be to build a heart atlas or database that can be used for automatic initialization. This may also allow rapid re-initialization during the procedure when the tracking approach fails due to unexpected causes.

### 5.8.3 Transfer Functions

We are also interested in developing sophisticated transfer functions for volume rendering that can provide customized and tuned visual cues in the mixed reality system [15]. Such transfer functions may enable the visualization of certain features without performing segmentation and may also allow more complicated visualization that renders both volumes and surfaces simultaneously.

# Bibliography

[1] J. T. Moore, M. W. A. Chu, B. Kiaii, D. Bainbridge, G. Guiraudon, C. Wedlake, M. Currie, M. Rajchl, R. V. Patel, and T. M. Peters, "A navigation platform for guidance of beating heart transapical mitral valve repair.," *IEEE transactions on bio-medical engineering*, vol. 60, pp. 1034–40, Apr. 2013.

[2] F. P. Li, M. Rajchl, J. A. White, A. Goela, and T. M. Peters, "Towards CT Enhanced Ultrasound Guidance for Off-pump Beating Heart Mitral Valve Repair," in *Augmented Reality Environments for Medical Imaging and Computer-Assisted Interventions Lecture Notes in Computer Science, Volume 8090*, pp. 136–143, 2013.

[3] P. Lang, P. Seslija, M. W. a. Chu, D. Bainbridge, G. M. Guiraudon, D. L. Jones, and T. M. Peters, "US-fluoroscopy registration for transcatheter aortic valve implantation," *IEEE transactions on bio-medical engineering*, vol. 59, pp. 1444–53, May 2012.

[4] O. Kutter, W. Wein, and N. Navab, "Multi-modal registration based ultrasound mosaicing," *Medical image computing and computer-assisted intervention : MICCAI ... International Conference on Medical Image Computing and Computer-Assisted Intervention*, vol. 12, pp. 763–70, Jan. 2009.

[5] A. Eklund, P. Dufort, D. Forsberg, and S. M. Laconte, "Medical image processing on the GPU - Past, present and future," *Medical image analysis*, vol. 17, pp. 1073–1094, June 2013.

[6] G. Pratx and L. Xing, "GPU computing in medical physics: A review," *Medical Physics*, vol. 38, no. 5, p. 2685, 2011.

[7] M. Modat, G. R. Ridgway, Z. a. Taylor, M. Lehmann, J. Barnes, D. J. Hawkes, N. C. Fox, and S. Ourselin, "Fast free-form deformation using graphics processing units.," *Computer methods and programs in biomedicine*, vol. 98, pp. 278–84, June 2010.

[8] P. Muyan-Ozcelik, J. D. Owens, J. Xia, and S. S. Samant, "Fast Deformable Registration on the GPU: A CUDA Implementation of Demons," *2008 International Conference on Computational Sciences and Its Applications*, pp. 223–233, June 2008.

[9] F. Li, P. Lang, M. Rajchl, E. C. S. Chen, G. Guiraudon, and T. M. Peters, "Towards real-time 3D US-CT registration on the beating heart for guidance of minimally invasive cardiac interventions," in *Proc. SPIE 8316, Medical Imaging 2012* (D. R. Holmes III and K. H. Wong, eds.), vol. 8316, p. 831615, Feb. 2012.

[10] X. Huang, J. Ren, G. Guiraudon, D. Boughner, and T. M. Peters, "Rapid dynamic image registration of the beating heart for diagnosis and surgical navigation," *IEEE transactions on medical imaging*, vol. 28, pp. 1802–14, Nov. 2009.

[11] D. R. Holmes, M. A. Wondrow, J. E. Gray, R. J. Vetter, J. L. Fellows, and P. R. Julsrud, "Effect of Pulsed Progressive Fluoroscopy on Reduction of Radiation Dose in the Cardiac Catheterization laboratory," *Journal of American College of Cardiology*, vol. 15, no. 1, pp. 159–162, 1990.

[12] K. Chida, H. Saito, H. Otani, M. Kohzuki, S. Takahashi, S. Yamada, K. Shirato, and M. Zuguchi, "Relationship between fluoroscopic time, dose-area product, body weight, and maximum radiation skin dose in cardiac interventional procedures.," *AJR. American journal of roentgenology*, vol. 186, pp. 774–8, Mar. 2006.

[13] J. Ender and S. Sgouropoulou, "Value of transesophageal echocardiography (TEE) guidance in minimally invasive mitral valve surgery.," *Annals of cardiothoracic surgery*, vol. 2, pp. 796–802, Nov. 2013.

[14] E. Altiok, M. Becker, S. Hamada, S. Reith, N. Marx, and R. Hoffmann, "Optimized guidance of percutaneous edge-to edge repair of the mitral valve using real-time 3-D transesophageal echocardiography," *Clinical research in cardiology : official journal of the German Cardiac Society*, vol. 100, pp. 675–81, Aug. 2011.

[15] J. S. H. Baxter, T. M. Peters, and E. C. S. Chen, "A unified framework for voxel classification and triangulation," in *SPIE Medical Imaging: Visualization, Image-Guided Procedures, and Modeling*, 2011.

# Appendix A

# Image Orientation

## A.1 Image Orientations

With the development of modern imaging techniques, such as CT, MRI and 3D ultrasound, 3D images have become more and more popular in medical fields for diagnosis, surgical planning, training, and guidance purposes. They can provide interior details of a patient's body and allow 3D visualization and modeling of chosen areas or structures, which helps the clinicians to have better understanding about the patient's condition.

One important thing to define before using a 3D image is the image orientation. Commonly, it is defined in the patient's coordinate with the head side denoted as "Superior", foot side as "Inferior", right hand side as "Right", left hand side as "Left", chest side as "Anterior", and back side as "Posterior".

Image orientation is also associated with how the images are stored in computers. Storing a 3D image in a computer, either in the physical memory or on the hard drive, is usually achieved by sequencing every point (voxel) in the image with a pre-defined order and then storing the whole sequence as a 1D array. In other words, if we denote the sequencing procedure as a function, $f$, it maps a three dimensional coordinate, $(x, y, z)$, to a non-negative integer, $i$, with one-to-one correspondence.

$$f : (x, y, z) \rightarrow i \tag{A.1}$$

The function $f$ must be reversible, so that the program which reads the image knows exactly how to map each point in the sequence back to the 3D volume space.

## A.2 Complications Associated with Image Storing

However, the sequencing order is not standardized. Different programs and data formats tend to have their own preference of what order to use for sequencing. Because of that, there is usually one field in the header of a 3D image which indicates the sequencing order used for the image in the form of either a transformation matrix or a three-letter annotation, such as "RAS". Here the annotation "RAS" stands for "Right, Anterior, and Superior". When a computer program reads this annotation, it knows that the first point in the 1D sequence corresponds to the right-anterior-superior corner point in the 3D volume. As the program goes through the whole sequence, it knows to fill the 3D volume first from right to left, then from anterior to posterior, and last from superior to inferior (Figure A.1).

It is possible to store and read one 3D volume with different sequencing orders. For example, a program can use the sequencing order of RAI orientation to read an image stored with RAS orientation and that will result in a flipped image in the I-S dimension. In Figure A.2, there is a 3D image containing an arrow pointing upwards stored with the RAS orientation, so the first point in the stored 1D array is the right-anterior-superior corner of the whole volume. However, if this image is then read by a program with the RAI orientation, the first point in the 1D array will be treated as the right-anterior-inferior corner and the order of filling the volume in the S-I dimension will be the reverse of how it is stored, so the upward-pointing arrow becomes a downward-pointing arrow.

Meta image format is the most commonly used data format in the scenario of this thesis. It stores a 3D image into two separate files, a *.mhd file which contains only the header informa-

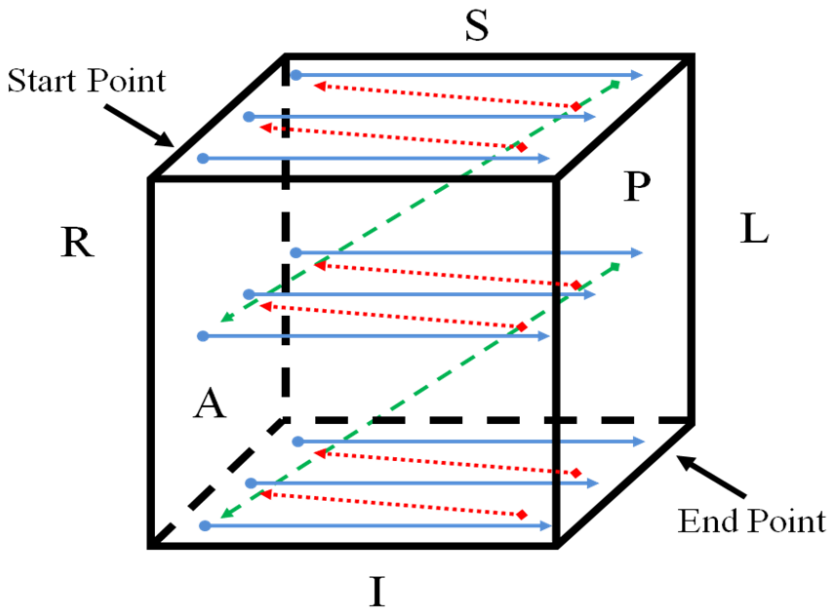


Figure A.1: Sequencing order of RAS orientation

tion as text and a *.raw file which contains the 3D volume as a 1D array. Meta image format allows the user to define the image orientation by editing the transform matrix in the *.mhd file, so that the user can use the image in whatever orientation they want with easy editing.

## A.3 Complications Associated with Image Registration

The reason why image orientation is so important is that images with different orientations may be impossible to be registered together, just like its impossible to register a left-hand coordinate system to a right-hand coordinate system. An illustrative example to explain the problem would be registering an image to its mirror image.

In Figure A.3, there is a moon-like object and its mirror image. If we try to align the original object to the mirror object in the 3D space by translation and rotation only, we will find it is impossible to align them together, because when the original object is moved and rotated to the backside, it is flipped. Such a phenomenon also occurs when people try to register two images with opposite orientations in one dimension, such as RAS and RAI.

A mathematical explanation of such a phenomenon can be given as this:

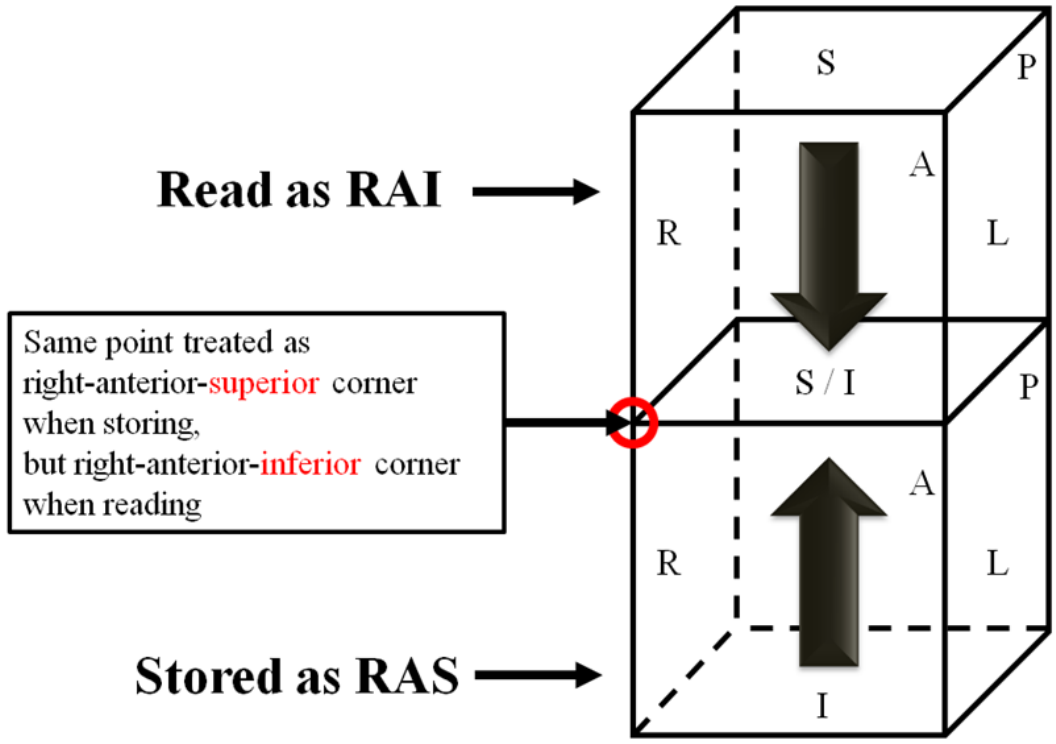


Figure A.2: Storing and Reading an Image with Different Sequencing Orders

Suppose there is a 3D coordinate system $XYZ$ and a 3D image $P$, of which each point is denoted by a 3D coordinate $P(x, y, z)$ (See Figure A.5). Now consider the $XZ$ plane as a mirror and flip the image along the $Y$ direction, so that the coordinate of each point in the mirror image becomes $P_1(x, -y, z)$. If we denote each point in the image as a vector $P := (x, y, z)'$, then the transform from $P$ to $P_1$ can be written in the matrix form:

$$P_1 = MP \tag{A.2}$$

where

$$M := \begin{pmatrix} 1 & 0 & 0 \\ 0 & -1 & 0 \\ 0 & 0 & 1 \end{pmatrix} \tag{A.3}$$

As we know, rigid registration attempts to align two images by rotation and translation and

a rigid registration can be written in a similar form as Equation A.2, which is

$$P_1 = RP + T \tag{A.4}$$

where $R$ is a $3 \times 3$ rotation matrix and $T$ is a $3 \times 1$ translation vector. The rotation matrix $R$ is a combination of the following three matrices, each of which deals with the rotation along one coordinate axis.

$$R_x := \begin{pmatrix} 1 & 0 & 0 \\ 0 & \cos\alpha & -\sin\alpha \\ 0 & \sin\alpha & \cos\alpha \end{pmatrix} R_y := \begin{pmatrix} \cos\beta & 0 & \sin\beta \\ 0 & 1 & 0 \\ -\sin\beta & 0 & \cos\beta \end{pmatrix} R_z := \begin{pmatrix} \cos\gamma & -\sin\gamma & 0 \\ \sin\gamma & \cos\gamma & 0 \\ 0 & 0 & 1 \end{pmatrix} \tag{A.5}$$

To simplify the problem, we can assume the origin of the coordinate system, which is the center of rotation, is at the center of image $P$. In that case, the translation vector $T$ is a zero vector, which leads to

$$P_1 = RP \tag{A.6}$$

Combing Equation A.2 and A.6, we can see whether or not it is possible to register image $P$ to $P_1$ with a rigid registration depends on if it is possible to find a rotation matrix $R$ that is identical to the transform matrix $M$ in Equation A.3. That is

$$R = M = \begin{pmatrix} 1 & 0 & 0 \\ 0 & -1 & 0 \\ 0 & 0 & 1 \end{pmatrix} \tag{A.7}$$

In the mean time, the rotation matrix $R$ should be the product of $R_x$, $R_y$, and $R_z$ regardless in which order are they multiplied. That is

$$R = \prod_{i=x,y,z} R_i \tag{A.8}$$

Combining Equation A.7 and A.8, we have

$$\prod_{i=x,y,z} R_i = M = \begin{pmatrix} 1 & 0 & 0 \\ 0 & -1 & 0 \\ 0 & 0 & 1 \end{pmatrix} \tag{A.9}$$

As we know, the determinants of the three rotation matrix are all 1. That is

$$|R_x| = |R_y| = |R_z| = 1 \tag{A.10}$$

Also, the determinant of matrix product is the product of the individual determinants, so we have

$$\left|\prod_{i=x,y,z} R_i\right| = |R_x| \times |R_y| \times |R_z| = 1 \tag{A.11}$$

However, the determinant of the transform matrix $M$ is -1.

$$|M| = -1 \tag{A.12}$$

Combining Equation A.9, A.11, and A.12, we notice that it is impossible to find a rotation matrix $R$ to make Equation A.7 valid. In another word, it is impossible to rigidly register an image to its mirror image.

With this approach, we can prove that if an image is flipped (or mirrored) in two dimensions, the result image can still be perfectly registered to the original image; if an image is flipped in all three dimensions, the result image cannot be registered to the original image.

In conclusion, for a 3D image registration problem, we must pay attention to the image orientation of the images to be registered. If there are differences in one or three dimensions,

such as RAS versus RAI or RAS versus LPI, it is impossible to correctly register those images together without changing the orientations.

# Appendix B

# iE33 Data Export and Conversion

## B.1 iE33 and the X7-2t Probe

Philips© iE33© xMATRIX echocardiography system is an ultrasound system designed for cardiac imaging purposes with real-time 3D imaging capability and it is claimed to be the world's first live 3D transesophageal echo (TEE) system. A commonly used probe for TEE scans with iE33 is the Philips X7-2t probe, where "X" stands for "matrix", "7-2" indicates the frequency range is 7-2 MHZ, and "t" stands for "transesophageal".

The iE33 system provides traditional single plane 2D, X-plane (or biplane) 2D, and live 3D scanning modes. The traditional 2D scan provides single plane B-mode images as most of the ultrasound systems. The biplane mode provides two intersected single-plane images simultaneously. One plane is kept stationary during the scan, while the other plane can be rotated and tilted. The live 3D mode provides real-time cone-shaped 3D images. The frame rate of the live 3D mode is normally around 20 Hz, whereas it can be increased to 30Hz with a reduced field of view. In addition, it also provides a full frame function which uses gating information to reconstruct an image with large FOV and high frame rate from several (typically four) heart beats.

## B.2 Export DICOM Data from QLAB©

The 3D data exported from the iE33 machine is stored as an encrypted DICOM format, which cannot be correctly read by a third-party DICOM reader. The specific software to read and visualize those data is called QLAB, which is developed and distributed by Philips itself (see Figure B.1).

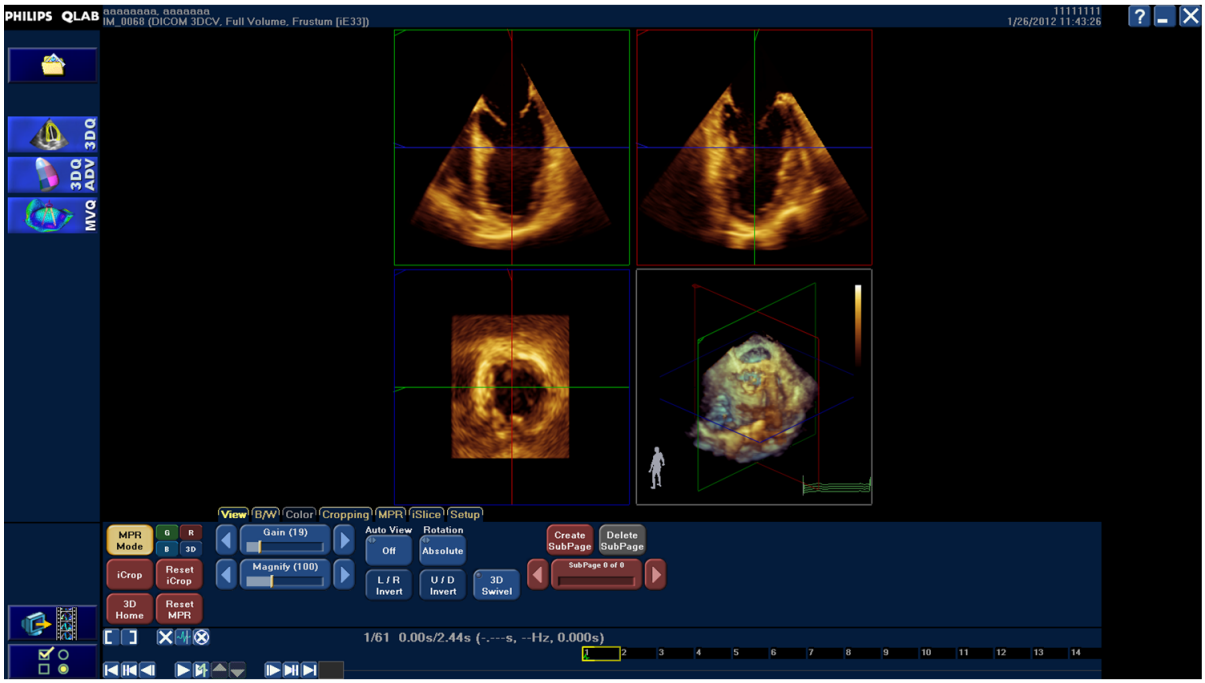


Figure B.1: A Screenshot of the QLAB platform

QLAB offers many functions for visualizing and analyzing the data. However, it does not provide a programming interface that allows users to develop their own functions and modules, such as segmentation and registration, and integrate them into QLAB. In order to apply user-defined functions, the data has to be exported as a normal DICOM data first and then be used in a different software platform.

QLAB offers a function to export the QLAB-specific 3D data to a non-encrypted DICOM format (An activation code is required to enable this function). However, there are still a few fields in the header of the exported data which are privately defined by Philips. Those fields include the size of dimensions, voxel spacing, and frame rate. For reference, those fields

together with their meanings are listed in Table B.2.

Table B.1: List of the Specifically-defined Fields in QLAB-exported DICOM Header and Their Meanings

| Fields | Meaning |
|---|---|
| dcminfo.Rows | Size of X dimension |
| dcminfo.Columns | Size of Y dimension |
| dcminfo.Private_3001_1001 | Size of Z dimension |
| dcminfo.PhysicalDeltaX | Voxel spacing in X dimension |
| dcminfo.PhysicalDeltaY | Voxel spacing of the Y dimension |
| dcminfo.Private_3001_1003 | Voxel spacing of the Z dimension |
| dcminfo.NumberOfFrames | Number of frames in a 4D data |

## B.3 Anonymizing the Data

Most of the research ethics approvals require the patients' data to be anonymized, but QLAB does not provide an auto-anonymizing function. Manually editing all the fields with patient names and IDs is very time-consuming. Further, the more complicated task is to eliminate the patient information integrated as bitmap images in both thumbnail and actual ultrasound images. A small piece of script is written in Matlab and converted to an executable command line programm to anonymize the data. The program does two things. First, it finds all the attributes with patient's private information, i.e. name, birthday, patient ID, etc., in the DICOM header and replace them with anonymous information. Second, it erases all the patient information in the bitmap images by reading the images as HEX code, finding specific HEX strings, and replacing the area indicated by the HEX string with background color. Thus, all the patient information is eliminated from the data.

## B.4 Export Streaming 4D Data

The 4D TEE data can be exported from the iE33 machine through an Ethernet cable and be integrated into a user-designed software platform. The programming interface including the

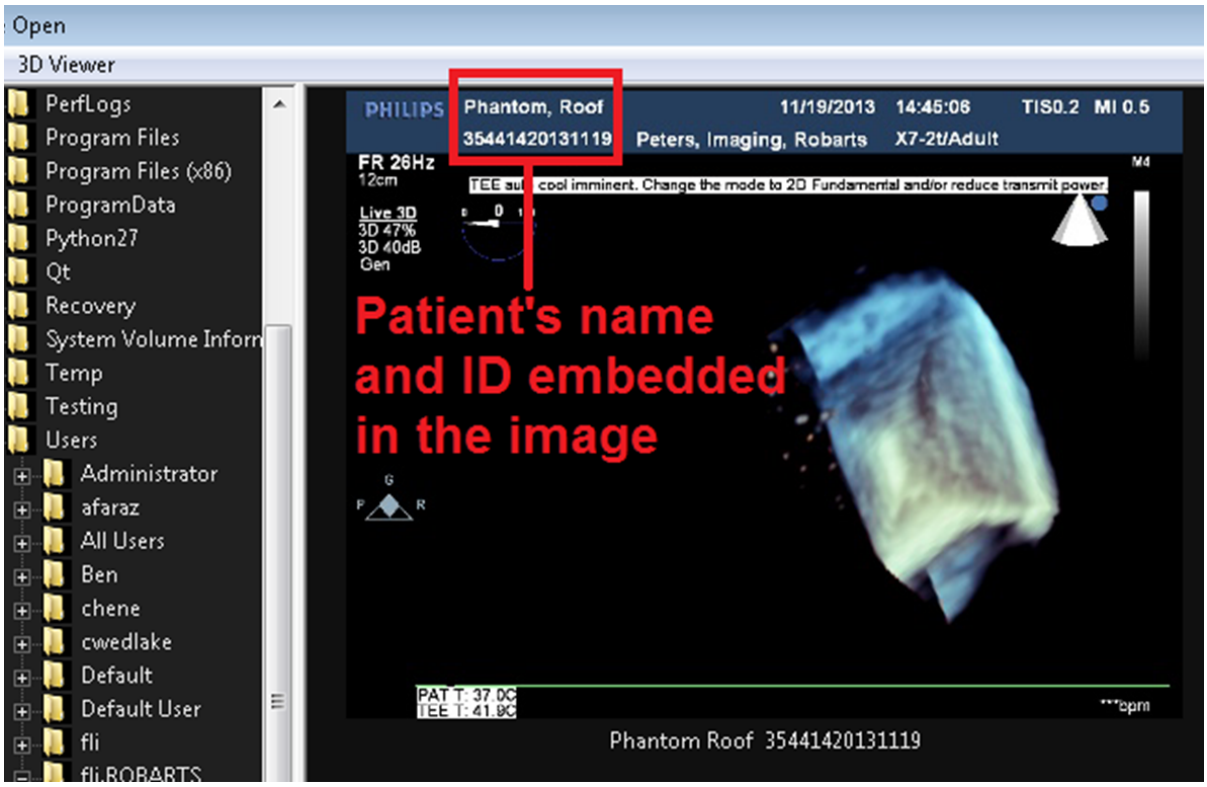


Figure B.2: A Screenshot of the QLAB platform

codes and *.dll files are confidentially provided by Philips Research North America, Briarcliff Manor, NY.

The working model of exporting 4D data is illustrated in Figure B.3. There are three components in the working model, the iE33 machine, the data conversion program, and user's own program. These three components form two client-server architectures. In the first client-server architecture, the iE33 machine works as a server that broadcasts the 4D frustum data continuously without caring if the data has been received or not. The executable program provided by Philips, working as a client in this architecture, receives the frustum data and convert it to a 3D Cartesian data. Then, the executable changes its role to be the server in the second client-server architecture. It sends out the converted 3D Cartesian data together with a "call-back" signal which informs user's program that a volume has been sent out. User's program, either a guidance platform, a visualization application, or a image processing software, works as a client in the second architecture and receives the Cartesian data when it is triggered by the "call-back"

signal.

A shortage of the streaming data is that it contains no header information other than the size of each dimension. The approach to obtain the voxel spacing is to build a look-up table of all the spacing values according to the scanning depth and then search the table for voxel spacing every time when a new depth is set.

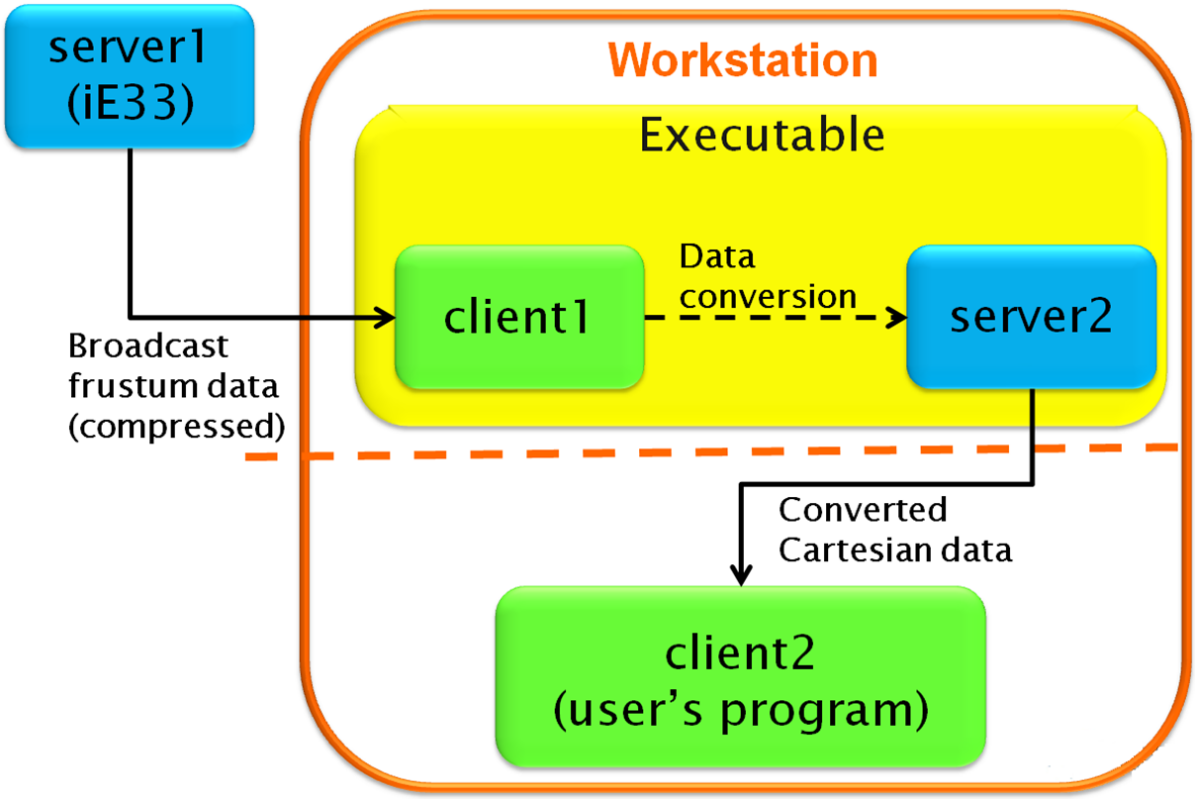


Figure B.3: Working Model of 4D Streaming Data Exporting

The standard operating procedure for setting up and testing a computer workstation to access iE33 4D streaming data is listed below:

1. Connect the iE33 to the workstation with a cross-over Ethernet cable. (There is a cross-over adapter in the lab, which can be attached to any normal Ethernet cable and make a cross-over cable.)

2. Run a DHCP server software on the workstation, so that it can automatically assign an IP address for the iE33. (OpenDHCPServer is available and located in "C: OpenD-

HCPServer" on the lab laptop. It can also be downloaded from SourceForge. The service can be started by running "RunStandAlone.bat" in command line.)

3. Check the IP address of iE33 with the following procedure. Press "setup" on the sliding keyboard → select "Print Network" on the screen → select "Network" → select "Network Device Utility" → find the IP address in the dialog box.

4. Ping iE33 and the workstation from each other and make sure each is visible to the other. (This may need some reboots.)

5. Register "..\StreamingData\Dll exes\Stream3d.dll. If you are using a 32-bit OS, this can be done by running "regsvr32 Stream3d.dll" in command line. If you are using a 64-bit OS, this can be done by the following procedure. Open the command line in administrator mode (Right click on cmd, choose "Run as administrator"). Go to directory "C:\Windows\SysWow64". Run the regsvr32 command in SysWow64.

6. Switch the scan mode to "live 3D" on iE33.

7. Run FrustumStreamTest in "..\StreamingData\Dll exes" with the command "FrustumStreamTest IPAddressOfiE33 port". Port is always 4013. It will show "receiving frustum data", if succeed.

8. Edit "..\Paul Streaming Code\StreamUS\server\3DUSTcpServer.bat". Go to the line "set addr=" and replace the IP address with iE33's IP address.

9. Run "3DUSTcpServer.bat" in command line. It will show "Waiting for client", if succeed.

10. Open Matlab (32-bit verstion) and set working directory to "..\Paul Streaming Code \StreamUS\StreamUS_matlab".

11. Run "StreamUS_init.m" in Matlab.

12. Run “script.m” in Matlab. It will show a slice from the streaming data, if succeed.

# Appendix C

# Copyright Releases

For the chapters in this thesis that were adapted from published articles, permission was sought to reproduce them in this thesis. Below are a copy of the copyright agreements that explicitly allow for the creation of derivative works.

# C.1 Releases for material in Chapter 2

## Consent to Publish

### Lecture Notes in Computer Science

Springer

**Title of the Book or Conference Name:** Information Processing in Computer Assisted Interventions 2013
**Volume Editor(s):** Purang Abolmaesumi, Leo Joskowicz, Pierre Jannin, Nassir Navab . .
**Title of the Contribution:** Generation of Synthetic 4D Cardiac CT Images for Guidance of Minimally Invasive Beating Heart Interventions
**Author(s) Name(s):** Feng P. Li, Martin Rajchl, James A. White, Aashish Goela, Terry M. Peters
**Corresponding Author's Name, Address, Affiliation and Email:** Feng P. Li, . . . . . .

When Author is more than one person the expression "Author" as used in this agreement will apply collectively unless otherwise indicated.

**§1 Rights Granted**

Author hereby grants and assigns to Springer-Verlag GmbH Berlin Heidelberg (hereinafter called Springer) the exclusive, sole, permanent, world-wide, transferable, sub-licensable and unlimited right to reproduce, publish, distribute, transmit, make available or otherwise communicate to the public, translate, publicly perform, archive, store, lease or lend and sell the Contribution or parts thereof individually or together with other works in any language, in all revisions and versions (including soft cover, book club and collected editions, anthologies, advance printing, reprints or print to order, microfilm editions, audiograms and videograms), in all forms and media of expression including in electronic form (including offline and online use, push or pull technologies, use in databases and networks for display, print and storing on any and all stationary or portable end-user devices, e.g. text readers, audio, video or interactive devices, and for use in multimedia or interactive versions as well as for the display or transmission of the Contribution or parts thereof in data networks or seach engines), in whole, in part or in abridged form, in each case as now known or developed in the future, including the right to grant further time-limited or permanent rights. For the purposes of use in electronic forms, Springer may adjust the Contribution to the respective form of use and include links or otherwise combine it with other works. For the avoidance of doubt, Springer has the right to permit others to use individual illustrations and may use the Contribution for advertising purposes.
The copyright of the Contribution will be held in the name of Springer. Springer may take, either in its own name or in that of copyright holder, any necessary steps to protect these rights against infringement by third parties. It will have the copyright notice inserted into all editions of the Contribution according to the provisions of the Universal Copyright Convention (UCC) and dutifully take care of all formalities in this connection in the name of the copyright holder.

**§2 Regulations for Authors under Special Copyright Law**

The parties acknowledge that there may be no basis for claim of copyright in the United States to a Contribution prepared by an officer or employee of the United States government as part of that person's official duties. If the Contribution was performed under a United States government contract, but Author is not a United States government employee, Springer grants the United States government royalty-free permission to reproduce all or part of the Contribution and to authorize others to do so for United States government purposes.
If the Contribution was prepared or published by or under the direction or control of Her Majesty (i.e., the constitutional monarch of the Commonwealth realm) or any Crown government department, the copyright in the Contribution shall, subject to any agreement with Author, belong to Her Majesty.
If the Contribution was created by an employee of the European Union or the European Atomic Energy Community (EU/Euratom) in the performance of their duties, the regulation 31/EEC, 11/EAEC (Staff Regulations) applies, and copyright in the Contribution shall, subject to the Publication Framework Agreement (EC Plug), belong to the European Union or the European Atomic Energy Community.
If Author is an officer or employee of the United States government, of the Crown, or of EU/Euratom, reference will be made to this status on the signature page.

**§3 Rights Retained by Author**

Author retains, in addition to uses permitted by law, the right to communicate the content of the Contribution to other scientists, to share the Contribution with them in manuscript form, to perform or present the Contribution or to use the content for non-commercial internal and educational purposes, provided the Springer publication is mentioned as the

07.02.2013
11:30

original source of publication in any printed or electronic materials. Author retains the right to republish the Contribution in any collection consisting solely of Author's own works without charge subject to ensuring that the publication by Springer is properly credited and that the relevant copyright notice is repeated verbatim.
Author may self-archive an author-created version of his/her Contribution on his/her own website and/or the repository of Author's department or faculty. Author may also deposit this version on his/her funder's or funder's designated repository at the funder's request or as a result of a legal obligation, provided it is not made publicly available until 12 months after official publication by Springer. He/she may not use the publisher's PDF version, which is posted on SpringerLink and other Springer websites, for the purpose of self-archiving or deposit. Furthermore, Author may only post his/her own version, provided acknowledgment is given to the original source of publication and a link is inserted to the published article on Springer's website. The link must be accompanied by the following text: "The final publication is available at link.springer.com".
Prior versions of the Contribution published on non-commercial pre-print servers like ArXiv/CoRR and HAL can remain on these servers and/or can be updated with Author's accepted version. The final published version (in pdf or html/xml format) cannot be used for this purpose. Acknowledgment needs to be given to the final publication and a link must be inserted to the published Contribution on Springer's website, accompanied by the text "The final publication is available at link.springer.com".
Author retains the right to use his/her Contribution for his/her further scientific career by including the final published paper in his/her dissertation or doctoral thesis provided acknowledgment is given to the original source of publication. Author also retains the right to use, without having to pay a fee and without having to inform the publisher, parts of the Contribution (e.g. illustrations) for inclusion in future work, and to publish a substantially revised version (at least 30% new content) elsewhere, provided that the original Springer Contribution is properly cited.

**§4 Warranties**

Author warrants that the Contribution is original except for such excerpts from copyrighted works (including illustrations, tables, animations and text quotations) as may be included with the permission of the copyright holder thereof, in which case(s) Author is required to obtain written permission to the extent necessary and to indicate the precise sources of the excerpts in the manuscript. Author is also requested to store the signed permission forms and to make them available to Springer if required.
Author warrants that he/she is entitled to grant the rights in accordance with Clause 1 "Rights Granted", that he/she has not assigned such rights to third parties, that the Contribution has not heretofore been published in whole or in part, that the Contribution contains no libelous statements and does not infringe on any copyright, trademark, patent, statutory right or proprietary right of others, including rights obtained through licenses; and that Author will indemnify Springer against any costs, expenses or damages for which Springer may become liable as a result of any breach of this warranty.

**§5 Delivery of the Work and Publication**

Author agrees to deliver to the responsible Volume Editor (for conferences, usually one of the Program Chairs), on a date to be agreed upon, the manuscript created according to the Springer Instructions for Authors. Springer will undertake the reproduction and distribution of the Contribution at its own expense and risk. After submission of the Consent to Publish form Signed by the Corresponding Author, changes of authorship, or in the order of the authors listed, will not be accepted by Springer.

**§6 Author's Discount**

Author is entitled to purchase for his/her personal use (directly from Springer) the Work or other books published by Springer at a discount of 33 1/3% off the list price as long as there is a contractual arrangement between Author and Springer and subject to applicable book price regulation. Resale of such copies or of free copies is not permitted.

**§7 Governing Law and Jurisdiction**

This agreement shall be governed by, and shall be construed in accordance with, the laws of the Federal Republic of Germany. The courts of Berlin, Germany shall have the exclusive jurisdiction.

Corresponding Author signs for and accepts responsibility for releasing this material on behalf of any and all Co-Authors.

**Signature of Corresponding Author:** **Date:** March 17, 2013

☐ I'm an employee of the US Government and transfer the rights to the extent transferable (Title 17 §105 U.S.C. applies)

☐ I'm an employee of the Crown and copyright on the Contribution belongs to Her Majesty

☐ I'm an employee of the EU or Euratom and copyright on the Contribution belongs to EU or Euratom

07.02.2013 11:30

## C.2 Releases for material in Chapter 3

**Consent to Publish**
**Lecture Notes in Computer Science**

Springer

**Title of the Book/Volume/Conference:** MIAR/AECAI 2013 (8090)

**Volume Editor(s):** Liao H, Linte CA , Masamune K, Peters TM and Zheng G

**Title of Contribution:** Towards CT Enhanced Ultrasound Guidance for Off-pump Beating Heart Mitral Valve Repair

**Author(s) name(s):** Feng P. Li, Martin Rajchl, James A. White, Aashish Goela, and Terry M. Peters

**Corresponding Author's name, address, affiliation and e-mail:**

**§ 1 Rights Granted**

The copyright to the Contribution identified above is transferred to Springer-Verlag GmbH Berlin Heidelberg (hereinafter called Springer-Verlag). The copyright transfer covers the sole right to print, publish, distribute and sell throughout the world the said Contribution and parts thereof, including all revisions or versions and future editions thereof and in any medium, such as in its electronic form (offline, online), as well as to translate, print, publish, distribute and sell the Contribution in any foreign languages and throughout the world (for U.S. government employees: to the extent transferable).

Springer-Verlag will take, either in its own name or in that of the Author, any necessary steps to protect these rights against infringement by third parties. It will have the copyright notice inserted into all editions of the Contribution according to the provisions of the Universal Copyright Convention (UCC) and dutifully take care of all formalities in this connection, either in its own name or in that of the Author.

If the Author is an employee of the U.S. Government and performed this work as part of their employment, the contribution is not subject to U.S. copyright protection. If the work was performed under Government contract, but the Author is not a Government employee, Springer-Verlag grants the U.S. Government royalty-free permission to reproduce all or part of the contribution and to authorize others to do so for U.S. Government purposes. If any of the above Authors on this agreement is an officer or employee of the U.S. Government reference will be made to this status on the signature page.

An author may self-archive his/her article on his/her personal website; however we request that acknowledgement is given to the LNCS publication and a link is inserted to the published article on Springer's website www.springerlink.com, LNCS online. The Author must ensure that the publication by Springer-Verlag is properly credited and that the relevant copyright notice is repeated verbatim.

The Author warrants that the work is original except for such excerpts from copyrighted works (including illustrations, tables, and text quotations) as may be included with the permission of the copyright holder and author thereof, in which case(s) the Author is required to indicate the precise source. Springer-Verlag has the right to permit others to use individual illustrations within the usual limits. The Author warrants that the work has not heretofore been published in whole or in part, that it contains no libelous statements and does not infringe on any copyright, trademark, patent, statutory rights or proprietary rights of others; and that he will indemnify Springer-Verlag against any cost, expenses or damages for which Springer-Verlag may become liable as a result of any breach of this warranty.

**§ 2 Delivery of the Work and Publication**

The Author agrees to deliver to the responsible Editor(s) on a date to be agreed upon the manuscript created according to the Instructions for Authors.

Springer-Verlag agrees to publish the said Contribution at its own cost and expense.

**§ 3 Author's Discount**

The Author is entitled to purchase for personal use (directly from Springer-Verlag) books published by Springer-Verlag at a discount of 33 1/3% off the list price. Resale of such books is not permitted.

**§ 4 Entire Agreement**

This agreement shall be deemed to be made under and shall be interpreted in accordance with the laws of the Federal Republic of Germany.

**Signature(s) of Author(s):** **Date:** 04.07.2013

# C.3 Releases for material in Chapter 4

SPIE **TRANSFER OF COPYRIGHT TO SOCIETY OF PHOTO-OPTICAL INSTRUMENTATION ENGINEERS (SPIE)**

**Title of Paper:** Ultrasound based mitral valve annulus tracking for off-pump beating heart mitral valve repair

**SPIE Paper Number: (xxxx-xx)** 9036-58 **Contact Author Email:** _____

**Author(s):** Feng P. Li, Martin Rajchl, John Moore, Terry M. Peters

*This signed statement must be returned to SPIE prior to the scheduled publication of the Proceedings or Journal in which the Paper will be published. The intent of this Agreement is to protect the interests of both SPIE and authors/employers and to specify reasonable rights for both parties related to publication and reuse of the material.*

---

**The undersigned hereby assign(s) to Society of Photo-Optical Instrumentation Engineers (SPIE) copyright ownership in the above Paper, effective if and when the Paper is accepted for publication by SPIE and to the extent transferable under applicable national law. This assignment gives SPIE the right to register copyright to the Paper in its name as claimant and to publish the Paper in any print or electronic medium.**

Authors, or their employers in the case of works made for hire, retain the following rights:

1. All proprietary rights other than copyright, including patent rights.
2. The right to make and distribute copies of the Paper for internal purposes.
3. The right to use the material for lecture or classroom purposes.
4. The right to prepare derivative publications based on the Paper, including books or book chapters, journal papers, and magazine articles, provided that publication of a derivative work occurs subsequent to the official date of publication by SPIE.
5. The right to post an author-prepared version or an official version (preferred version) of the published paper on an internal or external server controlled exclusively by the author/employer, provided that (a) such posting is noncommercial in nature and the paper is made available to users without charge; (b) a copyright notice and full citation appear with the paper, and (c) a link to SPIE's official online version of the abstract is provided using the DOI (Document Object Identifier) link.

   **Citation format:**
   Author(s), "Paper Title," Publication Title, Editors, Volume (Issue) Number, Article (or Page) Number, (Year).

   **Copyright notice format:**
   Copyright XXXX (year) Society of Photo-Optical Instrumentation Engineers. One print or electronic copy may be made for personal use only. Systematic reproduction and distribution, duplication of any material in this paper for a fee or for commercial purposes, or modification of the content of the paper are prohibited.

   **DOI abstract link format:**
   http://dx.doi.org/DOI# *(Note: The DOI can be found on the title page or online abstract page of any SPIE article.)*

If the work that forms the basis of this Paper was done under a contract with a governmental agency or other entity that retains certain rights, this Transfer of Copyright is subject to any rights that such governmental agency or other entity may have acquired.

By signing this Agreement, the authors warrant that (1) the Paper is original and has not previously been published elsewhere; (2) this work does not infringe on any copyright or other rights in any other work; (3) all necessary reproduction permissions, licenses, and clearances have been obtained; and (4) the authors own the copyright in the Paper, are authorized to transfer it, and have full power to enter into this Agreement with SPIE.

*WHO SHOULD SIGN.* This form must be signed by (1) at least one author who is not a U.S. Government employee and (2) the author's employer if the Paper was prepared within the scope of the author's employment or was commissioned by the employer. If not signed by all authors, the author(s) signing this Agreement represents that he/she is signing this Agreement as authorized agent for and on behalf of all the authors.

| Author's signature | Print name | Date (mm/dd/yyyy) |
|---|---|---|
| | Feng P. Li | 02/03/2014 |
| Author's signature | Print name | Date (mm/dd/yyyy) |
| | | |
| Authorized Employer signature | Print name Title | Date (mm/dd/yyyy) |
| | | |

**U.S. GOVERNMENT EMPLOYMENT CERTIFICATION**
A work prepared by a U.S. Government employee as part of his or her official duties is not eligible for U.S. Copyright. If all authors were U.S. Government employees when this Paper was prepared, and the authors prepared this Paper as part of their official duties, at least one author should sign below. If at least one author was not a U.S. Government employee, the work is eligible for copyright and that author should sign the Transfer of Copyright form above.

| Author's signature | Print name | Date (mm/dd/yyyy) |
|---|---|---|
| | | |

*Submit this form online at http://spie.org/myaccount*

*Director of Publications, SPIE, P.O. Box 10, Bellingham, WA 98227-0010 USA • Phone: 360/676-3290 (Pacific Time) • Fax: 360/647-1445 • Revised 14 May 2013*

# Curriculum Vitae

Name: Feng Patrick Li

## Post-secondary Education and Degrees

| | |
|---|---|
| 2009-* | PhD. Candidate in Biomedical Engineering<br>Robarts Research Institute, Western University, London, ON |
| 2009 | Double MSc. in Computer Science<br>Technical University of Berlin, Berlin, Germany<br>Shanghai Jiao Tong University, Shanghai, China |
| 2006 | BSc. in Computer Science<br>Shanghai Jiao Tong University, Shanghai, China |

## Awards & Scholarships

| | |
|---|---|
| 2014 | First prize in scientific poster competition at Imaging Network Ontario 2014 |
| 2009-2014 | Western Graduate Research Scholarship (WGRS) - (CAD $17500/yr) |
| 2011-2013 | Canadian Institutes of Health Research (CIHR)<br>Strategic Training Program in Vascular Research (CAD $12000/yr) |
| 2010-2011 | Computer Assisted Medical Intervention (CAMI)<br>Training Program Scholarship (CAD $10000/yr) |
| 2003-2005 | People Scholarship in Shanghai Jiao Tong University (RMB $3000) |

## Teaching

2013 Leading Teaching Assistant, Western University, London, ON
Faculty of Engineering - Dept. of Electrical and Computer Engineering
*Programming Fundamentals for Engineers*

2010-2013 Teaching Assistant, Western University, London, ON
Faculty of Engineering - Dept. of Electrical and Computer Engineering
*Programming Fundamentals for Engineers*

## Invited Talks

2014.06 *From Open Heart to Minimally Invasive Heart Surgery*
Retire with Strong Mind Program, London, ON

2103.06 *A Guidance System for Off-pump Beating Heart Mitral Valve Repair*
Innovation Centre of Computer Assisted Surgery, Leipzig, Germany

2012.11 *Towards Using Synthetic CT and Intro-op TEE Images in Guidance of Off-pump Beating Heart Interventions*
Computational Biomedicine, Imaging, and Modelling Center,
Rutgers University, Piscataway Township, NJ

2011.12 *Towards Model-Enhanced Real-time Ultrasound Guided Cardiac Interventions*
Department of Cardiology, Ruijin Hospital, Shanghai, PR. China

2011.11 *Towards Model-Enhanced Real-time Ultrasound Guided Cardiac Interventions*
Med-X Research Institute, Shanghai Jiao Tong University, Shanghai, PR. China

## Oral Presentations

2014 SPIE Medical Imaging 2014, San Diego, CA

2013 MICCAI Workshop on MIAR-AECAI 2013, Nagoya, JPN

2013 Intl. Conf. on IPCAI 2013, Heidelberg, GER

2013 Imaging Network Ontario (ImNO) 2013, Toronto, ON

2012 Intl. Conf. on ICBMI 2012, Wuhan, PR. China

2012 SPIE Medical Imaging 2012, San Diego, CA

# Poster Presentations

2014 Imaging Network Ontario (IMNO) 2014, Toronto, ON

2013 Image Guided Therapy Workshop (IGTWS) 2013, Crystal City, VA

2013 Imaging Network Ontario (IMNO) 2013, Toronto, ON

2012 MICCAI Workshop on AECAI 2012, Nice, FRA

2012 Imaging Network Ontario (IMNO) 2012, Toronto, ON

2011 MICCAI Workshop on AECAI 2011, Toronto, ON

2011 Intl. Cong. on CARS 2010, Berlin, GER

2011 Imaging Network Ontario (IMNO) 2011, Toronto, ON

2010 Margaret Moffat Research Day, London, ON

2008 Intl. Conf. on Pattern Recognition (ICPR) 2008, Tampa, FL

# Research Collaborations

2012-* Neochord Inc., Eden Prairie, MN

# Publications

## Peer-reviewed Journal Articles

1. F.P. Li, M. Rajchl, J.A. White, A. Goela, and T.M. Peters (2014). Ultrasound Guidance for Beating Heart Mitral Valve Repair Augmented by Synthetic Dynamic CT. IEEE Transactions on Medical Imaging. (In review).

2. F.P. Li, M. Rajchl, J. Moore, T.M. Peters (2014). A Mitral Annulus Tracking Approach for Navigation of Off-pump Beating Heart Mitral Valve Repair. Medical Physics. (In review).

3. M. Rajchl, J. Yuan, J. White, E. Ukwatta, J. Stirrat, C. Nambakhsh, F. Li, and T. Peters (2014). Interactive Hierarchical Max-Flow Segmentation of Scar Tissue from Late-Enhancement Cardiac MR Images. IEEE Transactions on Medical Imaging 33(1), 159-172.

4. G. Wang, S. Zhang, F. Li, L. Gu (2013), A New Segmentation Framework Based on Sparse Shape Composition in Liver Surgery Planning System, Medical Physics 40(5), 051913. (Made cover)

## Peer-reviewed Articles in Conference Proceedings

1. F.P. Li, M. Rajchl, J.T. Moore, and T.M. Peters (2014). Ultrasound based mitral valve annulus tracking for off-pump beating heart mitral valve repair. In: SPIE Medical Imaging, 90361M-90361M-9.

2. M. Rajchl, K. Abhari, J. Stirrat, E. Ukwatta, D. Cantor-Rivera, F.P. Li, T.M. Peters, and J.A. White (2014). Distribution of guidance models for cardiac resynchronization therapy in the setting of multi-center clinical trials. In: SPIE Medical Imaging, 90361V-90361V-7.

3. F.P. Li, M. Rajchl, J.A. White, A. Goela, and T.M. Peters (2013). Towards CT Enhanced Ultrasound Guidance for Off-pump Beating Heart Mitral Valve Repair. In: MIAR/AE-CAI, 136-143.

4. F.P. Li, M. Rajchl, J.A. White, A. Goela, and T.M. Peters (2013). Generation of Synthetic 4D Cardiac CT Images for Guidance of Minimally Invasive Beating Heart Interventions. In: Information Processing in Computer-Assisted Interventions (IPCAI). Springer Berlin Heidelberg, pp.11-20.

5. G. Wang, S. Zhang, F. Li, L. Gu (2013). Segmentation using Sparse Shape Model and Minimally Supervised Method in Liver Surgery Planning System, In: International IEEE EMBS Conference of the IEEE Engineering in Medicine and Biology Society.6075-8.

6. F.P. Li, J.A. White, M. Rajchl, A. Goela, and T.M. Peters (2012). Generation of Synthetic 4D Cardiac CT Images by Deformation from Cardiac Ultrasound. In: Augmented Environments for Computer-Assisted Interventions (AE-CAI). Springer Berlin Heidelberg, pp.132-141.

7. M. Rajchl, J. Yuan, J.A. White, M. Nambakhsh, E. Ukwatta, F. Li, J. Stirrat, and T.M. Peters (2012), A Fast Convex Optimization Approach to Segmenting 3D Scar Tissue from Delayed-Enhancement Cardiac MR Images, In: Medical Image Computing and Computer-Assisted Interventation (MICCAI). Lecture Notes in Computer Science. Springer Berlin Heidelberg, pp.659666.

8. F. Li, P. Lang, M. Rajchl, E. Chen, G. Guiraudon, and T. Peters (2012). Towards real-time 3D US-CT registration on the beating heart for guidance of minimally invasive cardiac interventions. In: SPIE Medical Imaging. International Society for Optics and Photonics, pp.831615-831615.

9. P. Lang, M. Rajchl, F. Li, and T. Peters (2011). Towards Model-Enhanced Real-Time Ultrasound Guided Cardiac Interventions. In: Intelligent Computation and Bio-Medical Instrumentation (ICBMI), 2011 International Conference on. IEEE, pp.89-92.

10. F. Li, P. Lang, M. Rajchl, E.C.S. Chen, G. Guiraudon, T.M. Peters (2011), Towards Real-time 3D US to CT Cardiac Image Registration for Minimally Invasive Cardiac Intervention Guidance, In: MICCAI workshop on Augmented Environments for Computer Assisted Interventions (AE-CAI).

11. F. Li, D. Bartz, L. Gu, and M.A. Audette, An Iterative Classification Method of 2D CT Head Data Based on Statistical and Spatial Information, In: International Conference on Pattern Recognition (ICPR), pp. 1-4.

## Other Conference Manuscripts & Abstracts

1. F.P. Li, M. Rajchl, J. Moore, and T.M. Peters (2014). Ultrasound Based Mitral Valve Annulus Tracking for Off-pump Beating Heart Mitral Valve Repair. In: Imaging Network Ontario (ImNO).

2. F. Li, M. Rajchl, J. Moore, C. Wedlake, and T. Peters (2013). CT-Enhanced Ultrasound for Guidance of Off-pump Beating Heart Interventions. In: National Image-Guided Therapy Workshop 2013, Arlington, VA. NCIGT.

3. M.Rajchl, F. Li, J. Moore, C. Wedlake, U. Aladl, and T. Peters (2013). Feature Tracking for Image guided Mitral Valve Repair. In: National Image-Guided Therapy Workshop 2013, Arlington, VA. NCIGT.

4. F. Li, J. White, M. Rajchl, A. Goela, and T. Peters (2013). Generation of Synthetic 4D Cardiac CT Images for Guidance of Off-pump Beating Heart Interventions. In: Imaging Network Ontario (ImNO).

5. F. Li, P. Lang, M. Rajchl, E.C.S. Chen, G. Guiraudon, and T.M. Peters (2012). Towards Real-time 3D US-CT Registration on the Beating Heart for Guidance of Minimally Invasive Cardiac Interventions. In: Imaging Network Ontario (ImNO).

6. F. Li, L. Gu, M.A. Audette, and T.M. Peters (2011), A Minimally Supervised Segmentation Method of Liver, Portal Vein, and Hepatic Vein on 3D Enhanced CT Abdomen Data, In: International Congress and Exhibition on Computer Assisted Radiology and Surgery (CARS).

7. E.C.S. Chen, J. McLeod, P. Lang, F. Li, and T.M. Peters (2011). Automatic Real-time 3D Ultrasound Calibration Using Single US Volume, In: International Congress and Exhibition on Computer Assisted Radiology and Surgery (CARS)

8. F. Li (2010). Dynamic Image Fusion for Guidance of Cardiac Therapies. In: Margaret Moffat Research Day.